Earth-Science Reviews 196 (2019) 102870

Contents lists available at ScienceDirect

Earth-Science Reviews

journal homepage: www.elsevier.com/locate/earscirev

Digital mapping of peatlands – A critical review

Budiman Minasny[a,*], Örjan Berglund[b], John Connolly[c], Carolyn Hedley[d], Folkert de Vries[e], Alessandro Gimona[f], Bas Kempen[g], Darren Kidd[h], Harry Lilja[i], Brendan Malone[a,p], Alex McBratney[a], Pierre Roudier[d,q], Sharon O'Rourke[j], Rudiyanto[k], José Padarian[a], Laura Poggio[f,g], Alexandre ten Caten[l], Daniel Thompson[m], Clint Tuve[n], Wirastuti Widyatmanti[o]

[a] School of Life & Environmental Science, Sydney Institute of Agriculture, the University of Sydney, Australia
[b] Swedish University of Agricultural Sciences, Department of Soil and Environment, Uppsala, Sweden
[c] School of History & Geography, Dublin City University, Ireland
[d] Manaaki Whenua - Landcare Research, Palmerston North, New Zealand
[e] Wageningen Environmental Research, PO Box 47, Wageningen, the Netherlands
[f] The James Hutton Institute, Scotland, United Kingdom
[g] ISRIC – World Soil Information, PO Box 353, Wageningen, the Netherlands
[h] Department of Primary Industries, Parks, Water, and Environment, Tasmania, Australia
[i] Luke, Natural Resources Institute, Finland
[j] School of Biosystems & Food Engineering, University College Dublin, Ireland
[k] Faculty of Fisheries and Food Security, Universiti Malaysia Terengganu, Malaysia
[l] Universidade Federal de Santa Catarina, Brazil
[m] Natural Resources Canada, Canada
[n] Natural Resources Conservation Service, United States Department of Agriculture, USA
[o] Department of Geographic Information Science, Faculty of Geography, Universitas Gadjah Mada, Yogyakarta, Indonesia
[p] CSIRO Agriculture and Food, Black Mountain ACT, Australia
[q] Te Pūnaha Matatini, The University of Auckland, Private Bag 92019, Auckland 1010, New Zealand

A B S T R A C T

Peatlands offer a series of ecosystem services including carbon storage, biomass production, and climate regulation. Climate change and rapid land use change are degrading peatlands, liberating their stored carbon (C) into the atmosphere. To conserve peatlands and help in realising the Paris Agreement, we need to understand their extent, status, and C stocks. However, current peatland knowledge is vague—estimates of global peatland extent ranges from 1 to 4.6 million km^2, and C stock estimates vary between 113 and 612 Pg (or billion tonne C). This uncertainty mostly stems from the coarse spatial scale of global soil maps. In addition, most global peatland estimates are based on rough country inventories and reports that use outdated data. This review shows that digital mapping using field observations combined with remotely-sensed images and statistical models is an avenue to more accurately map peatlands and decrease this knowledge gap. We describe peat mapping experiences from 12 countries or regions and review 90 recent studies on peatland mapping. We found that interest in mapping peat information derived from satellite imageries and other digital mapping technologies is growing. Many studies have delineated peat extent using land cover from remote sensing, ecology, and environmental field studies, but rarely perform validation, and calculating the uncertainty of prediction is rare. This paper then reviews various proximal and remote sensing techniques that can be used to map peatlands. These include geophysical measurements (electromagnetic induction, resistivity measurement, and gamma radiometrics), radar sensing (SRTM, SAR), and optical images (Visible and Infrared). Peatland is better mapped when using more than one covariate, such as optical and radar products using nonlinear machine learning algorithms. The proliferation of satellite data available in an open-access format, availability of machine learning algorithms in an open-source computing environment, and high-performance computing facilities could enhance the way peatlands are mapped. Digital soil mapping allows us to map peat in a cost-effective, objective, and accurate manner. Securing peatlands for the future, and abating their contribution to atmospheric C levels, means digitally mapping them now.

1. Introduction

Peatlands cover about 3% of the earth's land surface, holding between 113 and 612 Pg (Peta gram = 10^{15} g, or equivalent to Gigatonne) of carbon (C) (Jackson et al., 2017; Köchy et al., 2015). This is equivalent to about 5–20% of the global soil C stock, 15–72% of atmospheric C, and 18–89% of global terrestrial C biomass. Peatlands can be found in arctic, boreal, temperate, and tropical regions (Fig. 1). Types of peatland vary, but all have accumulated a significant amount of organic matter over a long period (Wieder et al., 2006). Under

* Corresponding author.
E-mail address: budiman.minasny@sydney.edu.au (B. Minasny).

https://doi.org/10.1016/j.earscirev.2019.05.014
Received 9 June 2018; Received in revised form 14 January 2019
Available online 30 May 2019
0012-8252/

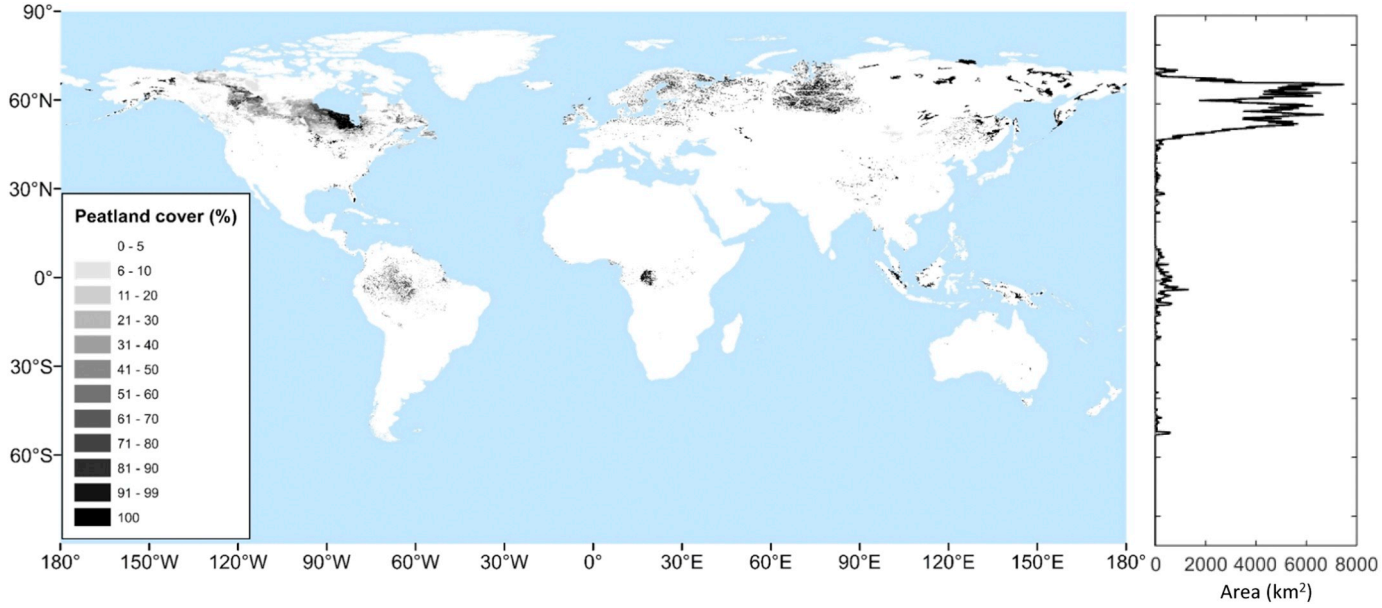

Fig. 1. A global estimate of peatland and its distribution along the latitude (map from Xu et al., 2018, creative common).

natural conditions, peatlands are carbon sinks with an estimated accumulation rate between 0.5 and 1 mm per year since the last glacial period. For over 1000 years, peatlands have been mined for fuel and fertilizer, and used for grazing and agriculture. Agricultural use requires draining the peat, causing consolidation, enhanced peat decomposition, and subsequent land subsidence (Hoogland et al., 2012).

Climate change and rapid land use change have turned peatlands into carbon source ecosystems. Peat mining, drainage, agriculture, and potential negative feedback with the warming environment are releasing the carbon stored in peats, and adding to atmospheric carbon dioxide (CO_2). Concerns of elevated greenhouse gas emissions from degraded peatlands have sparked international interest. The EU 2030 climate and energy framework emphasises that forests, agricultural land and wetlands (and thus peatlands), will play a central role in realising the Paris Agreement. Under this framework, from 2021, all EU member states need to report on the emissions and removals of greenhouse gases from wetlands (European Parliament, 2018). Other global initiatives on peatlands include the FAO (Joosten et al., 2012), the UN Framework Convention on Climate Change (UNFCCC), the International Union for the Conservation of Nature, and the establishment of the Global Peatlands Initiative.

Global peatlands are degrading and immediate action is necessary to prevent further decline. Comprehensive, worldwide mapping is essential to better understand peatland extent and status, and to protect peatland from further degradation. Research into and monitoring of peatland should be improved to provide better maps and tools for rapid assessment to support action and multi-stakeholder engagement (Crump, 2017).

Much effort is focused on measuring aboveground biomass, however C stored in peat can be 10–30 times larger than its aboveground biomass. As such, C loss and potential emissions reduction are better targetted in areas of deep peat (Law et al., 2015). However, mapping peatland extent and its C stock is not a simple exercise. Nearly 100 years ago, soil surveyor William Edgar Tharp from the U.S. Soil Survey explained that the first problem in mapping peat soils lies in defining the extent of the investigation (Tharp, 1924). Peat occurs worldwide but as fragmented pockets. Consequently, it has often been neglected by soil surveyors, as evidenced by the lack of large-scale digital soil mapping studies on peat (see Table 4).

Traditional mapping approaches determined peatland extent and distribution by manually delineating peat based on aerial photography (Cruickshank and Tomlinson, 1990; Vitt et al., 2000). With advances in digital soil mapping (DSM) (McBratney et al., 2003), soil C has been successfully mapped throughout the world, and global estimates of soil C stocks have improved over the last decade (Arrouays et al., 2014). However, digital mapping efforts specific to peatlands are modest and global C stock estimates for peatlands vary considerably, between 113 and 612 Pg (Jackson et al., 2017).

Digital mapping techniques can help generate accurate peatland maps and identify regions with the highest threats, priorities, and drivers of change. These maps can also be used in climate models to assess the sensitivity and feedback to future climate change. Protecting, restoring, and managing peatlands can be offered as part of the national climate change mitigation policy to achieve the Paris Agreement (Crooks et al., 2011).

This article aims to review the state-of-the-art of digital mapping of peatlands, methods for estimating C stock, and highlights some opportunities and challenges to accurately measuring and monitoring the world's peatlands. Section 2 describes peatland definitions and formation. Section 3 describes how carbon stocks in peatland are currently calculated. Section 4 provides an overview of global and regional estimates of peatland, highlighting the variability in these values and proposing some reasons for this variability. Section 5 presents 12 case studies of national or regional peatland mapping. Section 6 reviews 90 studies that have explicitly mapped peatlands using digital techniques, illustrating the biggest gaps in digital peat mapping and the main avenues to improve mapping. Section 7 reviews some proximal and remote sensors that are useful for mapping peat.

2. Peatland definition and formation

2.1. Peatland definition, types, and ecosystem services

There is no globally accepted definition for ‘peatland’. In this paper, we use the broad definition from Joosten and Clarke (2002):

- Peat is a sedentarily accumulated material consisting of at least 30% (dry mass) of dead organic material.
- A peatland is an area with or without vegetation with a naturally accumulated peat layer at the surface.

The term “mire” describes a wetland ecosystem where peat

accumulates (Moore and Bellamy, 1974) or a peatland where peat is currently being formed (Joosten, 2009), although it is difficult to know if peat is still forming or not.

The definition of 'organic soil' varies between soil classification systems. Organic layer thickness is usually part of the description. According to the World Reference Base for Soil Resources (WRB) and the USDA soil taxonomy, histosols must have organic materials ≥ 40 cm overlying unconsolidated soil materials. The USDA system specifies that the organic materials should have at least 12–18% organic carbon (OC). Histosols can be further distinguished into sapric, hemic, and fibric categories based on their decomposition stages; however the classification criteria could also be different according to different systems (Kolka et al., 2016). Other national classification systems may have a different definition of organic soils.

In the ecology literature, peatlands are distinguished from other landscapes based on morphology and landscape position (bogs, convex raised above the surrounding landscape, acid and nutrient-poor and fens, flat or concave situated in depressions with higher pH and richer nutrient content), and land use potential. Classifications include ombrogenous peats (or ombrothropic) that are fed only by precipitation, and geogenous (or geo or minerothropic) that are also fed by water which has been in contact with the mineral bedrock or substrate (Joosten and Clarke, 2002).

Despite covering only 3% of the earth's land surface, peatlands provide many ecosystem services (Kimmel and Mander, 2010) including:

- Biomass production for agricultural use including horticulture, dairy, and forestry.
- An energy source. Peat has been extracted as an energy source or fuel and horticultural growing media.
- Carbon storage. Peat is one of the largest C stores per unit area.
- Water regulation. Peat serves as a water reservoir and as part of the hydrological cycle which can mitigate flood via water absorption.
- Climate regulation. As one of the largest terrestrial C components, peat influences the direction and magnitude of carbon cycle-climate feedbacks.
- Biodiversity support including unique habitats for rare and endemic species.
- Research and education. Peatland is not currently well understood or documented, offering great scope for research and education.
- Recreation and art. Peatland can serve as a natural recreation area and contribute to art.

2.2. Rates of formation

Based on radiocarbon date estimates, peatland has been accumulating since the last glacial maximum, some 20,000 years ago. Average global peatland C accumulation rates were reported at 20–140 g C $m^{-2} yr^{-1}$ (Mitra et al., 2005). Yu et al. (2010) found that northern peatland formation peaked around 11,000–9000 years ago (average accumulation rate of 18.6 g C m^{-2} yr), tropical peatland formation began > 20,000 years ago and peaked about 8000–4000 years ago, and southern peatland formation peaked about 17,000–13,500 years ago. They noted the dominant factors controlling peatland formation in northern regions are climate and seasonality.

In Ireland, for example, peatland is divided into blanket bog and raised bogs (Hammond, 1979). A third type: fen, has been extensively drained and only a very small area remains. Raised bogs are found primarily in the middle of Ireland whereas blanket bogs are found predominantly along the western seaboard and in mountainous areas (Connolly and Holden, 2009; Renou-Wilson et al., 2011).

Raised bogs and blanket bogs have different genesis, both of which have been influenced by drainage, climate, hydrology, geomorphology, nutrient status and glacial geology. Raised bogs developed in the post-glacial lacustrine environment left after the retreat of the British-Irish Ice Sheet. Over time, as the lakes themselves are infilled with dead vegetation, conditions suitable for peat moss (Sphagnum) growth occurs. This is followed by the "accumulation of water-saturate peat above the original water surface" (Van Breemen, 1995). The surface becomes disconnected from the groundwater and the peatland becomes an ombrotrophic bog. The genesis of blanket bogs is related to a combination of the deterioration of the climate and land clearance between 5100 and 3100 BP. Increased rainfall led to the paludification of soils and the formation of blanket bogs on relatively flat or gently sloping areas (Van Breemen, 1995).

Meanwhile in the tropics, peat is mostly governed by sea level and monsoon intensity. Coastal peat swamps in the tropics developed as organic matter accumulated on marine clay and mangrove deposits of river deltas and coastal plains during the mid- to late Holocene (5000 years ago). Peat deposits in a bog in Kalimantan, Indonesia, date back to the Late Pleistocene around 26,000 years ago (Page et al., 2004). Accumulation was most rapid in the early Holocene (~11,000–8000 years ago) and continued at a reduced rate until now (Page et al., 2004). These peatlands mostly occupy low altitude coastal and sub-coastal environments but may extend inland for distances of > 150 km along river valleys and across catchments. Conditions that encourage peat accumulation are poor drainage, permanent waterlogging, high rainfall, and substrate acidification. Most of the peatlands of Southeast Asia have a characteristically domed, convex surface. Their water and nutrient supply are derived entirely from rainfall (ombrogenous) and the organic substrate on which plants grow is nutrient-poor (Andriesse, 1988). Reported accumulation rates were 39 to 85 g C $m^{-2} year^{-1}$ in the Peruvian Amazon (Lähteenoja et al., 2009), 1.3 to 529 g C $m^{-2} year^{-1}$ in Indonesia, 6.6 to 38 g C $m^{-2} year^{-1}$ in Brazil (Silva et al., 2013), and 46 to 102 g C m^{-2} year in Panama (Upton et al., 2018).

2.3. Peat domes

Peat swamps or bogs usually accumulate in mounds, also called peat domes, where waterlogged peat accumulates above the level of the surrounding stream system. Peat dome development is described by a conceptual model of water flow, an interplay between the water table and organic matter accumulation (Andriesse, 1988). Peat starts accumulating in an initial depression. In regions between two rivers, the accumulation of peat tends to canalize the main flow of water within the basin. The accumulation continues with vertical and horizontal growth of peat (as a dome) which restricts the inflow of water until it only receives rainfall as a water supply.

Several studies have tried to model peat dome development. Ingram (1982) modelled the limiting shape of a temperate peat dome based on the soil physics principle as a balance between rainfall and groundwater flow. The model states that the steady-state shape of a peat dome is an elliptic function of a ratio between recharge and hydraulic conductivity. The dome shape is mainly due to impeded drainage. Using morphological field data from a pristine peat forest in Brunei Darussalam, Cobb et al. (2017) developed a mathematical model that predicts the shape of a peat dome. The model showed that in areas bound by rivers, dome formation starts at the edges. The interior of the peat dome continues growing at an approximately uniform rate, and the rate of carbon sequestration is proportional to the area of the still-growing dome interior. The model also predicted that once the peatland surface is sufficiently domed, water is shed so rapidly that waterlogging ceases and peat can no longer accumulate. The shape of the dome sets a limit on how much carbon a peat dome can sequester and preserve, and fluctuations in net precipitation on timescales from hours to years can reduce long-term peat accumulation.

While process-based models have been developed and calibrated on a small (field) scale, empirical models still offer the most practicable approaches for mapping peatlands (Fig. 2).

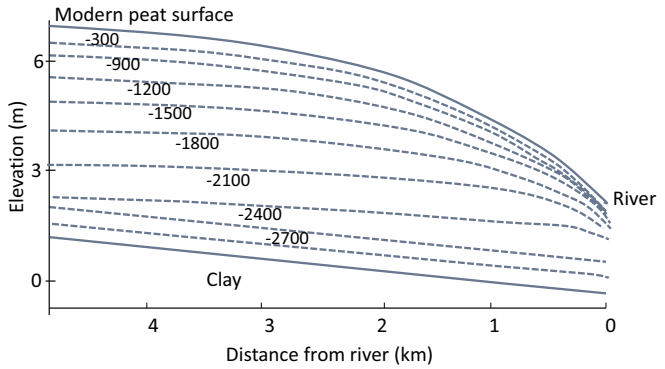

Fig. 2. Modelled morphogenesis of Mendaram peat dome in Brunei Darussalam showing the shape of peat dome over time, including modelled peat surface (number beside contours represent the number of years BP). The deepest peat layers before 2250 years BP represent uniformly deposited mangrove peat on a gently sloping clay plain (based on Cobb et al., 2017).

2.4. Drivers of peat distribution

The factors of peat formation and distribution have been studied at different spatial scales (Limpens et al., 2008). Like soil carbon (Wiesmeier et al., 2019), there is a hierarchical process governing the development of peat (Fig. 3).

At a global scale over a millennial time scale, rainfall distributed continuously during the growing season allows biomass production and inhibits decomposition by maintaining the groundwater table. Cooler temperatures decrease evaporation, extending the available supply of water, and decreasing decomposition. Prolonged periods of drought (< 40 mm rain/month) and warmer months (temperature $> 10\,^{\circ}C$) limit peat development (Lottes and Ziegler, 1994). Charman et al. (2015) reaffirmed that climate is the most important driver of peatland accumulation rates over millennial timescales in the continental USA, but that successional vegetation change is a significant additional influence. At the landscape and regional scale the hydrology, topography and land cover affect C fluxes from the plants to peat, water, and the atmosphere. The presence of certain species of vegetation adapted to waterlogged and nutrient-poor conditions is a useful indicator of peatlands. At a local scale the depth of the water table and vegetation composition are good predictors for peat respiration (Limpens et al., 2008).

The range of environmental factors controlling organic matter accumulation at different spatial scales is summarised in Fig. 3. These factors affect our ability to map peat at various spatial scales (extent and resolution). The spatial scale required for mapping also depends on the required use and application. For example, global reporting would only require coarse-scale information, while local management requires detailed peat thickness and water information. Thus, one way to improve peat mapping is to identify indicators that are useful for quantification peat extent and carbon stock as a function of spatial scales (Wiesmeier et al., 2019). Specific remote and proximal sensors can be used as predictors for peat extent and C stock at a range of scales.

The scale of required peatland mapping influences the choice of mapping technique. As discussed, at the global and continental scale, climate and vegetation appear to be important drivers of peatland distribution (Xing et al., 2015), which can be represented with global climate and vegetation maps. At the landscape scale, topography, vegetation, and hydrogeology are important factors (Buffam et al., 2010), and these factors can be represented via Digital Elevation Models (DEM), optical and radar images. At the local scale, detailed hydrology, biochemistry, and plant-soil interactions can be represented via high-resolution proximal and remote imaging techniques such as Lidar, electrical resistivity survey and detailed vegetation indices (Fig. 3).

3. Accounting for C stock in peat

Accounting for C stored in peatland is essential for inventory and conservation purposes (Law et al., 2015). The amount of C in peat depends on the peat's extent, thickness, and density, and can be calculated in two ways—a deposition model and an accounting model.

Carbon content based on peat deposition rates is calculated as:

$$C_s = \sum_{j}^{t} A_i \times \overline{Cr_i}. \quad (1)$$

where C_s is Carbon stock in unit mass (Mg), A is the area, and $\overline{Cr}$ is the

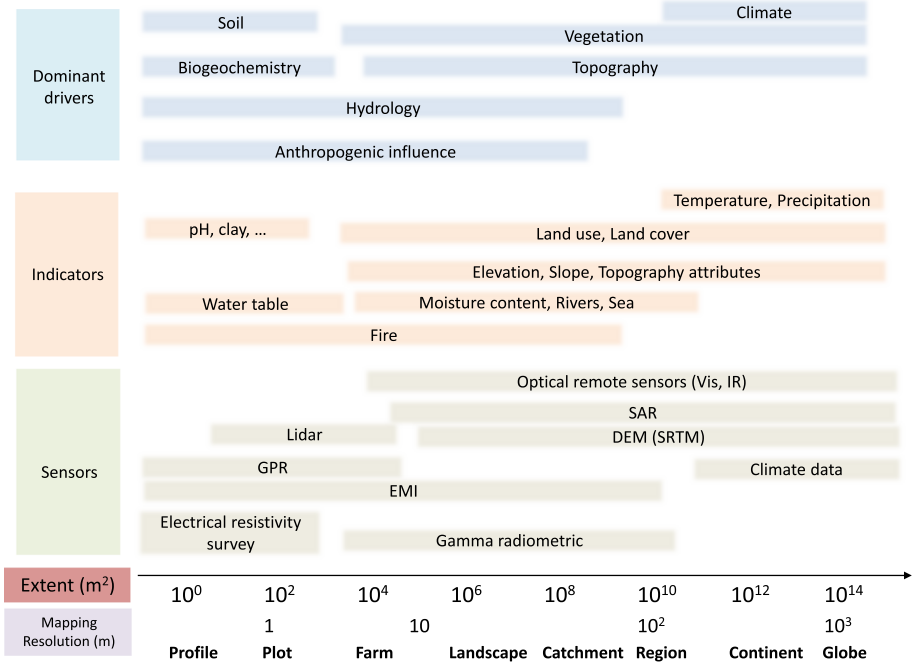

Fig. 3. Drivers of peat formation, indicators of peat occurrence, and sensors that can be used to measure the indicators as a function of spatial scale.

average C accumulation rate (in Mg m^{-2} kyr) for period j and t is the age of the peatland (kyr) (Yu et al., 2010). The average C accumulation rates can be estimated from radiocarbon dating. For example, in Finland there was a monotonic increasing trend in apparent carbon accumulation rates during the Holocene, from ~ 15 g C m^{-2} yr^{-1} in the early Holocene to ~ 45 g C m^{-2} yr^{-1} in the late Holocene. Models that take into account the loss of peat C through decomposition have also been developed (Yu et al., 2010). Such models are useful for large scale estimates where field observations are not available.

Another way of calculating C stock is based on empirical data. First, an average carbon density C_d (in Mg m^{-2}) is calculated for a particular peat type or unit based on n observations:

$$\overline{C_d} = \sum_{i}^{n} \overline{C_{c_i}} \times \overline{\rho_{b_i}} \times \overline{d} \quad (2)$$

where C_c is organic carbon content by mass (g of C/g of dry soil), ρ_b is bulk density (in Mg/m^3), and d is peat thickness (m). Carbon stock is then calculated for m peat type classes or units in the area:

$$C_s = \sum_{i}^{m} \overline{C_{d_i}} \times \overline{A_i} \quad (3)$$

This accounting method is preferred in field to regional scale surveys as it is based on empirical observations.

To use the above formulas and calculate C stock in peat, estimates of peat thickness, bulk density, and C content are required.

3.1. Peat thickness

Peat thickness (or depth to mineral layer) is an important variable that needs to be measured in the field. Changes in water content can cause peat to shrink and swell (Camporese et al., 2006). Parry et al. (2014) reviewed approaches for estimating peat thickness. The easiest method is manual probing or coring. Probing involves pushing an extendable metal pole (~ 1 cm in diameter) into the ground until it hits a resistance or mineral layer, then recording the depth and the geographical position with a global positioning system (GPS). The Russian peat borer, also called the Macaulay corer (Jowsey, 1966) was designed to sample peat materials at depth as well. It has a chamber within the corer which traps samples when the corer is twisted. The main issues with manual coring or probing are that small-scale local variability affect the results, and the volume of measurement is relatively small. Section 7.1 discusses proximal sensors for measuring or inferring peat thickness.

3.2. Bulk density

Peats have a low bulk density (BD) compared to mineral soil, and BD varies considerably within an area. In addition to calculating C stock, BD is a useful indicator or predictor of several physical characteristics including hydraulic conductivity, smouldering combustion vulnerability, and water retention (Thompson and Waddington, 2014). Bulk density has a close relationship with the degree of peat decomposition, with lower values indicating less decomposition. Päivänen (1969) found a value of around 0.09 Mg m^{-3} in undecomposed peats to 0.23 Mg m^{-3} in decomposed peats (Silc and Stanek, 1977). In tropical peatlands, natural peats can have a BD of 0.05 Mg m^{-3} or less, and compacted peat has a density of around 0.15 Mg m^{-3} (Kool et al., 2006).

Bulk density is well-predicted from organic matter content in mineral soils, and pedotransfer functions have been developed to estimate BD from soil organic matter content as measured by the loss on ignition (LoI) method. However, this relationship does not hold for soil with high organic matter content or peats (Adams, 1973).

A study from the blanket peatlands on Dartmoor, England, found that BD decreases with depth while the C content increases with depth (Parry and Charman, 2013). However, in tropical peatlands, BD under forest slightly increases with depth, but in oil palm plantations compaction causes an increase in surface BD (Tonks et al., 2017).

3.3. Carbon content

The best way to measure C content in organic soils and peat is the loss on ignition (LOI) method. A sample is dried, weighed, placed in a furnace set at 550 °C to 'burn off' the organic matter (OM), then weighed again. The mass loss after ignition is attributed to OM. Carbon content is derived from the OM content using the van Bemmelen conversion factor of 0.58. Carbon is assumed to be 58% of OM, however this value is variable. From 20 peat samples in Indonesia, Farmer et al. (2014) found a factor of 0.53 more accurately represented the C content of OM. Meanwhile, Klingenfuß et al. (2014) evaluated this conversion factor for various peatlands in Northern Germany and found that the factor varies between 0.49 and 0.58, mostly influenced by the botanical origin of peat-forming plants. Sphagnum peats have a lower C content (0.49) compared to peats of vascular plants (0.58) and amorphous peats (0.51).

Warren et al. (2012) proposed that for tropical peats with a C content > 40%, C density can be predicted based on BD:

$$C_d = (468.72 \times BD) + 5.82. \quad (4)$$

Farmer et al. (2014) showed that the accuracy of Eq. (4) is reduced with increasing BD density and suggested that Eq. (4) was applicable for BD values between 0.05 and 0.16 g cm^{-3}.

Rudiyanto et al. (2016a) compiled a dataset of 568 observations from tropical peatlands with BD values between 0.01 and 0.57 g cm^{-3}, and C content ranges between 0.11 and 0.62 g g^{-1}. They showed that at C contents above 0.5 g g^{-1}, there is no relationship between C_c and BD. For peat with a BD < 0.25 g cm^{-3}, they found an average value of C_c of 0.549 g g^{-1}, and within these values, C_c values are constant with varying BD values. Thus, C_d can be estimated from an average C content ($\overline{C_c}$ in g g^{-1}), multiplied by BD:

$$C_d = \overline{C_c} \times BD = 0.5491 \pm 0.0218 \times BD \quad (5)$$

The equation above is in contrast with the regression approach of Warren et al. (2012) and Farmer et al. (2014) who fitted a linear regression to the data.

In Canada, Bauer et al. (2006) developed pedotransfer functions for estimating C density of peat based on field-based variables (stratigraphic depth and material type), and laboratory measurements (BD and ash content). They warned that these estimates are only for use in regional surveys.

4. Global and regional estimates of peatland and carbon stock

Global and regional estimates of peatland areas and their C stock vary wildly according to the definition of peat, assumed C density, and thickness (Tables 1 & 2). Most estimates are based on very rough country inventories and reports such as by the FAO (Andriesse, 1988), World Bank (Bord na Mona, 1984), and World-Energy-Council (2013). Indonesia, for example, has estimates ranging from 130,260 to 265,600 km^2 (Table 2). Despite the uncertainty of the values and assessment methodology, these estimates are still being used in scientific reports and decision making.

Global peatland area was estimated between 3.3 and 4.6 million km^2 (Table 1). Most global peat maps (e.g. Yu et al., 2010) are created by compiling regional and national peat maps, and histosols from the Harmonized World Soil Database (HSWD) (Nachtergaele et al., 2009). The HSWD is a global soil map product at a resolution of 30 arc-second (about 1 km × 1 km at the equator) which was combined with regional and national maps as an update to the 1:5 million FAO-UNESCO Soil Map of the World.

Estimates of global C stock in peatland is even more variable,

Table 1
Estimates of global and tropical peatlands area and C stock with calculated C density and average thickness.

Extent	Area (10^6 km^2)	C stock (Pg)	C density (kg m^{-2})	Average peat thickness (m)	Assumed C content (kg m^{-3})	Author
Global	3.9–4.1	329	82.6	1.5	55	(Maltby and Immirzi, 1993)
Global			77.6	1.0	77.6	(Batjes, 1996)
Global	3.8	447	120.8	2.2	55	(Joosten, 2009)
Global	4.0	612 (530–700)	153.0	2.8	55	(Yu et al., 2010)
Global (Histosols)	3.3	113	34.2	1.6	55	(Köchy et al., 2015)
Global	4.013					(Kolka et al., 2016)
Global		543		2		(Jackson et al., 2017)
Global (Histosols)	0.65-1.55					(Hengl et al., 2017)
Global	4.232					(Xu et al., 2017)
Global	4.632	597.8				(Leifeld and Menichetti, 2018)
Tropics	0.41	70.0	168.7	3.1	55.0	(Maltby and Immirzi, 1993)
Tropics	0.44	88.6 (82–92)	200.9	4.0	50.4	(Page et al., 2004)
Tropics	0.40	24.2	60.5	1.2	50.4	(Köchy et al., 2015)
Tropics	1.70	350	205.8	4.1	50.4	(Gumbricht et al., 2017)

between 113 and 612 Pg. The large variation between estimates could be due to the different definitions of peatlands and the assumed C density and peat thickness. The average global C density for histosols (0–100 cm) according to Batjes (1996) is 77.6 (std. dev. 36.5) kg/m^2, which is double the values calculated by Köchy et al. (2015) but half of the number by Yu et al. (2010). Criteria for peat thickness range from 0.3 m in Finland and Ireland, up to 0.6 m in New Zealand (Table 2).

Table 2 shows some estimates of peat areas (km^2) for selected counties and regions which are reviewed in this paper. The global studies gave variable estimates of peat area, and many studies used estimates from Andriesse (1988) which was based on Bord na Mona (1984), an initiative on using peat as fuel (Clarke, 2010). The numbers quoted from global studies are full of uncertainties. According to Andriesse (1988), this is due to several factors:

- Numbers are copied from the literature and accepted without checking the accuracy of the data.
- Estimates are based on the coarse scale FAO-UNESCO World Soil Map.
- Peatlands have variable definitions and classifications in different countries.

It is discouraging to find that after 30 years, we still do not have better estimates of global peat information. While countries in Europe have come together for a compiled European peatland map (Tanneberger et al., 2017), information from other parts of the world remains sketchy. Additionally, rapid land use change such as clearing for agriculture means existing maps are quickly outdated. A more accurate estimate of global peatlands, as well as the ability to rapidly update maps, is essential to address climate change concerns.

Table 2. Estimates of peat areas (km^2) for selected counties based on international publications and country estimate.

5. National peatland mapping: 12 case studies

Mapping peat presents different challenges in different countries. Varying definitions and peat types, difficult access, and the quality of legacy data mean that no one mapping technique will suit all nations. The time and monetary cost of traditional soil surveys are too prohibitive for mapping on a national scale, while inconsistencies between mappers can present challenges. In response, some institutions are turning to digital soil mapping (DSM) to refine existing maps and generate new ones. Conventional soil maps still contain valuable soil data that can be extracted and used to update existing maps, while remote sensors can estimate several soil properties at once (see section 7). These reduce the need for expensive, on-the-ground, soil assessments.

This section describes peat mapping attempts by 12 countries, including challenges to mapping in that country. The case studies start with countries using conventional mapping approaches and work up to nations that use digital soil mapping techniques.

5.1. Brazil

In the Brazilian Soil Classification System (SiBCS), peat soils are considered Organossolos—poorly evolved soils consisting of organic material of black, very dark grey or brown colour. The exact area of Organossolos in Brazil is debatable. In the 1: 5000,000 map *Solos do Brasil* approximately 2200 km^2 of *Organossolos Háplicos Hêmicos* were identified, corresponding to 0.03% of the country. However, the Organossolos are also mapped in association with Podzols, Gleysols, Fluvisols and Arenosols (Dos Santos et al., 2011), and the value may be inflated. Using legacy data from 129 profiles of high OC content, Valladares (2003) estimated peats covered 6100 km^2 corresponding to around 0.07% of the Brazilian land area. The study by Pereira et al. (2005) estimated of 10,000 km^2 of Organossolos, or just over 0.1%. Considering that Brazil has > 12,200 km^2 of mangroves, distributed across > 7000 km of its coastline where the presence of organic soils is likely, the exact area of Organossolos is still uncertain.

Organossolos are difficult to quantify accurately as they occur as inclusions in complex areas of hydromorphic soils and mangroves, which are often difficult to discriminate. In addition, Pereira et al. (2005) also pointed out that—for the entire country—only coarse-scale soil maps are available which cannot accurately represent Organossolos. Further complications arise considering that soils with a high OC content can be found throughout Brazil (Fig. 4) (Beutler et al., 2017). Based on the legacy data examined by Valladares (2003), Organossolos can be found from sea level (0 m) in poorly drained environments, up to 2000 m in low temperature and cool climate environments (mountainous regions). Most occur between < 10 m and 800–1600 m.

Table 2
Estimates of peat areas (km^2) for selected counties based on international publications and country estimate.

Country/ Region	Peat areas (Bord na Mona, 1984) (km^2)	Peat areas (Joosten, 2009) (km^2)	Peat areas (World-Energy-Council, 2013) (km^2)	Peat areas (Gumbricht et al., 2017) (km^2)	In-country estimate of peat areas (km^2)	Criteria of peat thickness as organic soil (m)	National peat definition
Finland	104,000	79,429	89,000	–	66,214	0.3	Histosols (USDA Soil Taxonomy)
Sweden	70,000	65,623	66,000	–	61,186	0.4	
Canada	1,500,000	1,133,926	1,113,280	–	1,136,000	0.4	Organic soil with > 17% organic carbon content accumulations (Soil Classification Working Group, 1998) over 40 cm in thickness (National Wetlands Working Group, 1997).
Scotland	–	–	–	–	17,263	0.5	Peat soil has a minimum of 60% organic matter in the surface horizon, and > 50 cm thick (Soil Survey of Scotland, 1984).
Netherlands	2800	3450	–	–	4029	0.4	The Dutch soil classification system (De Bakker and Schelling, 1989) distinguishes two types of organic soils: peat soils (peat layer > 40 cm thick and starting within 40 cm from the surface) and peaty soils (peat layer 10–40 cm thick and starting within 0.4 m from the surface). The peat soils are further subdivided into thin (peat layer 40–120 cm thick) and thick (peat layer > 120 cm thick) peat soils.
USA	569,400	223,809	625,001	–	234,006	0.4	Histosols, soils with a surface organic layer > 40 cm thick. Permafrost-affected organic soils are classified as the Histels suborder in the Gelisols order (Kolka et al., 2016).
Ireland	11,800	11,090	11,800	–	14,475	0.3 on drained 0.45 on undrained	Organic soil materials which have sedentarily accumulated and have at least 30% (dry mass) organic matter over a depth of at least 45 cm on undrained land and 30 cm deep on drained (Hammond, 1979).
Indonesia	170,000	265,500	206,950	225,420	130,260	0.5	Organosol, soils with organic layer > 50 cm, and organic C content > 12% (Subardja et al., 2016)
Australia	1330 (Queensland)	10,828	1350	–	11,900	0.4	Organosols, soils that are not regularly inundated by saline water and either have > 0.4 m of organic materials within the upper 0.8 m or have organic materials to a minimum depth of 0.1 m if directly overlying rock or other hard layers (Isbell 1996).
Tasmania	–	9910	–	–	9610	0.4	As above.
New Zealand	15,000	1961	3610	–	2505	0.3, 0.4	Soils that have horizons that consist of organic soil material that within 60 cm of the soil surface are either —30 cm or more thick and are entirely formed from peat or other organic soil materials that have accumulated under wet conditions (O horizons), or —40 cm or more thick and are formed from partly decomposed or well decomposed litter (F and H horizons) (Hewitt, 2010).
Chile	10,470	10,996	10,472		32,605	0.4	Histosols of USDA Soil Taxonomy
Brazil	15,000	54,730	23,875	312,250	2200	0.4	Organossolos, poorly evolved soils made up of organic material of black, very dark grey or brown colour (Embrapa Solos, 2013).

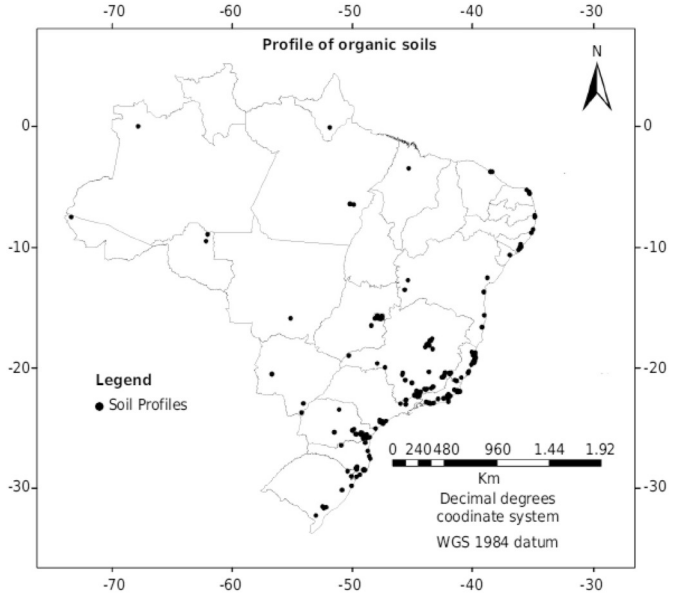

Fig. 4. Distribution within Brazil of soils with high content of organic C (Beutler et al., 2017, Creative Commons License).

5.2. Chile

The exact extent and location of peatland in Chile is uncertain. The latest data from the National Forest Corporation (CONAF) traditional mapping approach reported a total area of 32,605 km^2, around 4.31% of the country. In Chile, peatlands are found in two main areas. In the north of the country, "bofedales", the high altitude peatland of the Andes can be found with an area about 308.5 km^2 (Fig. 5). These are unique ecosystems which survive despite the arid to hyper-arid conditions of the area (Squeo et al., 2006). They are usually dominated by *Juncaceae* and *Bofedales* (Villagrán and Castro, 1997) and have historically been used for grazing by wild and domestic animals. They usually have a higher rate of C accumulation than boreal peatlands and the biggest threat to them is climate change and decreasing rainfall. Llanos et al. (2017) estimated accumulation rates in areas of Peru with similar conditions to the Chilean bofedales, ranging between 10 and 350 g C m^{-2} y^{-1}.

The largest group of peatlands are in the south of the country, starting at around 39.5° S and extending to Chilean Patagonia. The southern peatlands are dominated by Sphagnum, accumulating, on average, 16 g C m^{-2} y^{-1} (McCulloch and Davies, 2001). Peatlands with sphagnum vegetation can be identified using optical and radar images (Fig. 6). Due to its relative isolation, Patagonian peatlands are usually under low human pressure, but peatlands closer to populated areas are starting to be harvested. Human activity such as roads or mega-projects like hydroelectric power plants also threatens these vulnerable ecosystems (Rodrigo and Orrego, 2007).

In Chile, peatlands are currently recognised as a non-metallic resource in the Mining Code, giving priority to extraction over conservation. Like most of the national legislation related to natural resources, this code was issued during a 17-year-long dictatorship and needs a complete re-evaluation.

5.3. Indonesia

Peat maps of Indonesia can be divided into two groups: national and local scales. At a national scale (1:250, 000) there are several versions of the peat extent and thickness map. The first one is in a vector format made by an NGO, Wetlands International, in 2004 (WI map, Fig. 7) (Wahyunto et al., 2006; Wahyunto and Subagjo, 2003; Wahyunto and Subagjo, 2004). The WI map was digitized manually based on legacy source data from the Land Resource Evaluation and Planning Project (1985–1990), the Bogor Agriculture and Land Research Center, Land System Maps from the Regional Planning Program for Transmigration, RePPProT (1985–1989). These maps were derived from manual delineateion based on Landsat satellite imageries of 1990 and 2002.

Subsequently, the WI map was updated by the Ministry of Agriculture in 2011 and again in 2018 (MoA map) (BBSDLP, 2011; BBSDLP, 2018). The Ministry of Environment and Forestry also published its version in 2011–2013 (MoEF map). The MoA map was derived from the WI map with additional peatland data and soil maps of Indonesia delineated with the help of SPOT5 images. Although both the WI and MoA maps may underestimate peatland extent and thickness (Hooijer and Vernimmen, 2013) and have a relatively coarse scale (1: 250,000), these maps are still useful as an indication of peat extent (Warren et al., 2017). Recently, the MoA map became the official government map of peatlands in Indonesia.

Before the 1990s, peatlands were considered marginal lands and exploited without environmental concerns. In 1995, the Mega Rice Project attempted to develop 1 million ha of peatlands in Central Kalimantan for rice cultivation (Indonesian Presidential Decree No. 82/ 1995). The project failed miserably. Rice did not grow, and the heavily drained peats were degraded, fuelling fires during extended dry seasons. Rapid deforestation, excessive peatland drainage, and intensive fire have increased carbon gas emissions to the atmosphere via the loss of biomass (Margono et al., 2014b), peat oxidation (Itoh et al., 2017), and combustion (Page et al., 2002). With increasing awareness of climate change issues – particularly greenhouse gas emissions from agricultural sectors and land and forest fires – peat management has become a controversial issue in Indonesia. The Indonesian government attempted to restore degraded peatlands by issuing Government Regulation (PP) No. 71 Year 2014 and No. 57 Year 2016, on the conservation and management of peat ecosystems. Peatland with a thickness > 3 m must be conserved. In 2016, the Indonesian government also established the peatland restoration agency (Badan Restorasi Gambut, BRG) to coordinate and facilitate peat restoration. One essential factor in peatland restoration is the availability of a high-resolution peat map.

For effective spatial planning and policy making, a local peat map with a resolution of 1:50,000 or spatial resolution of 30 m or finer is required. Many studies discriminate between peatlands based on satellite imageries (visible and infrared bands) (Wijedasa et al., 2012; Yoshino et al., 2010), and radar images (Hoekman et al., 2010; Novresiandi and Nagasawa, 2017). Others tried to map thickness solely based on elevation (Jaenicke et al., 2008). Only a few studies have used digital mapping techniques to map peat thickness (for example, Illés et al., 2019).

Rudiyanto et al. (2016b) and Rudiyanto et al. (2018) proposed an open digital mapping methodology as a cost-effective way to map peat thickness and estimate C stock in Indonesian peatlands. The method uses open data in an open-source computing environment. The digital mapping methodology predicts field observations with a range of factors that are known to influence peat thickness distribution such as DEM from the Shuttle Radar Photography Mission (SRTM), geographical information, and radar images using machine-learning models. This method also provides the uncertainty of the estimates according to error propagation rules. This approach has been used to map 50,000 ha of peatlands in the eastern part of Bengkalis Island in Riau Province. Results showed that the digital mapping method can accurately predict the thickness of peat, explaining up to 98% of the variation of the data with a median relative error of 5% or an average error of 0.3 m. The procedure also incorporates uncertainty of estimates of peat thickness and C density for estimating C stock. The estimate of the cost and time required for map production is two to four months with a cost between $0.3 to $0.5 per ha. This DSM method can be upscaled to map peatlands for the whole of Indonesia.

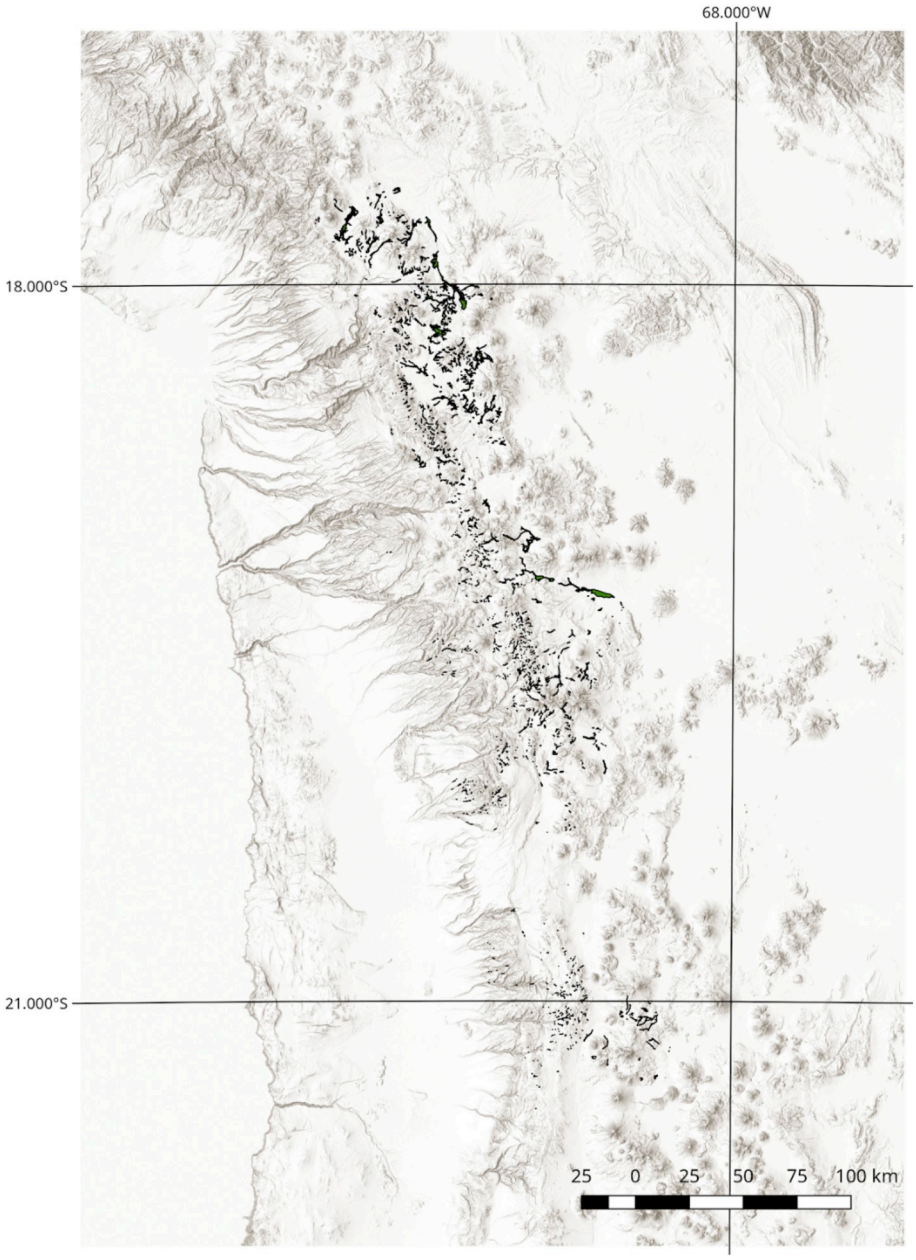

Fig. 5. Location of bofedales (data from CONAF).

5.4. New Zealand

National-scale soil maps have been published at a 1:50,000 scale as part of the New Zealand Land Resource Inventory (NZLRI, Lynn et al., 2009), and distributed as part of the Fundamental Soil Layers (FSL, Landcare-Research, 2000). The NZLRI polygons boundaries were drawn manually based on stereoscopic analysis of aerial photographs along with field verification. The dominant soil type was assigned to each polygon. The FSL dataset pre-date the newer S-Map project (Lilburne et al., 2012), which at the time of writing (late 2018) covers about 30% of the country. National peat maps have been derived from the FSL dataset by selecting the soil polygons mapped as organic under the NZSC. The resulting map (Fig. 8) was improved by adding an undisturbed peatland map that was mapped using expert interpretation of aerial imagery used by Ausseil et al. (2015).

5.5. Ireland

Peatlands in Ireland are heterogeneous and complex (Fig. 9). They include everything from intact fully functioning bogs to drained agricultural pastures, and this presents mapping challenges. Hammond (1979) produced a map of Irish peatlands, combining fieldwork and older data including the 1921 Geological Survey map (Anonymous, 1921). Hammond (1979) calculated that peatlands comprised 17.2% of the national land area. Connolly et al. (2007) produced the Derived Irish Peat Map (DIPM), a probability map of peatland extent, by combining several maps (CORINE 1990 (O'Sullivan, 1992)) and The General Soil Map of Ireland (Gardiner and Radford, 1980) within a GIS and calculating the probably of peatlands occurring at a location. The DIPM calculated peatland extent to be 13.8%. In 2009, Connolly and Holden produced an updated version of this map (Fig. 9) based on newly

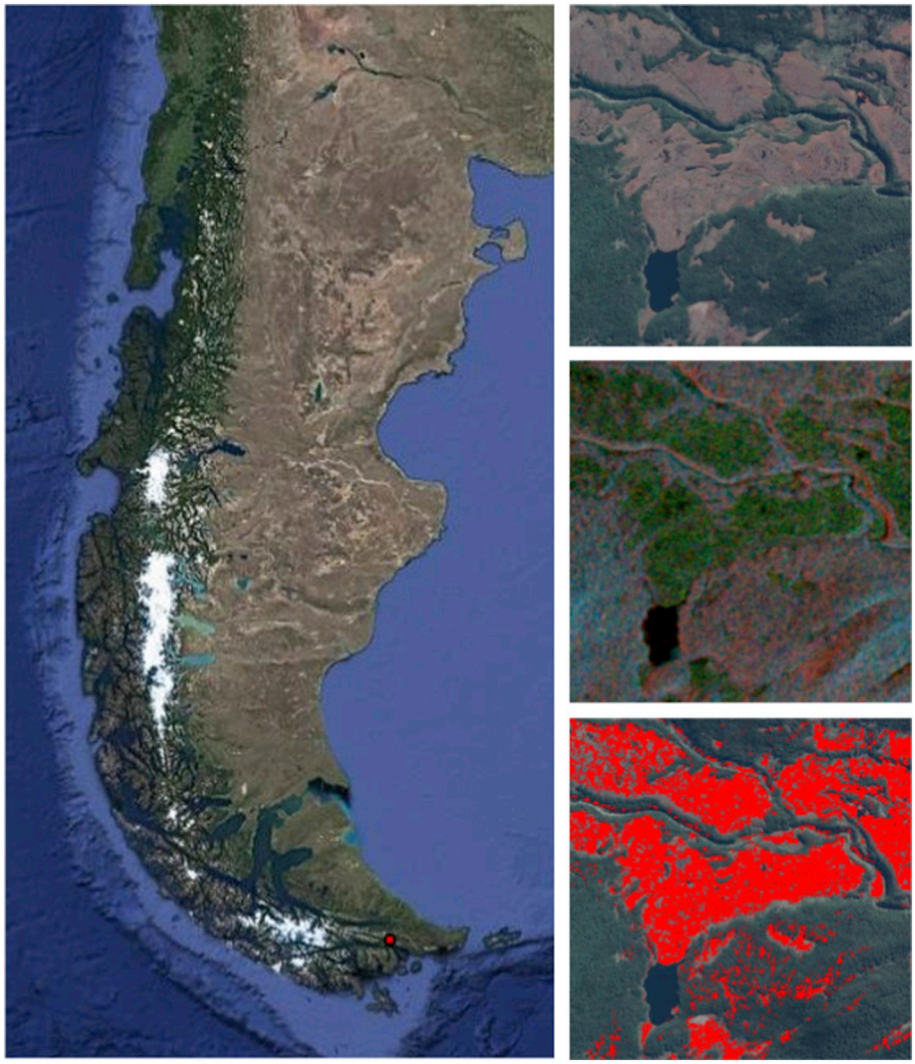

Fig. 6. The identification of peat extent in an area in Patagonia (red dots in the left figure). The green areas correspond to Sphagnum peatland which can be recognised via Sentinel 1 composite of different polarisations angles. Bottom right is a classification of peatland based on Sentinel 1 and 2 data.
(For interpretation of the references to colour in this figure legend, the reader is referred to the web version of this article.)

released spatial data including CORINE 2000 and the Indicative Soil Map of Ireland (Reamonn Fealy, personal communication by email). The extent of peatland in the DIPM version 2 was 20.6%, however, many identified small area peatlands (< 7 ha) were excluded. Their inclusion would increase the peatland extent to 25% of the national land area. The recent publication of digital soil maps in the Irish Soils Information System (Creamer et al., 2014) does not add any clarity as Hammond's peatland map was used to represent peatlands in this new national soil map.

Uncertainty around the full spatial extent of peatlands and their condition may have implications for the governmental strategy for using wetlands as a part of the GHG mitigation strategy under the Paris Agreement (National Mitigation Plan, 2017; National Peatland Strategy, 2015). Significant challenges remain to map the extent and condition of Irish peatlands. These challenges relate to climate change mitigation, ecosystem service provision and natural capital. In particular, the lack of extensive information on the impact of degradation on DOC losses may also present issues in terms of net ecosystem C balance, though much more work is needed on this issue.

5.6. USA, with an example from Minnesota

Based on the SSURGO (Soil Survey Geographic database, map scale between 1:12,000 to 1:63,360), Histosols in the USA are estimated at 100,794 km^2 or 1.28% of the country. Including Alaska, Puerto Rico, and Hawaii (according to STASGO2, a general soil map of USA at 1:250,000), histosols account for 152,837 km^2 or 1.64% of the land area. The total peatland in the USA, including 88,994 km^2 of histels in Alaska, is around 242,000 km^2 or 2.6% of the land area (Fig. 10).

The state of Minnesota has approximately 2.5 million hectares of peatlands, most of which occurs in the northern part of the state. St. Louis County lies in the northeast part of the state and has several large peatlands, as well as hundreds of smaller ones. Mapping the peatlands took place mainly between 1992 and 2010, as part of the National Cooperative Soil Survey. Most of the peatlands in Minnesota are one of two topographical types and they both occur in St. Louis County. The first is small and confined to depressions—usually ice-block depressions—in the landscape. These peats are formed by when sediment accumulates in the depressions, aquatic plants grow, and organic matter accumulates. Soil types would be mostly classified as Hemists and Saprists.

The other type of peat occurs on flat or nearly level landscapes. In both Minnesota and St. Louis County, the predominant landscapes with extensive larger peatlands of this type are glacial lake plains. These peatlands blanket the landscape, formed from surplus moisture and slowly permeable underlying soil materials. Soil types here are mostly Hemists and Fibrists.

The challenges in mapping were to consistently identify soil types

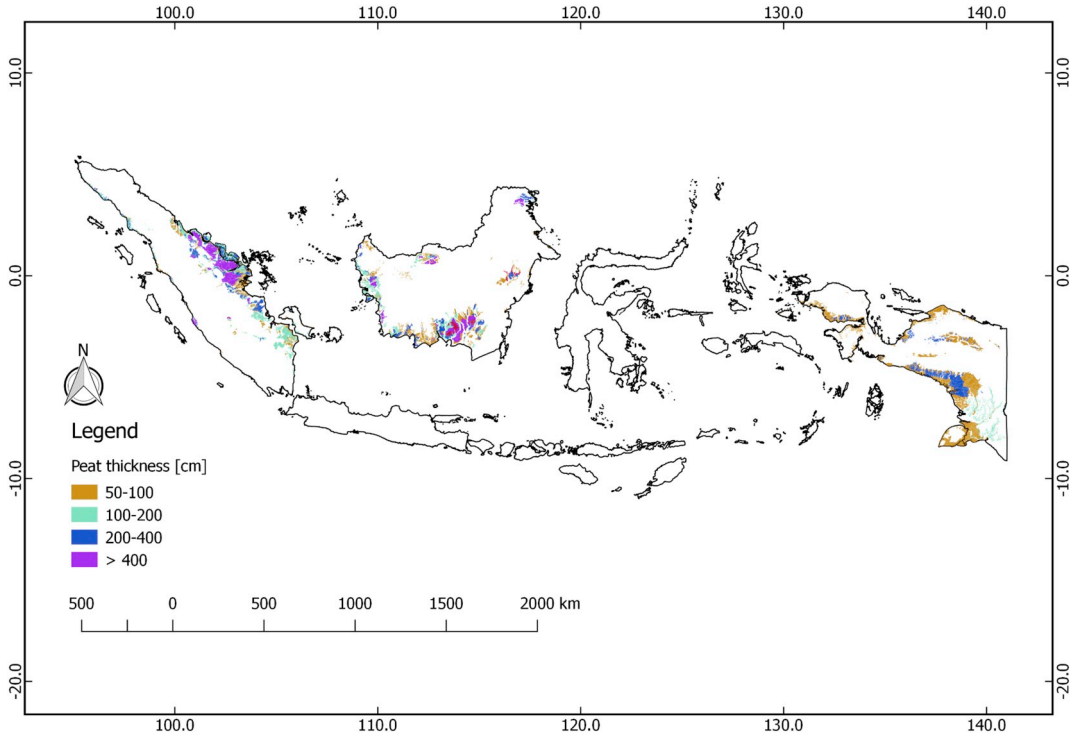

Fig. 7. The peat extent and thickness map of Indonesia from the Wetland International 2004 1:250,000 map.

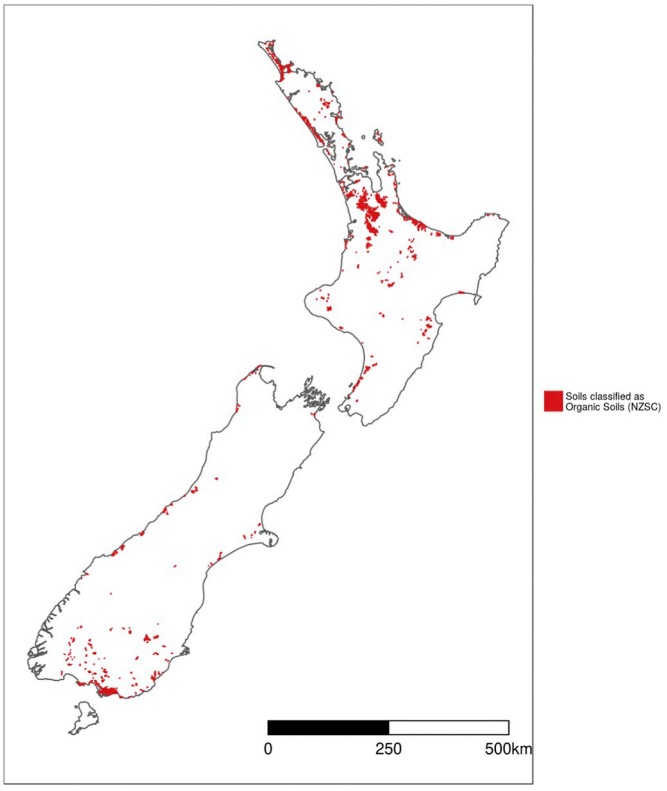

Fig. 8. Distribution of peatlands in New Zealand.

and correlate them to ecological sites. Early in the project it became clear that using estimates of unrubbed and rubbed fibre content to classify materials resulted in inconsistencies between mappers. Researchers adopted the Von Post method of identifying the degree of decomposition to more accurately identify and separate saprists, hemists, and fibrists.

Researchers identified a relationship between hydrology, soil type and vegetation. Peatlands found in smaller closed depressions tend to receive moisture and nutrients from surrounding uplands. Those that were wetter generally supported deciduous shrubs or grass/sedge vegetation and were more decomposed than saprists. Dryer areas supported more mixed vegetative cover with some trees and ericaceous shrubs. These were mapped as hemists. In many cases, the larger peatlands supported a complex vegetative pattern. These complexities may stem from underlying subtleties in the landscape that affect the hydrology, subsequent chemistry, and degree of decomposition. Areas near the centre of the landscape are mainly raised bogs that receive their moisture from rainfall and support sphagnum moss, ericaceous shrubs, and black spruce. They have a convex cross-section and are the driest part of the peatlands. These areas were mapped as fibrists. Areas around the margins of the raised bogs were mapped as hemists. These areas were wetter and generally have few stunted trees and sphagnum mosses. Water tracks that had a flat or concave cross-section and channel water through these peatlands also occur between raised bogs and were also mapped as hemists. After this model was developed, these individual areas within the larger peatlands were separated mainly using air photo interpretation.

Predictive models for mapping peat thickness has been tested by Buffam et al. (2010) for a smaller area in northern Wisconsin. They found that mean peat thickness for small peat basins could be predicted from basin edge slope at the peatland/upland interface calculated from a DEM.

5.7. Australia

Literature regarding the extent and nature of peatlands in Australia are well summarised in Pemberton (2005), Whinam and Hope (2005), and Grover (2006). Outside Tasmania, peatlands in Australia are not extensive as the climate does not favour their formation (Cambell, 1983). Because of their small extent, peats often do not appear on soil maps and there is no accurate estimate of their extent in Australia (McKenzie et al., 2004). An estimate of the area of organic soils in mainland Australia (excluding Tasmania) based on the Atlas of

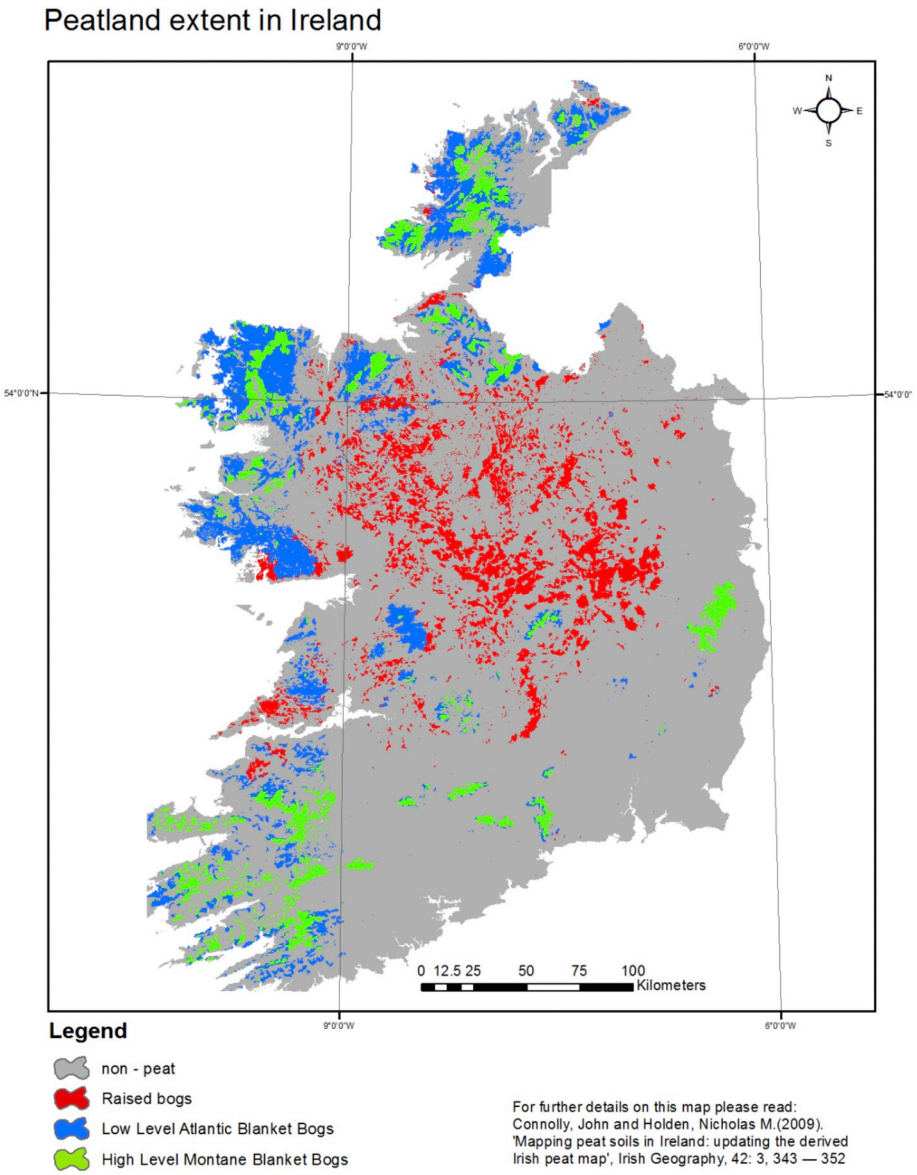

Fig. 9. The extent of peatland in Ireland.

Australian Soils which is at a coarse scale of 1:2000,000 (Northcote et al., 1960–68) is around 2300 km^2.

There has been limited detailed mapping of peat formation in Tasmania. Field data is scarce due to the access constraints in the inhospitable south-west wilderness environments. Pemberton (1989) undertook considerable fieldwork throughout the south-west region while mapping the Land System of Tasmania, producing 1:250,000 nominal-scaled conceptual land system component maps based on grouped similarities of rainfall, elevation, vegetation, topography and soils. These maps were later updated to include soil order estimates of each land system component (Cotching et al., 2009) (Fig. 11A). The approximate total area of peatland in Tasmania is 9600 km^2. However, it must be stressed that many of these components are conceptual, rather than field mapped, at a scale of 1:250,000.

More recently, a DSM approach (McBratney et al., 2003) was applied by the Department of Primary Industries Parks Water and Environment (DPIPWE) in Tasmania as regional contributions to the Soil and Landscape Grid of Australia (Grundy et al., 2015). Part of this was to map soil organic carbon (SOC) content at 80 m resolution across the whole state for standard GlobaSoilMap (Arrouays et al., 2014) depths (Kidd et al., 2015). Using these DSM surfaces, a depth-weighted mean of each layer was used to generate an estimated SOC content map across the state for 0 to 30 cm. This was then split into areas of SOC $<$ 18% as being non-peat soils, and SOC $>$ 18% being considered peat soils (Isbell, 2002). Fig. 11B shows the predicted extent of peat soils (SOC $>$ 18%) using the Tasmanian depth-weighted DSM.

While generally showing similar spatial patterns to the land systems derived in Fig. 11A estimates (south-west peat predominance), the DSM products show more spatial detail and are better aligned with terrain. Average annual rainfall and terrain-based derivatives were found to be the most important predictors of SOC in Tasmania (high rainfall and lower slopes) (Kidd et al., 2015). The DSM peat-estimate (0 to 30 cm, SOC% $>$ 18) corresponds to a total area of 11,478 km^2. However, this mapping appears to be missing areas of coastal peat soils (many classified as Podzols) around the far north-west, north-east, Flinders and King Islands, and was produced using limited site data in the south-west. This map should also be considered as a regional estimate of peat extent, due to the sparsity of calibration data used.

5.8. Scotland

A recent work by Poggio et al. (2019) explored the use of legacy soil

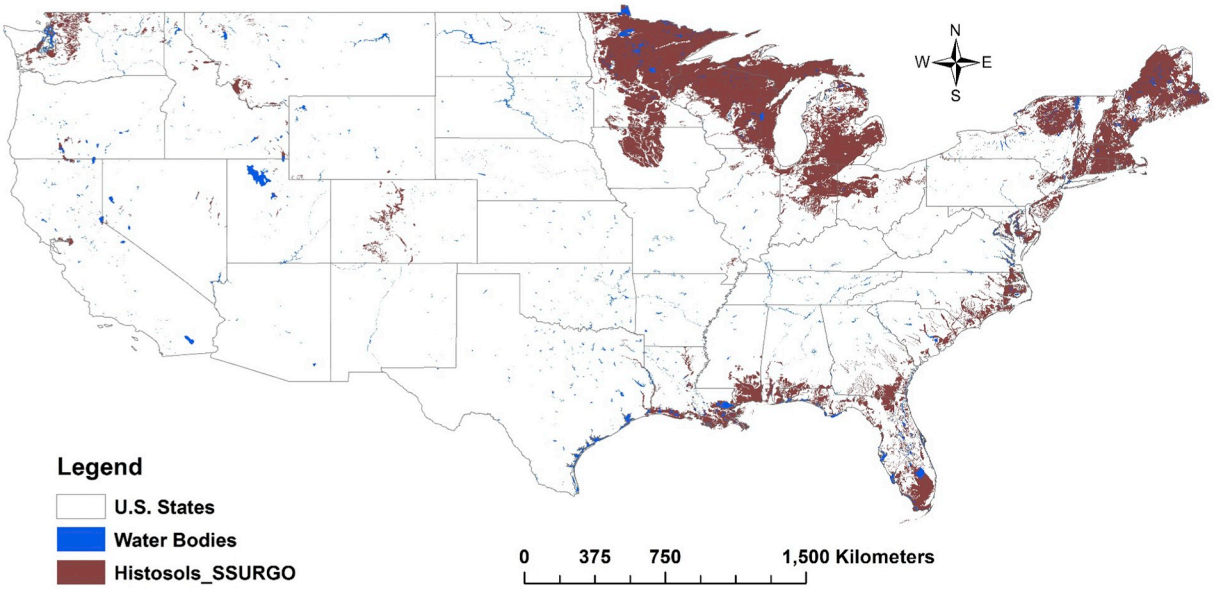

Fig. 10. Histosols in the conterminous USA based on SSURGO.

data for mapping the extent of peatlands in Scotland using the DSM approach. The primary sources of data are the Soil Survey of Scotland (MLURI, 1984) that developed the classification and soil mapping system for the 1:250,000 soil map of Scotland, and a number of studies on mapping of habitats and vegetation, some of which is typically associated with peatlands (Joint Nature Conservation Committee, 2011; MLURI, 1993; Morton Rowland et al., 2011).

The Scottish Soils Database contains information and data on soils from locations throughout Scotland. It contains the National Soil Inventory of Scotland (NSIS) profiles described on a regular 5 km grid of locations (Lilly et al., 2010) and data from a large number of soil profiles taken to characterize the soil mapping units. The total number of soil profiles is about 7000. The profiles were classified according to a Scottish classification (MLURI, 1984), and for mapping purposes, they were re-classified in three classes (Bruneau and Johnson, 2014):

- Mineral soils: soils without a thick organic horizon.
- Organo-mineral soils: soils with a thick organic horizon but not peat (e.g., peaty podzol, peaty gley).
- Peats: organic soils deeper than 50 cm.

The study used covariates that are freely and globally available, described peat distribution directly or indirectly, and scorpan factors topography, vegetation, climate, and geographical position.

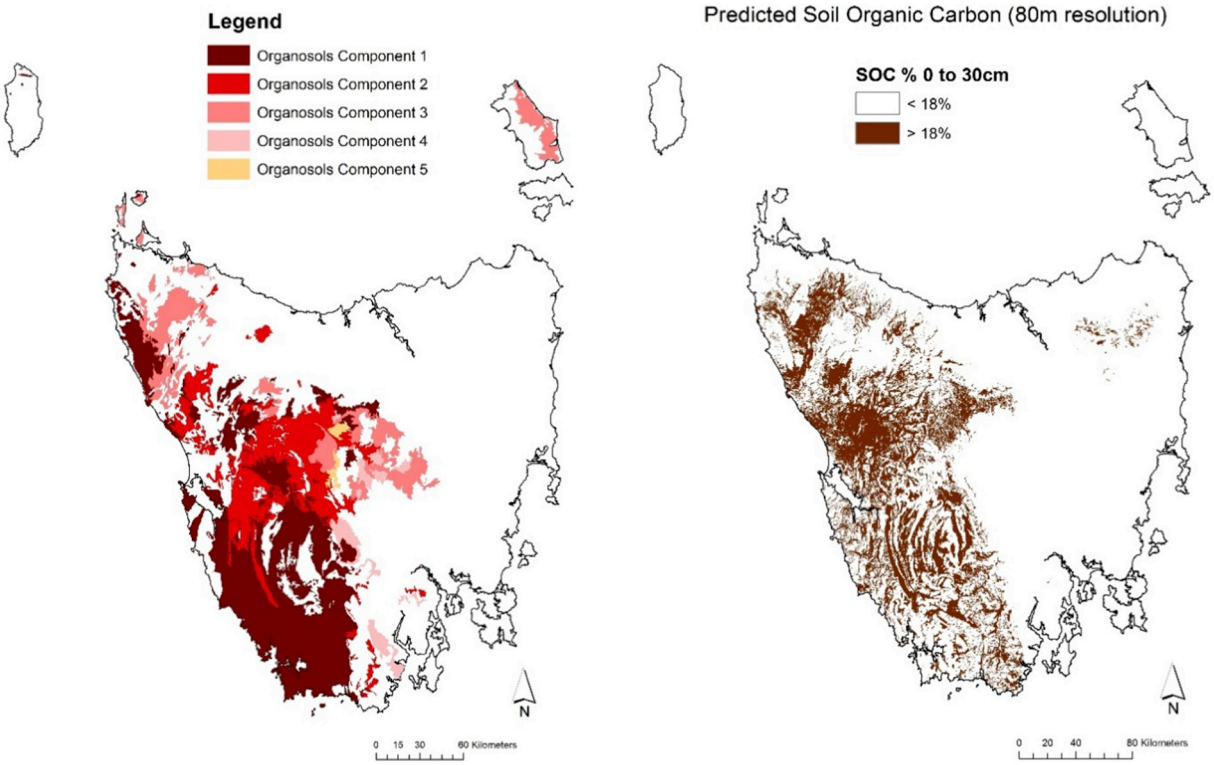

Fig. 11. (A) Dominant organosols soil units in Tasmania from the 1:250,000 land system map. (B) DSM predicted organic soils with SOC > 18%.

The Sentinel-1 (S1) mission provides data from a dual-polarization C-band Synthetic Aperture Radar (SAR) instrument. This includes the S1 Ground Range Detected (GRD) scenes, processed using the Sentinel-1 Toolbox to generate a calibrated, ortho-corrected product. Each scene was pre-processed with Sentinel-1 Toolbox using the following steps: thermal noise removal, radiometric calibration, and terrain correction using the SRTM 30. The final corrected images were converted to decibels via the log scaling = 10 x $\log_{10}$(value) and quantized to 16-bits. The data were pre-processed, prepared, mosaicked and downloaded from Google Earth Engine (Gorelick et al., 2017). The VV and VH polarization for the images available in 2016 were used to calculate seasonal median values (i.e., spring, summer, autumn, and winter) of the ratio of the two polarisations.

Sentinel-2 (S2) is a wide-swath, high-resolution, multi-spectral imaging mission. It supports Copernicus Land Monitoring studies including the monitoring of vegetation, soil and water cover, as well as observation of inland waterways and coastal areas. Each band represents Top of Atmosphere (TOA) reflectance scaled by 10,000. The data were mosaicked and downloaded from Google Earth Engine (Gorelick et al., 2017).

The SRTM DEM with no-data voids (Jarvis et al., 2006) was used to derive terrain attributes. All covariates were resampled to 100 m × 100 m resolution using the median of each grid cell.

An extension of the scorpan-kriging approach, i.e., hybrid geostatistical Generalized Additive Models (GAM; (Wood, 2006)), combining GAM with kriging (Poggio and Gimona, 2014) was used in the modelling. The modelling steps were: 1) fitting a GAM to estimate the trend of the variable, using a spatial smoother with covariates; and 2) kriging GAM residuals as a spatial component to account for local details.

The model showed a good overall accuracy of 72% with a Kappa coefficient of 0.58 for predicting the three soil classes. The validation statistics showed an accuracy for peat of 59%. The organo-mineral soils are difficult to separate from peat and have an accuracy of 50%. This mix-up is probably due to the vegetation similarity between the shallower peats and the organo-mineral soils.

The most important covariates in the model were the topographic features and the information derived from Sentinel 1 in the vegetative season. Sentinel 2 provided useful information despite the limited temporal availability.

Fig. 12 shows the probability of each pixel to be considered as peat. The highest values can be found on the island of Lewis, on the west coast and the mountainous areas. This result is in agreement with the patterns identified with traditional soil mapping (MLURI, 1984). The total area of peatland in Scotland found in this study is about 30% of the total area of Scotland, with differences and variability due to model and covariates used.

The use of radar data is very important in cloudy regions such as Scotland. Digital soil mapping allows the integration of recent remote sensing data into the modelling, and it allows the production and communication of a measure of uncertainty for the output maps.

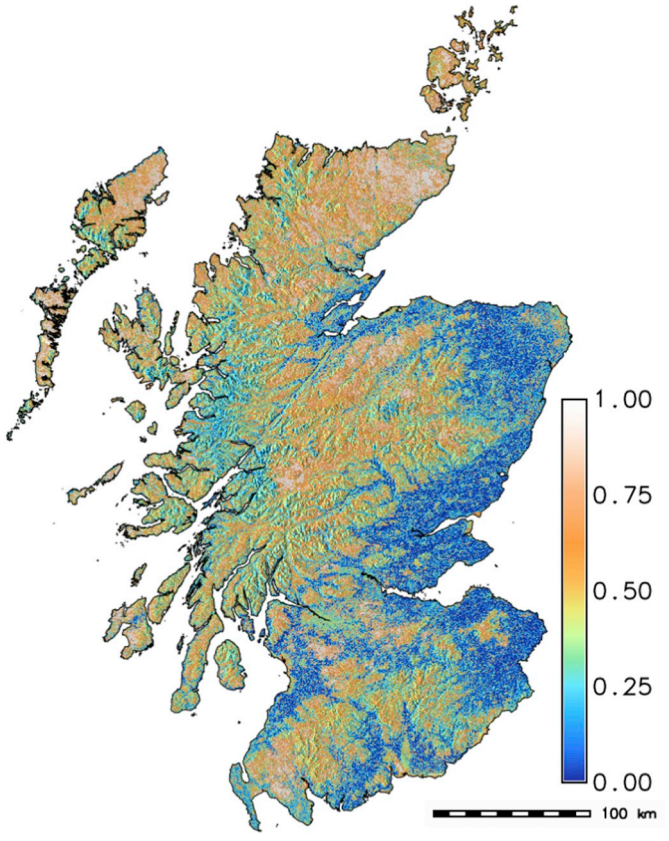

Fig. 12. A probability map of peat soils in Scotland based on digital soil mapping approach.

5.9. The Netherlands

The Dutch National Soil Map at scale 1:50,000 was finalized in the early 1990s, after more than three decades of surveying. Approximately 15 years after the map was completed it became evident that the map was becoming outdated, especially for areas with organic soils. Large areas of organic soils are drained and under intensive agricultural use that causes oxidation and compaction of peat.

A reconnaissance survey of peat soils in the eastern part of the Netherlands showed that the area of peat soils had reduced by about 50% (De Vries et al., 2009). Since the 1:50,000 soil map is the most important source of soil information in the Netherlands, the Dutch government commissioned an extensive updating programme in 2008. Approximately 400,000 ha of peatland were marked to be surveyed, targeting thin peat soils, and thick peat soils in the north of the country.

Though the programme started with conventional soil mapping, after two years it became evident that completing the update with conventional mapping was not feasible. Instead, DSM would be used. A first experiment to update the 1:50,000 soil map with DSM was published in 2009 (Kempen et al., 2009), though the focus was not on solely on organic soils. The authors used a multinomial logistic regression model. A few years later, this method was extended to account for spatial autocorrelation for an area with organic soils in the province of Drenthe (Kempen et al., 2012a). The authors showed that DSM could produce soil class maps that were as accurate as maps produced with conventional mapping but at a fraction of the cost (Kempen et al., 2012b).

Building on this research, in 2012, a method was developed to operationalize DSM to update the 1:50,000 map for the peatlands. Instead of mapping soil classes directly, this method mapped soil classes from two quantitative diagnostic soil properties: the thickness and starting depth of the peat layer. From these two properties, five major soil groups were constructed. The method implemented a two-step simulation approach because the sampling data were zero-inflated. In the first step, peat presence/absence indicators were simulated from probabilities of peat occurrence that were predicted with a generalized linear model. In the second step, conditional peat thickness values were simulated from kriging with external drift predictions. The indicator and peat thickness simulations were combined to obtain simulations of the unconditional peat thickness. A similar approach was followed for the starting depth. From the simulated soil properties, probability distributions of soil groups were derived, thus taking uncertainty fully into account. These groups were further refined with information on static soil properties derived from the 1:50,000 map to obtain soil classes according to the 1:50,000 legend. The prediction models used a set of newly acquired point data and legacy point data that were updated for peat thickness before being used. The uncertainty associated with the

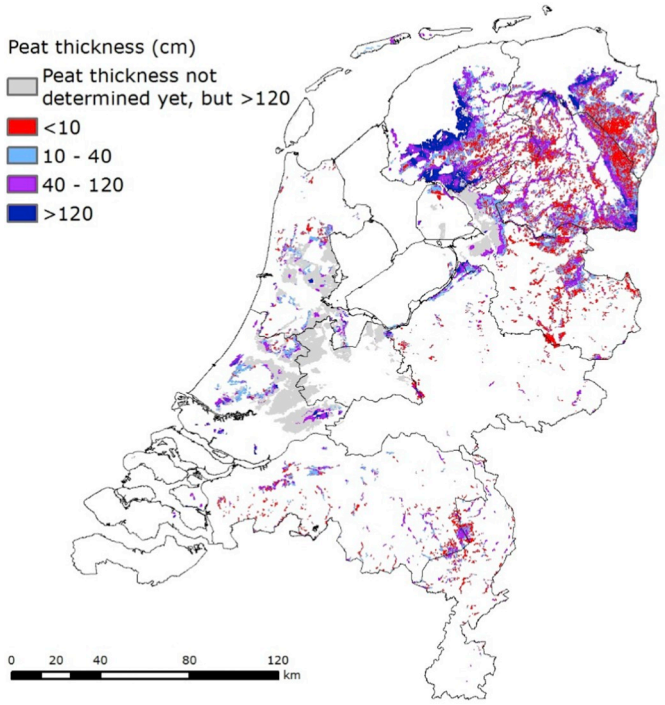

Fig. 13. Updated peat thickness map of the Netherlands. The grey-shaded areas in the western part of the country were not surveyed. These areas were mapped as thick peat soils on the 1:50,000 map and since the original peat layers in these areas were typically 2 to 6 m thick, it was assumed that these soils would still be classified as 'thick peat soils'.

Table 3
Surface area distribution of peat thickness classes in the Netherlands according to the original 1:50,000 national soil map (1995) and the updated version of the map (2014). The column 'Change' indicates the relative change in the areal extent.

Peat thickness	1995		2014		Change
	ha	%	ha	%	%
0–10 cm	0	0	90,580	23	
10–40 cm	221,926	55	162,593	40	−27
40–120 cm	98,672	24	94,574	23	−4
> 120 cm	82,270	20	55,121	14	−33
Total	*402,868*	*100*	*402,868*	*100*	

updated peat thickness values in the legacy dataset was quantified and accounted for by the prediction models. The method is described extensively by Kempen et al. (2015) and De Vries et al. (2014) for mapping a 187,525 ha area in the northern peatlands. The method was then applied to other regions with organic soils. By 2014, the 1:50,000 map was updated for 403,000 ha of peatlands. Peat layer thickness was tested via auger at 7300 new sampling sites. The peat mapping programme resulted in a new updated peat thickness map (Fig. 13).

Table 3 provides an absolute and relative overview of the surface area distribution of the peat thickness classes according to the 1:50,000 soil map from 1995 and the updated map from 2014. The results show that the surface area with organic soils shrank by almost 25%, while the surface area for which originally thick peat soils were mapped shrank by 33% and now cover 14% of the updated area. As a result, 40% of peaty soils will now be classified as mineral soils (having < 10 cm peat in the profile). For the thin and thick peat soils, approximately 30% of the area dropped into a lower peat thickness class.

Table 3. Surface area distribution of peat thickness classes in the Netherlands according to the original 1:50,000 national soil map (1995) and the updated version of the map (2014). Column 'Change' indicates the relative change in the areal extent.

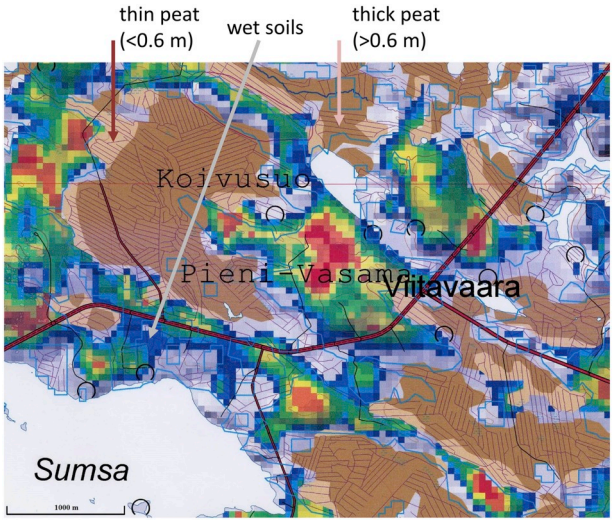

Fig. 14. The thickness of peat mapped with classified airborne radiometric potassium (K) in the Koivusuo area, Finland.

5.10. Finland

The Geological Survey Finland (GSF) surveys about 30,000 ha of Finland's 9 million hectares of peatlands every year. For the past four decades, GSF has studied approximately 2 million hectares of peatlands, most of which were drained peatlands. This information is needed for public officials to set policies on agriculture and forestry practices, along with the protection of habitat and groundwater, and setting aside peatlands for recreational use. GSF's knowledge was also crucial in mapping peatlands for the Finnish Soil database 1:250,000 (Lilja and Nevalainen, 2006) as a joint project between GSF and the Natural Resources Institute Finland.

The mapping process delineates peat deposits using topographic maps (1:20,000), topographic databases (1:10,000), aerial photographs, and the GSF peat database. In the topographic database, the minimum area for a mire was 1000 m^2 and for a paludified area 5000 m^2 The peat database had > 10,000 records of mires larger than 20 ha and over 900,000 drilling points. Mire thickness is quite variable in Finland—some are very thin, especially in Western Finland (Ostrobothnia), while deeper mires are commonly found in smaller areas where the topography is fluctuating. Using classified airborne radiometric potassium (^{40}K) data with peat drilling data, the thickness of peat deposits were separated in two classes: 1) Thinner than 0.6 m and 2) thicker than 0.6 m. Wet soils, mostly in low topographic positions, were also identified (Fig. 14). In Northern Finland (Lapland) GPR measurements were also used to scale radiometric data (Väänänen et al., 2007).

Important development work during the mapping project was the classification of airborne geophysical data for the further interpretation of peatlands. The mires were divided to three categories of thickness by radiation attenuation of ^{40}K%: paludified areas < 0.3 m (0.6–0.9%), thin peats (0.3–0.6%) and thick peats (< 0.3%) (Väänänen et al., 2007). Special attention was paid to the thickness of peat on narrow mire patterns, where the topography varied sharply. Because of the mires, the agricultural peatlands (fields) were also separated by reference points and field observations.

Peatland information from the Finnish Soil database has been used in numerous projects and recently in the creation of national SOC-map of Finland as part of the Global SOC map. GSF peat researchers have introduced a new three-point grid mapping system for mapping

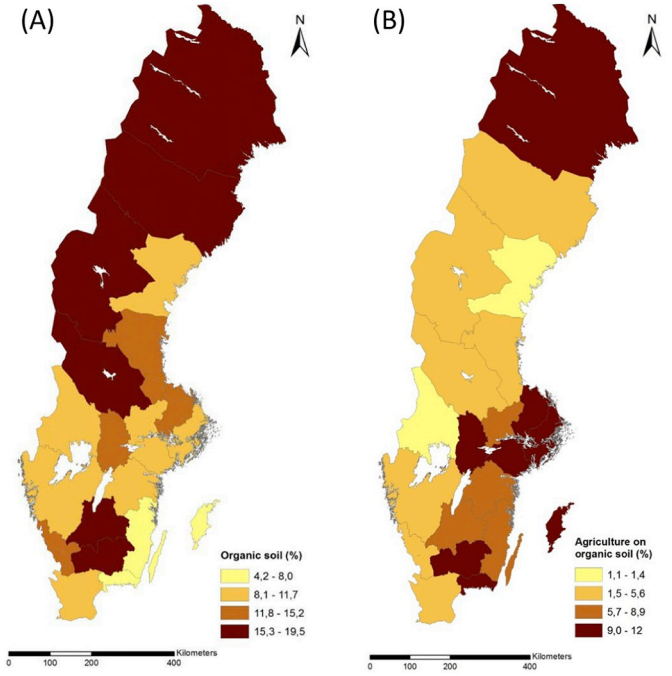

Fig. 15. (A) Distribution and coverage (% of total land area) of organic soils in each county in Sweden (B) Distribution and coverage of organic soil (% of total agricultural area) in each county in Sweden (from Pahkakangas et al., 2016).

peatland. The approach takes full advantage of GPS, field computers, and high-speed data analysis to create digital datasets that give better aerial coverage over traditional methods, and are ideal for 3D modelling.

5.11. Sweden

The area of peat in agricultural land in Sweden was estimated by Hallgren and Berglund (1962) and more recently, using digitized maps by Berglund and Berglund (2010) and Pahkakangas et al. (2016).

Organic soil data was retrieved from the Swedish geological survey (SGU). The GIS-database has one layer of information on peat type at 0.5 m depth, and one layer with shallow peat. Most of the country was mapped with high precision (1:25,000–1:100,000) but some of the northwestern parts of the country were mapped with less detail (1:750,000). For some minor areas where no soil information from SGU was available, low ^{40}K gamma radiation was used as a proxy for peat soil, since water filled peat soil blocks the radiation (Ek et al., 1992). A ^{40}K radiation value of 1.4 or less was used as an indication of peat soil (Berglund and Berglund, 2008). The total area of peat in Sweden is estimated to be 6,118,644 ha (Pahkakangas et al., 2016) and the distribution of organic soil in each county is shown in Fig. 15A.

To access European Union (EU) subsidies, all farmers in EU countries must report their land use. This information is stored in databases regulated by the Swedish board of agriculture. The agricultural land is divided into “blocks” and can be retrieved as map layers for GIS analysis. Based on this data, 3,232,039 ha of land in Sweden is defined as agricultural land and represents 7.9% of the total Swedish land area.

A map of organic soils in Sweden was created using the databases from SGU with soil information. In areas lacking this information gamma ^{40}K data was used. Using ArcGIS 10.3.1 this was cross referenced with the map of agricultural land, generating a map of agricultural land on peat. The total area of organic soil used in agricultural production is estimated to be 225,722 ha (7% of the total agricultural area). About 80% is used as arable land and 20% for pasture. The distribution of agriculture on the organic soil within each county is shown in Fig. 15B.

5.12. Canada

Peatland mapping in Canada can be traced back to the Canada Land Inventory (Coombs and Thie, 1979), which used aerial photography acquired from the 1940s to the 1960s to delineate areas suitable for forestry and agriculture (1:250,000 scale), from those with excess soil moisture (i.e. wetlands, of which a majority peatlands). Synthesizing this data with soil pedon data culminated in the Soil Landscapes of Canada product, a polygonal 1:1,000,000 scale soil survey which covers the entire landmass of Canada. Derivatives of the Canada Land Inventory and Soil Landscapes of Canada were soon adapted to mapping peatlands (Tarnocai, 1984), with the current edition (Tarnocai et al., 2011) using a map scale of around 1:1,000,000. This map estimated a total peatland area of 1.13×10^6 km^2, or 12.5% of the total land area.

Remote sensor-derived peatland maps in Canada are split between comprehensive nation-wide or continental products, and more regional analyses. The Canada Wetland Inventory (Fournier et al., 2007) is based primarily on 30 m Landsat supervised classification, and covers much of the southern and managed boreal forest of Canada, with limited coverage in northern regions. Recently, multi-sensor remote sensing methods have yielded excellent results at high resolution in smaller, regional studies. Hird et al. (2017) produced peatland maps of the Alberta province using multispectral satellite data, DEM, synthetic aperture radar (SAR) with training data from forest inventory plots (Fig. 16). Bourgeau-Chavez et al. (2017) used a similar approach including a study area with high permafrost abundance. Airborne LiDAR mapping has shown strong potential to delineate peatland at high resolutions (e.g. Millard and Richardson, 2013; Chasmer et al., 2016), though LiDAR coverage is very limited. Most surveys are sparse, but there is some comprehensive coverage near urban areas, agricultural lands, and some actively managed forests. Airborne radiometric methods have not been widely used in Canada to map peatlands. National land cover maps primarily derived from multispectral imagery that capture open peatlands, such as the EOSD product from Wulder et al. (2008), classify only very broad peatland classes such as moss and open wetland. They do not distinguish between forested peatland and uplands with a similar conifer forest cover. Similarly, the North American Land Change Monitoring System (Latifovic et al., 2017) defines a distinct open wetland class, though many of the boreal grassland and shrubland classifications far below the northern tree line are themselves likely to be peatlands.

Given the large area of treed and forested peatlands in Canada, forest inventory has also been used to map much of the peatlands in Canada with a significant tree component. At a national scale, 250 m resolution maps of forested and treed peatland have been produced by Thompson et al. (2016) for the entire boreal land area of Canada. Forest inventory methods however, cannot capture treeless peatlands more common in northern regions, in maritime climates, and sites recently burned in wildfires.

Few peatland maps cover the entire Canadian land area, and more intensive mapping efforts using multi-sensor remote sensing methods often only cover small fractions of the estimated 113 Mha of peatlands in Canada (Tarnocai et al., 2011). To produce optimal peatland maps that span the large gradient of forest cover and composition, successful peatland mapping syntheses should incorporate terrain metrics, optical multispectral and radar remote sensing, as well as forest inventory and structured data as a cohesive product. To date, this synthesis does not exist, and existing peatland maps compromise on resolution and scale (Tarnocai et al., 2011), or more limited accuracy at either end of the vegetation spectrum, be it in open systems (Thompson et al., 2016) or densely forested ones (Bourgeau-Chavez et al., 2017).

5.13. Summary

Based on these 12 case studies, national approaches to peat mapping vary based on access to peatland and available resources. EU countries

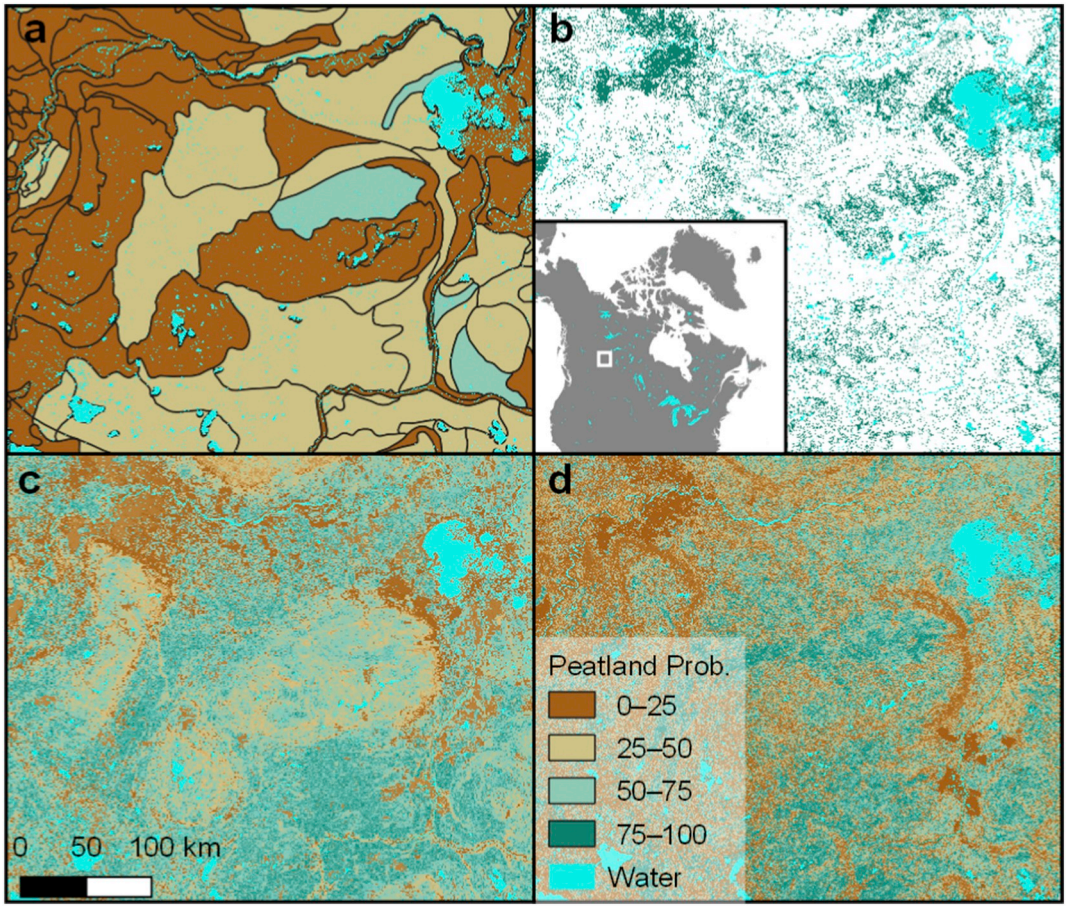

Fig. 16. Comparison of four peatland maps over the same area of northeastern Alberta, Canada using the same colour scale (see panel d). Panel (a) is Tarnocai et al. (2011) with peatland proportion per polygon, including both bogs and fens. Panel (b) is the North American Land Cover Monitoring System from Latifovic et al. (2017), with any pixels classified as wetland, shrubland, or grassland-lichen-moss coloured as 75–100%. Panel (c) is the forested and treed peatland map from Thompson et al. (2016); panel (d) is the wetland probability map from Hird et al. (2017).

with a rich data infrastructure—such as Finland and Sweden—can provide accurate peat maps using country-wide gamma radiometric surveys. Examples from the two countries show that shallow peats can be distinguished from deeper ones using gamma ^{40}K.

The USA has the most detailed soil maps derived from conventional mapping methods (map scale between 1:12,000 to 1:63,360). Regions such as the Netherlands and Scotland have traditional soil maps at a coarser scale, and have updated peat extent and thickness maps at a finer resolution using DSM. The Netherlands have also mapped peat thickness at a fine scale. These countries benefitted from having good legacy soil data and expertise in DSM. The Scotland example demonstrated that an accurate and consistent peatland map at a country scale can be made using freely-available covariates. The DSM maps were at least as accurate as conventional maps, but were created at a fraction of the cost. Tasmania is planning to update its peat map (extent and thickness) using the DSM approach.

Canada has used remote sensing approaches and DSM techniques to map large areas (Hird et al., 2017). Digital soil mapping approaches have been trialled in several areas in Indonesia, but not extended to a national scale. The challenge is convincing countries such as Indonesia, Chile, Brazil, and other nations with a large area of peatlands to adopt DSM techniques for country-wide peatland mapping. In these countries, peatlands are often in pockets and difficult to access, suggesting mapping efforts should focus on combining remotely sensed images and field observations.

6. A review of digital peat mapping studies

6.1. Digital soil mapping

Digital soil mapping (DSM) studies are framed based on the *scorpan* spatial prediction function approach (McBratney et al., 2003):

$$P_x = f(s, c, o, r, p, a, n) + e \quad (6)$$

Where peat properties at spatial position x is a function of soil factors (s), climate (c), organisms which include land use, human effects, and management (o), relief (r), parent materials (p), age or time (a), spatial position (n), and e is the spatially correlated errors. This model links field observations (e.g. the presence of peat or thickness of peat) to spatial environmental variables that are captured by proximal or remote sensors via a spatial prediction function f. The model assumes the factors are in steady-state, and the observations should cover the entire range of variation in covariates so that the model can be extrapolated to the whole area. The form of f can be a simple linear model, logistic regression, or machine learning models such as regression trees and random forests (Table 4).

Minasny and McBratney (2016) stated that DSM requires three components: the input in the form of field and laboratory observational methods, the process used in terms of spatial and non-spatial soil inference systems, and the output in the form of spatial soil information systems, which includes outputs in the form of rasters of prediction along with the uncertainty of prediction.

Table 4
Studies on mapping peat characteristics using digital approaches, arranged based on extent of the study area.

Area	Extent (km^2)	Map grid spacing (m)	Mapped Peat characteristics	Calibration data	Covariates	Prediction model	Model Validation*	Map Uncertainty*	Reference
Global	510×10^6	50,000	Peatland cover	Legacy soil maps	Climate maps, soil maps	Classification tree	IV	N	(Wu et al., 2017)
Tropics and subtropics countries	4.7×10^6	232 m	Tropical wetlands and peatlands	275 field work data	MODIS, monthly mean precipitation, monthly evapotranspiration,SRTM, wetness index	Expert rule classification	N	N	(Gumbricht et al., 2017)
Congo basin	3.7×10^6	50	Peat extent	9 ground transects length 2.5–20 km, 250 m spacing along transect (n = 211)	SRTM DEM, ALOS PALSAR, Landsat	Maximum likelihood classification	CV	Y	(Dargie et al., 2017)
Central Siberia, Russia	3.0×10^6	10,000	Wetland types		ENVISAT, ScanSAR (C-band) and QuikScat (Ku-band) scatterometer data	Simple threshold-based classification	N	N	(Bartsch et al., 2007)
Southeast Asia	2.5×10^6		Peat swamp landcover	Legacy soil maps	GeoCover landcover, MODIS, SRTM	ISODATA clustering	N	N	(Yoshino et al., 2010)
Sunda land: Peninsular Malaysia, Sumatra, and Borneo	2×10^6	30	Peat swamp forest	Legacy soil maps	Landsat 5 and Landsat 7 multi-temporal images	Supervised classification	IV	N	(Wijedasa et al., 2012)
Indonesia	1.9×10^6	60	Wetland cover	Wetland map	SRTM DEM, Landsat, ALOS PALSAR	Bagged classification tree	N	N	(Margono et al., 2014a)
Kalimantan	743,330	100	Land cover	Expert judgement	ALOS PALSAR	Unsupervised classification	Qualitative	N	(Hoekman et al., 2010)
West Siberia lowland, Russia	592,440		Peat extent, thickness & C stock	Legacy soil maps and observations	Multispectral satellite data (vis-IR)	Geostatistical interpolation	IV	N	(Sheng et al., 2004)
Finland	338,000		Peat deposits	Legacy soil maps	Gamma radiometric K	Manual classification	N	N	(Lilja and Nevalainen, 2006)
Alberta, Canada	340,000	30	Peatland ecosystem type	Field data, systematic and random sampling	ALOS PALSAR, ERS-1 & ERS-2, Landsat 5 TM	Random Forests	IV	N	(Bourgeau-Chavez et al., 2017)
Northern Ireland	141,130	50	Peat and mineral soil class and C stock	6862 Topsoil samples	Gamma radiometric, DEM	Linear mixed model	CV	Y	(Rawlins et al., 2009)
Taiga zone of West Siberia	140,000		peatlands/mires		Landsat 7 and indication characteristics of the vegetation	phytoindication method	N	N	(Bazanov et al., 2009)
St. Petersburg region of Russia	100,000	30	Spectral characteristics of peat	Ground data	Landsat	Expert knowledge	N	N	(Krankina et al., 2008)
St. Petersburg region, Russia	80,000	1000	Fractional cover of peatlands		MODIS	Reduced major axis (RMA) regression model	Y	N	(Pflugmacher et al., 2007)
The Puna and High Andean ecoregions of northwestern Argentina	143,000	30	Two categories: Peatbog and No Peatbog	53 digitized polygon based on Google Earth	Landsat TM 5 and 8	Maximum likelihood classification	N	N	(Izquierdo et al., 2015)
Pastaza-Marañón basin (Peruvian Amazonia	120,000	30	Peat cover	Transects at 13 accessible wetland sites	Landsat TM	Supervised classification	N	N	(Lähteenoja et al., 2012)
Sweden	35,000	200	Agricultural peat extent	Digitized maps of Quaternary deposits	Airborne gamma K data	Gamma K classes	Local validation	N	(Berglund and Berglund, 2010)
Scotland	80,000	100	Peat or mineral soil cover	Legacy soil data (n = 721)	DEM, Landcover, Soil map, Monthly mean temperature and rainfall, Geology map, Landsat	Artificial neural Network	IV	N	(Aitkenhead, 2017)
Ireland	84,000	300	Peat extent	Soil maps	Peatland Map of Ireland, Land Cover	Expert rules	IV	N	(Connolly and Holden, 2009)

(*continued on next page*)

Table 4 (*continued*)

Area	Extent (km^2)	Map grid spacing (m)	Mapped Peat characteristics	Calibration data	Covariates	Prediction model	Model Validation*	Map Uncertainty*	Reference
St Petersburg, Russia	80,000	1000	Peatland extent/cover	Forest inventory map	MODIS	Correspondence analysis	N	N	(Pflugmacher et al., 2007)
Amazonian Peru	35,600	30	peatland vegetation types	Legacy data, 218 ground data for classification, 24 forest census plots, 33 peat cores	Landsat TM, ALOS PALSAR, SRTM DEM	Image classification	N	N	(Draper et al., 2014)
Mackenzie River Basin, Canada	25,000	1: 50000	Peat depth, peat C distribution	203 peat depth from different sites		Ordinary kriging	Y	Y	(Beilman et al., 2008)
South Sumatra, Cental Kalimantan, West Papua	15,000	1000	Peat dome volume	542 field observations	SRTM DEM, Landsat TM	Manual delineation and kriging	N	N	(Jaenicke et al., 2008)
Drenthe province, the Netherlands	16,750	25	Peat & mineral soil classes	16,282 soil profile descriptions	DEM, groundwater level map, landcover, paleogeography, geomorphology, soil map	Multinomial logistic regression	CV	Y	(Kempen et al., 2009)
Drenthe, the Netherlands	16,750		Soil types in peatlands	125 sampling locations	27 environmental covariates from DEM, DEM+ point measurements, land cover, soil, Paleogeography maps	The generalized linear geostatistical model (GLGM)	Y	Y	(Kempen et al., 2012a)
Serra do Espinhaço Meridional (SdEM), Brazil	11,801	30	Peat extent	Field work	Aerial photographs, Google Earth, Landsat and radar images	maximum likelihood supervised classification	Y	N	(Silva et al., 2013)
Periglacial terrain, European Russian Arctic	17,500	2.4 and 30	High-resolution mapping of ecosystem carbon storage	field observations	QuickBird satellite images, Landsat TM images	multiple level segmentation for classification	Y	N	(Hugelius et al., 2011)
Zoige, Tibet Plateau China	18,000	60	Peat extent	Expert judgement	Landsat	Segmentation based on reflectance & clustering	N	N	(Fan, 1988)
Djoge, Tibetan Plateau	10,000	30	Landcover (incl. peatland)	Field survey	Landsat TM	Supervised classification	N	N	(Kumpula et al., 2004)
Denmark	7300	250	Peat extent (presence of peat) over 2 periods	Legacy soil descriptions (n = 25,739)		Indicator kriging	N	Y	(Greve et al., 2014)
Northern Highlands Lake District, Wisconsin, USA	7000		Peat thickness & C stock	Field survey	DEM	Linear regression	N	Y	(Buffam et al., 2010)
Alberta, Canada	5900	1	Burn depth	Plot survey	Temporal multispectral Lidar	Linear interpolation	N	N	(Chasmer et al., 2017)
Central Kalimantan, Indonesia	2800	30	Peat burn scar depth	41 sites from transects of 20 km long	Lidar DTM, Landsat TM	Linear interpolation	N	N	(Ballhorn et al., 2009)
Ecuadorian páramo	2715	30	Peatland cover & carbon stock	Field observations, preferential sampling (max. Walking distance of 4 km)	Multitemporal Landsat TM, PALSAR, RADARSAT-1, SRTM/ASTER DEM	Random Forest	N	N	(Hribljan et al., 2017)
Loreto, Amazonian Peru	2700	30	Peatland cover	Forest plot, determined systematically	Landsat TM, ALOS PALSAR, SRTM DEM	Random Forest	N	N	(Hergoualc'h et al., 2017)
Ogan Komerang Ilir, South Sumatra	6100	90	Peat thickness, C stock	Legacy data	SRTM DEM	A power model	N	N	(Rudiyanto et al., 2015)
Ogan Komerang Ilir, South Sumatra and Katingan, Central Kalimantan, Indonesia	6100, 932	30	Peat thickness, C stock	Legacy data Based on transect sampling	SRTM DEM, Distance to rivers, Landsat TM	Cubist Regression tree, Random Forests	IV	Y	(Rudiyanto et al., 2016b)

(*continued on next page*)

Table 4 (*continued*)

Area	Extent (km^2)	Map grid spacing (m)	Mapped Peat characteristics	Calibration data	Covariates	Prediction model	Model Validation*	Map Uncertainty*	Reference
Tanjung Puting National Park, Indonesia	4000	30	Peat classes	Legacy peat map	TerraSAR-X, Landsat TM	Canonical discriminant analysis	N	N	(Wijaya et al., 2010)
Okefenokee Swamp, Southeast Georgia, USA	3702	500	Peat and sand surface, peat thickness	Survey data	GPS survey, topography maps, airphoto	kriging	N	N	(Loftin et al., 2000)
Across Canada		250	Treed boreal peatlands	Inventory ground plots from the Canadian National Forest Inventory (NFI) (n = 540)	Biophysical and bioclimatic raster data	logistic regression model, boosted regression tree (BRT) model	N	N	(Thompson et al., 2016)
James Bay Lowlands in Far North Ontario, Canada	1756	5	Peatland types, Peat thickness & C stock	140 ground observations via random sampling	SPOT 5	Supervised classification for peat extent & kriging for peat thickness & C stock	N	N	(Akumu and McLaughlin, 2014)
Moscow Oblast	1500	10	Peatbogs and peatlands with different area gradations		SPOT 5		N	N	(Sirin et al., 2014)
Usa River basin, Northeast European Russia	1625	2.4, 30	Land cover classification and C stock	Soil map, soil samples for SOC via transects and stratified random sampling	Quickbird, Landsat	Segmentation classification	N	N	(Hugelius et al., 2011)
Usa River Basin, west of the Ural Mountains, northeastern European Russia	1625	2.4	Mapping the degree of decomposition and thaw remobilization potential of soil organic matter		High-resolution land cover map		N	N	(Hugelius et al., 2012)
Keminmaa, central boreal region of south-western Finnish Lapland	1100	5	Peatland biotopes	48 dataset for training; 58 for testing	HyMap™ imaging spectrometer, dielectric permittivity (ε), electrical conductivity (σ), and pH, and site types	Unsupervised classification with partitioning around medoids (PAM), fuzzy mapping with multiclass Support vector machine classification	Y	N	(Middleton et al., 2012)
Isle of Lewis, Scotland	2200	60	Peatland class	Ground truth data	Aerial photograph, Landsat image	Ordination analysis	EV	N	(Stove and Hulme, 1980)
North-east of Lewis, Scotland	500	30	Peatland class	Field data	Landsat TM	PCA, Unsupervised classification, Neural networks	N	N	(Brown et al., 2007)
Dartmoor, south-west England	1000	250	Peat thickness	Field data via stratified sampling (n = 1000)	slope, elevation	Regression	EV	N	(Parry et al., 2012)
Dartmoor, South West England	471	5	Mapping blanket peatland SOC, bulk density and carbon content	29 cores	Peat thickness map	grid-based map algebra, regression between bulk density, carbon content and depth	N	N	(Parry and Charman, 2013)
Dartmoor, South West England	406	50	Peat thickness and C stock	1334 field observations	Lidar-derived terrain attributes and gamma radiometric data	Linear regression	Y	Y	(Gatis et al., 2019)
Dartmoor, South West England	122	250	Peat thickness	425 field observations	DEM (5 m resolution) derived attributes	Regression kriging	CV	Y	(Young et al., 2018)
Sites across England, Scotland, Wales and Ireland	100–1000	200	Peat extent	Legacy soil maps	Gamma radiometric	Manual interpretation	N	N	(Beamish, 2014)
Isle of Man, UK	500	0.2	Peat extent	Sampling at 4 sites (n = 462)	Aerial photograph	Supervised classification	IV	N	(Weissert and Disney, 2013)
Eastmain, Québec, Canada	600	10	Wetland classification	image segmentation	SPOT-4,	Object-based classification	N	N	(Grenier et al., 2008)

(*continued on next page*)

Table 4 (*continued*)

Area	Extent (km^2)	Map grid spacing (m)	Mapped Peat characteristics	Calibration data	Covariates	Prediction model	Model Validation*	Map Uncertainty*	Reference
Bengkalis, Sumatra, Indonesia	500	30	Peat thickness, C stock	Legacy data	SRTM DEM, ALOS PALSAR, Sentinel 1, Distance to rivers	Cubist Regression tree, Random Forests	IV	Y	(Rudiyanto et al., 2016b)
Lake Kuortane, Western Finland	787	25	Landcover class (inl. Peatland)	Aerial imagery class	ALOS PALSAR	Probabilistic Neural Network	IV	N	(Antropov et al., 2014)
Blue Gem coal bed, Kentucky, USA	838	304.8	Geochemical map in peat bog	45 samples/locations	25 attributes	Kriging interpolation using sequential Gaussian simulation	N	Y	(Geboy et al., 2013)
Great Dismal Swamp National Wildlife Refuge, VA, USA	450	0.7	Peat Burn depth, C loss	Field observations	Pre- and Post-fire Lidar	Monte Carlo Simulation	N	Y	(Reddy et al., 2015)
Madre de Dios River of Peru	294	30	Peat extent and peat volume	800 locations on 35 peatlands, and 429 locations with peat thickness measurements on 10 peatlands	Landsat	maximum-likelihood classification for peat occurrence and interpolation for peat depth	N	N	(Householder et al., 2012)
Wicklow Mountains, Ireland	100	1000	Peat thickness	621 field observations via transects, 100 m interval	Elevation, slope and disturbance data	Peat inference model	EV	N	(Holden and Connolly, 2011)
Scotty Creek basin, Northwest Territories, Canada	152	2	Peatland class	Legacy peatland type map	RADARSAT-2	Support Vector Machine	IV	N	(Merchant et al., 2017)
West of Ireland	117	1.84	Peatland drain	Field data	Geoeye-1 multispectral image	Object-based image analysis	N	N	(Connolly and Holden, 2017)
Alfred Bog, southeastern Ontario, Canada	100	8	Peatland classification	500 randomly located points	LiDAR derivatives	Random Forest (RF)	Y	Y	(Millard and Richardson, 2015)
James Bay, Quebec, Canada	100–200	0.6	Peatland degradation	Ground control point	Aerial photo, Quickbird panchromatic image	Object-based Image classification	N	N	(Dissanska et al., 2009)
Mer Bleue Ontario, Lac St Pierre, Quebec Happy Vall Canada	200	30	Wetland class	Airphoto interpretation	Landsat, RADARSAT-1 DEM	Decision tree based on expert knowledge	N	N	(Li and Chen, 2005)
Mer Bleue, Ontario, Canada	35	8	Wetland class	Airphoto interpretation	Lidar, RADARSAT-2	Random Forests	IV	N	(Millard and Richardson, 2013)
Siak, Riau, Indonesia	50	100	Peat extent	Artificial observations	PALSAR	Image classification using expert rule	N	N	(Novresiandi and Nagasawa, 2017)
Bacho, province of Narathiwat, Thailand	30	10–200	Peat thickness and volume	426 field observations		Indicator kriging	N	Y	(Saito et al., 2005)
Ballynahone Bog and Slieve Beagh, N. Ireland	14 20		Peat thickness	Field observations: auger & GPR	Airborne radiometric data	Kriging and cokriging	N	Y	(Keaney et al., 2013)
Kami-Sarobetsu, Japan	15	20	Surface peat properties; C, N, bulk density	33 surface (0 − 20) field observations	PALSAR, NDVI & Lidar DSM	Multiple linear regression	N	N	(Takada et al., 2009)
Alfred Bog, Southern Ontario	17	30	Peatland landcover	330 observations	RADARSAT, Landsat 8	Random Forests	N	N	(White et al., 2017)
Bleaklow Plateau in northern England	7.8	2	gullies in upland peatlands		LiDAR DEM	Gully models	N	N	(Evans and Lindsay, 2010)
Boundaries of Finland	6.25	30	Treeless peatlands	Digitizing treeless peatland polygons	Landsat 7 ETM +	Sequential maximum a posteriori (SMAP), Maximum likelihood (ML) classification, Clustering	N	N	(Haapanen and Tokola, 2007)

(*continued on next page*)

Table 4 (*continued*)

Area	Extent (km^2)	Map grid spacing (m)	Mapped Peat characteristics	Calibration data	Covariates	Prediction model	Model Validation*	Map Uncertainty*	Reference
BOREAS, Manitoba, Canada	5		Peat (vegetation) types	72 vegetation plots	Compact Airborne Spectrographic Imager (CASI) reflectance data	Ordination and cluster analysis	N	N	(Thomas et al., 2003)
Värnamo, Gislaved, Lindesberg, Dorotea, Murjek, Sweden		30	Wetland classification		Topographic map, Landsat TM	Classification by thresholds and maximum-likelihood classification	N	N	(Bronge and Näslund-Landenmark, 2002)
Wedholme Flow, UK	4	30	Landcover class & C stock		Landsat TM, IKONOS	Maximum likelihood classification	N	N	(Crichton et al., 2015)
Polder Groot-Mijdrecht, The Netherlands	4	25	Peat thickness, Peat subsidence	433 auger observations	Soil maps, hroundwater levels, Elevation from Lidar	Kriging & Mechanistic Model	EV	Y	(Hoogland et al., 2012)
Peak District, North Central England	1	2	Mapping gully networks and depth, lead concentrations in peatland catchments		Lidar DEM	Gully models	N	N	(Rothwell et al., 2010)
Cors Fochno the west coast of Wales, UK	1		Peat (vegetation) types	86 vegetation plots	Hyperspectral data	Ordination and PLS	CV	N	(Harris et al., 2015)
Lakkasuo mire in southern Finland	2	1	mire site type, main type, dominant tree species, nutrient level	ground data	Lidar DEM & derived terrain variables	Supervised classification: Random Forest (RF), Support Vector Machines (SVM), and the k-Nearest Neighbor (kNN) methods	N	N	(Korpela et al., 2009)
The Rahivere bog, eastern Estonia	0.91	5	bog morphology, thickness and geometry of the peat body	Thirteen peat cores	GPR profiles, Topographic elevations from air-borne image	Kriging	N	N	(Plado et al., 2011)
TAHURA Muaro Jambi, Sumatra, Indonesia	58 ha & 5 ha	0.1	Peat burn depth	Field observations	Lidar (pre-fire) & UAV (post-fire)	Landcover classification	N	N	(Simpson et al., 2016)
7 fields within rhin-Havelluch, Northeast Germany	7–20 ha	1	Soil C density	Field data	Lidar, electromagnetic induction (EMI)	Regression & kriging	N	N	(Koszinski et al., 2015)
Großes Moor, Northern Germany	35 ha	0.5	Peat thickness, SOC, and SOC stock	34 soil cores (to 1 m depth)	ECa from electromagnetic induction (EMI), DEM from laser scanning	Multiple linear regression	N	N	(Altdorff et al., 2016)
Alpot Moor peat dome, Peak District National Park, UK	10 ha	2	Concentration of magnetic minerals (0–10 cm)	Field transects	Lidar DEM	Multiple linear regression	N	N	(Rothwell and Lindsay, 2007)
Wedholme Flow, UK	7.8	4	Peatland class	Ecological survey	IKONOS multispectral image, Lidar	Maximum likelihood classification	N	N	(Anderson et al., 2010)
Cranberry bogs in Massachusetts, USA	0.5–19 ha		Peat thickness	GPR survey	soil map units, and surficial geology	Linear model	N	N	(Kennedy et al., 2018)
La Grande River watershed, Quebec, Canada	0.2–2	9	Land cover class and Peat type	Field data	RADARSAT-1	Image classification	N	N	(Racine et al., 2005)
Alpine peatland in the Helen Creek watershed, Banff National Park, Canada	1.23 ha	0.05, 0.10, 0.25, 0.50, 1.00, and 2.00	Microtopography of the peatland	15,286 points of real-time kinematic (RTK) GPS survey and 116 photos	Orthophoto	Structure from motion with multiview stereo photogrammetry (SfM-MVS) and ground-based photos	Y	Y	(Mercer and Westbrook, 2016)
Stordalen mire, northern Sweden		0.5 m to 25 m	Mapping high latitude peatland hydroperiod	field measurements of water table depth at DOY 130 to 251 between 2003 and 2010	ALOS PALSAR and LiDAR-derived elevation	Random forests	Y	N	(Torbick et al., 2012)

* Validation: IV = internal validation (random withheld or systematic split of data into calibration & validation), CV = cross validation, EV = external validation, validation from an independent dataset, N = no validation.

6.2. Review of digital mapping studies

Peat mapping studies pre-2000 often use air photos or Landsat imageries to delineate peat areas. Pala (1982) used Landsat images and a classification tool to identify the location and extent of wetlands types over a 1700 km^2 area in North Ontario, Canada, while Stove (1983a, 1983b) used Landsat images and principal component analysis to discriminate between peat types in Scotland. Similarly, Fan (1988) classified Landsat images to identify peatlands in the Tibetan plateau.

Post-2000 there has been an increased interest in mapping peat using information derived from satellite images. These studies mainly involve delineating landcover from remote sensing, ecology, and environmental field studies. The beginning of the 2000s also saw the increased availability of spatial data (digital elevation model, satellite imageries), the availability of computing power for processing data, the development of data-mining tools and GIS (Minasny and McBratney, 2016). These factors helped push research in digital soil mapping, and enhanced publications of peat mapping using a variety of remote sensing products.

Table 4 presents 90 studies that have explicitly mapped peatlands using digital techniques. All but two studies were published in 2001 or later.

Table 4. *Studies on mapping peat characteristics using digital approaches.*

In the proceeding sections, we will discuss the main factors that can help drive more accurate peatland mapping.

6.3. How did these studies map peat?

Scale and resolution: Peatland has been mapped from a global to a field scale, with a median extent of the study area between 1000 and 2000 km^2 at a resolution of 30 m, coinciding with Landsat and STRM DEM. The finest resolution is at 0.1 m with LiDAR, and the coarsest is 0.5° or 50 km. Resolution of the images corresponds to the mapping extent and utility. For example, the 30 m resolution image may only be suited for regional mapping but cannot detect small pockets of peatlands in highland areas (Silva et al., 2013).

Who and where: These studies were mainly published in the fields of geography and remote sensing (38%), ecology & environment (36%), soil science (25%). The study areas are in Canada (18%), Russia (12%), Indonesia (11%), England (11%), Ireland (6%), Peru (5%), and the remaining 37% from other parts of the world.

What was mapped: As most studies are from remote sensing and ecological journals, peat is mapped as part of wetland types or landcover types (26%). Studies that map the extent of peat over an area (of peat or non-peat class) can be found in 17% of the studies, and 17% of the studies mapped the type of peats. Peat thickness is only explicitly mapped in 18% of the studies, and C stocks were calculated in 11% of the studies. The studies also variously mapped different parameters such as peat burn depth, gully erosion, and peat degradation.

Inputs: Peatland or landcover classification is based on legacy soil or land cover maps, field observations, or expert interpretation. Studies based on field survey (as opposed to using legacy soil samples) are collected from a low number of field observations because of access. For example, the study by Dargie et al. (2017) was based on 211 samples collected along transects in a relatively large area in the Congo basin. Soil science studies tend to use legacy soil samples. Countries with rich soil databases tend to have a large number of samples, e.g. Denmark with a sampling density of 3 samples/km^2, Drenthe province Netherlands 6/km^2, and Parry et al. (2012) collected 1 sample per km^2 in the Dartmoor area in south-west England.

Covariates: About 25% of the studies use a single source for the covariate, such as Landsat or ALOS PALSAR images. The most recent studies used 2 or 3 sources for covariates, which was termed multi-sensor (optical and radar), or multi-temporal images (Bourgeau-Chavez et al., 2017; Hribljan et al., 2017). The most common covariates used are Landsat images (31%), followed by Lidar (18%), ALOS PALSAR (13%), and SRTM DEM (12%). While climate was identified as a major factor in large-scale peat formation, it is absent in all of the surveyed studies in Table 4. This is in contrast with mineral soil carbon mapping studies, where climate layers are commonly used in regional mapping (Minasny et al., 2013).

Validation: 64% did not perform any validation and only 5% of the studies performed external validation. As machine learning tools are data hungry and tend to overfit calibration data, there is a need for a more robust validation measures in peat mapping studies.

Uncertainty: Only 19% of the studies define the uncertainty of the map. Producing a map of peat type, extent, thickness or carbon stock should be accompanied by its confidence of prediction.

6.4. Interpolation functions

6.4.1. Classification approach

Supervised classification is the most common approach for mapping peat type. Peat extent is mapped by classifying optical and radar images using a supervised classification algorithm (e.g., maximum likelihood, logistic regression or machine learning algorithms). Unsupervised classification is also used by clustering algorithms to group satellite imageries (such as Landsat) into landcover classes and assigning landcover type to these classes. Classification can also be done using field observation data of peat type (White et al., 2017).

There is no general rule on which classification methods work best; however, unsupervised classification is generally used in areas with few field observations while supervised classification works well where there is general site knowledge or field observations. Studies on soil class mapping indicated that complex machine learning models tend to be more accurate than simple or moderately complex models (e.g. logistic regression) (Brungard and Boettinger, 2010).

In ecological and geographical studies, peat observations are collected on a transect or based on a convenient sampling procedure. This sampling design is common in tropical forests where access is limited. A subset of these samples will measure peat thickness using an auger. The general workflow is based on land cover classification, and is summarised as follows:

- Land cover is mapped using a supervised classification with satellite images.
- Peat thickness and C density are calculated from field data. A core sample is usually divided into n layers, and bulk density and C content measured for each layer. The carbon density C_d (Mg m^{-2}) is calculated using the following equation:

$$C_d = \sum_{i}^{n} C_{ci} \times \rho_{bi} \times d$$

where, C_c is organic carbon content by mass (g of C/g of dry soil), ρ_b is bulk density (in Mg/m^3), and d is peat thickness (m).

- An average C density for each land cover is calculated.
- The average C stock (in Mg) is applied to each land cover (i = 1,.., m) multiplied by its area A and C stock (Cs) was calculated as:

$$C_s = \sum_{i}^{m} C_{di} \times A_i.$$

6.4.2. Regression approach

Studies using regression models commonly relate peat observations using various regression functions. The simplest form is interpolating peat thickness data using ordinary kriging (Keaney et al., 2013). Kriging

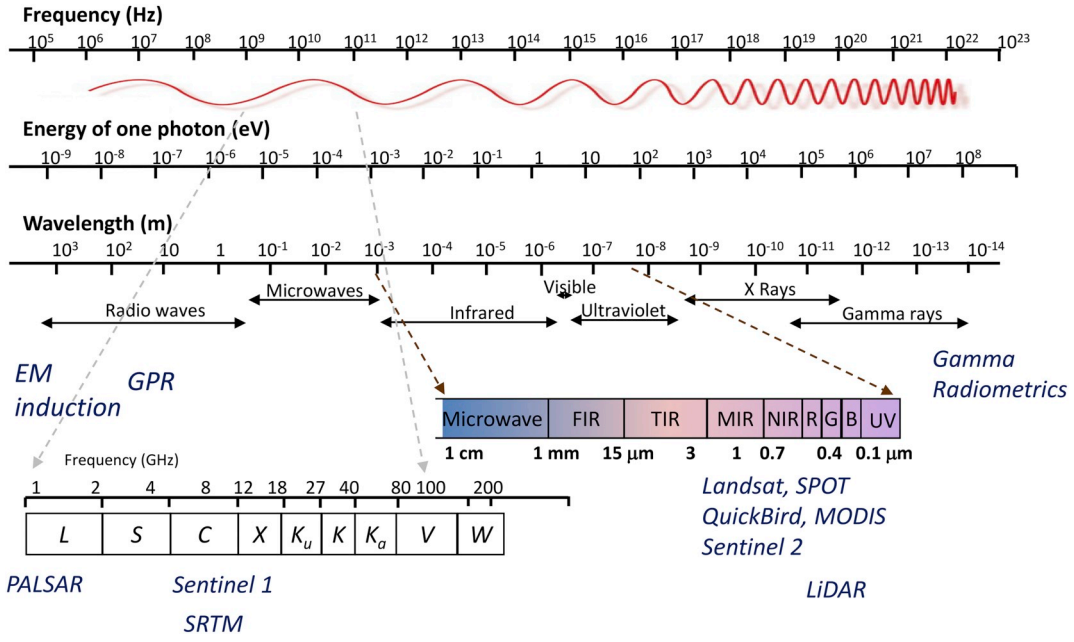

Fig. 17. The electromagnetic spectrum, highlighting areas useful for sensing peat.

works well when there are dense field observations with good spatial coverage.

For much of the world, optical and radar images are freely available, and can be used as covariates to predict peat. Field observations can be intersected with layers of environmental data or covariates, and a model fitted by various means. This model is then used to predict all other locations on the raster.

In some of the studies, explicit spatial models were derived to predict peat thickness, such as regression analysis from terrain attributes (e.g., elevation and slope) (Holden and Connolly, 2011; Parry et al., 2012); a peat thickness inference model (Holden and Connolly, 2011); a power function of the distance to a river (Hooijer and Vernimmen, 2013); an exponential function of elevation and slope (Parry et al., 2012); and an empirical function of elevation (Rudiyanto et al., 2015).

Only a few papers used regression and machine learning models to derive a spatial prediction of peat thickness (Aitkenhead, 2017; Rudiyanto et al., 2016b). Only a limited study that combined regression with kriging of the model residuals, termed regression kriging (Young et al., 2018).

Studies in digital soil mapping indicate that machine learning models tend to work better than linear regression (Rudiyanto et al., 2017). However, the prediction accuracy is more sensitive to training sample size compared to the model type used (Somarathna et al., 2017).

6.5. Summary

These 90 studies show that although peat type varies throughout the world, peat can be mapped using the DSM approach. Mapping at a resolution of 30 m can be done quite accurately using freely-available remotely-sensed information. Multi-source covariates (radar and optical) provide geographical information, elevation, optical, and radar images provide better information than a single covariate. Adding multi-temporal dimensions to optical and radar covariates provide useful information for mapping peat type, and machine learning models provide better accuracy than linear models. Some notable gaps in current peat mapping are:

- Uncertainty needs to be quantified.
- Climate, as a major factor in peat formation, should be considered when mapping peat at a regional scale or larger.

The next section provides a more detailed discussion on sensors that can improve peat mapping.

7. Using sensors to improve peat mapping

Mapping peat needs covariates that can reflect its extent or thickness, or factors related to peat formation. However, the tools that produce those covariates operate at different spatial scales, as shown in Fig. 3. Fig. 17 shows the electromagnetic spectrum and highlights areas that are useful for sensing peat: radio waves, microwaves, infrared, and gamma rays. The following sections describe common proximal and remote sensing systems that could be used for peat mapping.

7.1. Proximal geophysical methods for sensing peat thickness

Proximal sensors refer to sensors that operate close to the ground. Typically, the horizontal resolution of those sensors is between 0.1 and 1 m, and the vertical resolution is 0.01–0.1 m. Proximal sensors can cover an area between 1 m^2 to 1000 ha (Fig. 3) and penetrate up to tens of meters. Many proximal sensors used in geophysical surveys have been tested to measure peat thickness. Most of them are based on the unique electrical properties of peat, i.e., its high water content (Comas and Slater, 2004). Peat has a high porosity (around 90%) and is mostly saturated, and thus its electrical conductivity (or inverse of resistivity) depends mainly on its water content and concentrations of the dissolved ions. Walter et al. (2015) found that electrical conductivity is also related to peat decomposition stages, with values generally below 3 mS cm^{-1} and lower values found on undecomposed peats (around 0.2 mS cm^{-1}).

The relative dielectric permittivity (ε_r) of a material is the ability to polarize electrically. It is measured by the speed of an electromagnetic wave travelling through it. The dielectric permittivity of dry organic material is quite low, around 1.5, 2–3 for dry mineral materials, and 80 for water. Since peat contains a high amount of water, its dielectric permittivity is around 63 ± 8 (Parry et al., 2014), much higher than saturated soil at around 25–30.

A suite of instruments in the broad field of electromagnetic (EM) geophysics have been employed for measuring peat (Heagy et al., 2017). To map peatland, these instruments measure physical electrical conductivity (or resistivity), and electric permittivity. Measuring EM

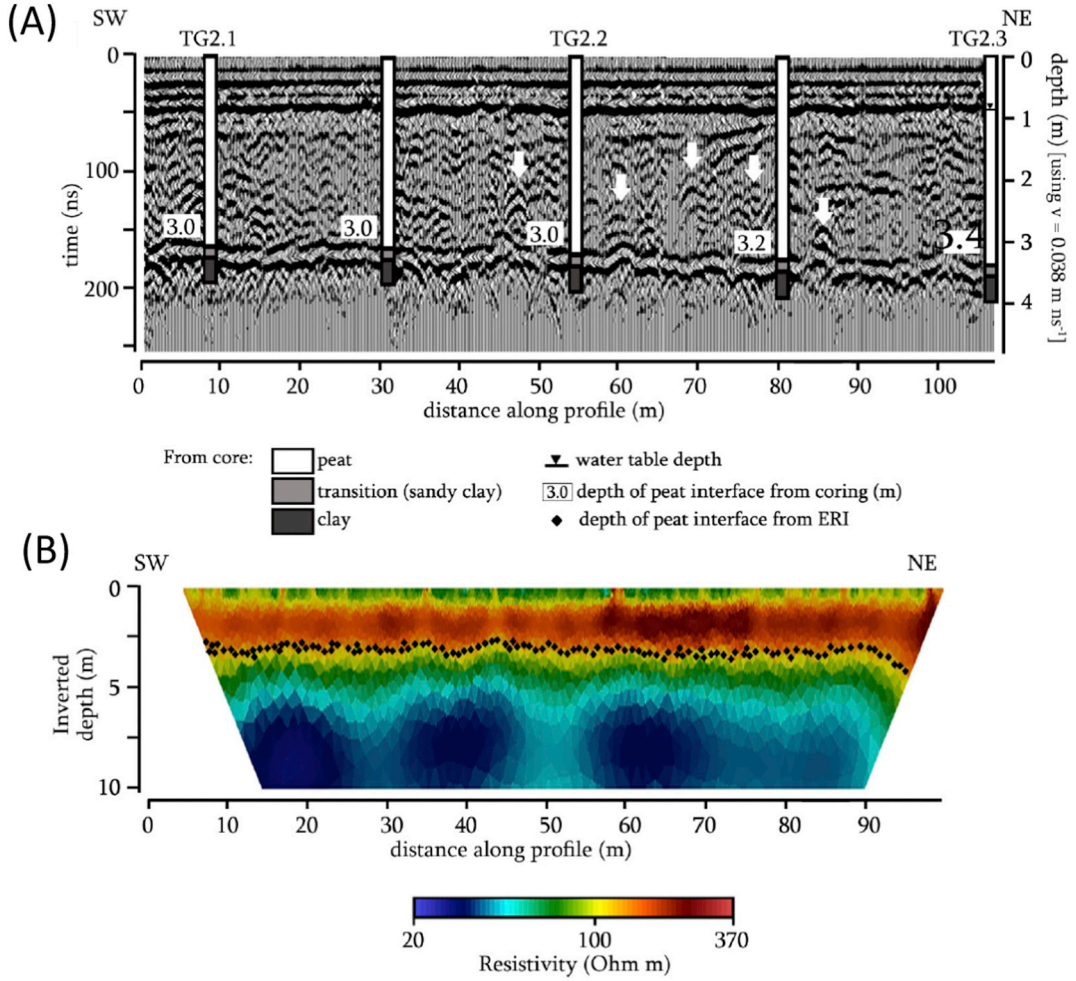

Fig. 18. (A) GPR with 100 MHz antennae profile on a transect in West Kalimantan: TG2.1–TG.2.3 and two additional core samples with layer thickness; (B) inverted image of resistivity survey using a four-electrode Wenner-type array with 1 m electrode spacing. The dots represent interpreted peat–mineral soil interface. Figure from Comas et al. (2015), Creative Common License.

data on the ground surface helps predict information about subsurface physical properties. Based on numerical models of Maxwell's equations, a model can predict the EM responses given the subsurface properties. In soil mapping, it is more common to measure the EM responses and find a set of subsurface properties that match. This is known as the 'inverse problem'.

7.1.1. Ground penetrating radar

Ground penetrating radar (GPR) is an active proximal sensing method. It is based on electromagnetic wave propagation which measures the soil dielectric permittivity. GPR has been used since the 1980s (Bjelm, 1980) and 1990s (Warner et al., 1990). It sends short pulses of high frequency (10–1000 MHz) EM waves through the ground surface. The wave propagates downwards and is reflected when it encounters boundaries between layers which have differences in permittivity. Depth is estimated from the wave velocity—from the time between transmission and detection of the wave. Lower frequency waves penetrate deeper into the ground, however resolution decreases.

GPR signals can penetrate up to 10 m in peatlands, with a resolution of 10–15 cm (Slater and Reeve, 2002). As peat has a dielectric permittivity of around 50–70, and saturated mineral soils around 25–40, it is relatively easy to tell the two media apart. Variation in the degree of peat decomposition may also cause a change in GPR response (Lowe, 1985; Warner et al., 1990). Reflections from boundaries between different types of peat deposits can be identified. Holden et al. (2002) also showed that GPR could be used to map out natural soil pipes in blanket peat. Most studies were in northern America and Europe.

There is a limitation for peat mapping when the electrical conductivity of peat is high. EM wave propagation is attenuated, reducing the depth of penetration. Comas et al. (2015) evaluated a GPR system (100 MHz) for mapping tropical peatland in Indonesia. They found that GPR is effective for mapping shallower peat (3–4 m), and able to pick up the peat/mineral interface up to a one centimeter resolution. However, this system could not detect peat deeper than 9 m. Campos et al. (2017) used GPR to detect buried peat bogs in highlands of Minas Gerais in Brazil, identifying four peat bog typologies such as "entrenched bogs", "subsurface bogs", "structural bogs", and "hanging bogs".

Most GPR studies are done on transects, using field coring to calibrate the EM wave velocity (Fig. 18A). Rosa et al. (2009) indicated from a study in Quebec, Canada, that at least 30 calibration points are required to minimize the EM velocity error in each survey.

7.1.2. Electrical resistivity imaging

Also called electrical tomography, electrical resistivity imaging is one of the oldest geophysical investigation techniques (Daily et al., 1992). It involves burying metal electrodes in the ground, applying a voltage, and measuring the resistance to the flow of the electric current. A typical resistivity survey system consists of four or more equally spaced metal electrodes (a 'Wenner array'), inserted into the soil. An AC-power source supplies current flow between the two outer electrodes and the resultant voltage difference between the two inner

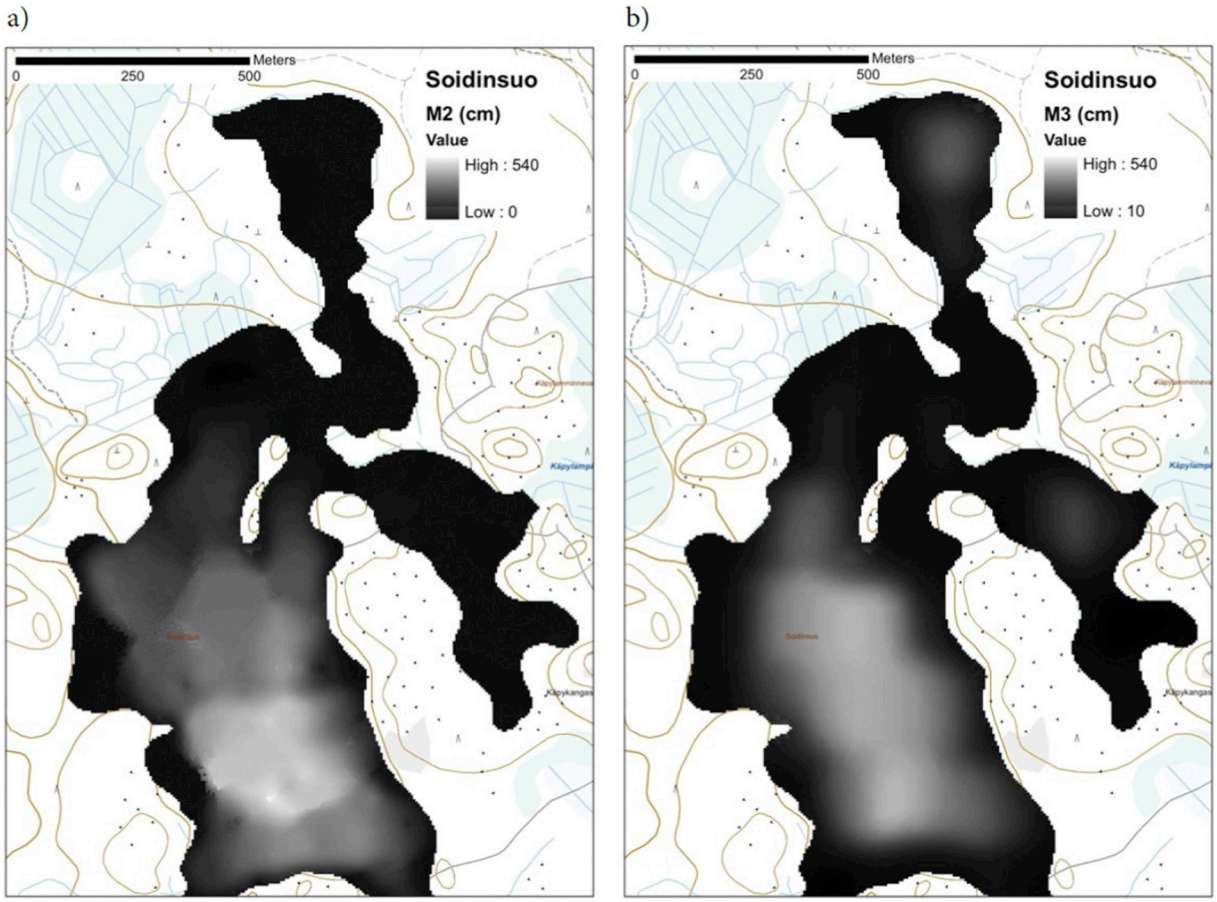

Fig. 19. Peat thickness estimated using a) electromagnetic induction data with 1D layer inversion, and b) ground penetrating radar (GPR) and drilling data. (From Airo et al., 2013, used with permission).

electrodes is measured. By placing many electrodes along a transect, the system can generate an image of the electrical resistivity variation in 2-D (along the transect and with depth) (Comas et al., 2015). The electrical measurements can be "inverted" by using a model describing the flow of electricity in soils.

Resistivity imaging is time-consuming, mostly done on a transect, and few full 3-D inversions have been performed. An example from Comas et al. (2015) in Fig. 18B shows different layers of material with different resistivities along a 100 m transect. The upper layer (60 and 200 Ω m) correlates with peat layer, and the underlying layer with high resistivity (200 and 300 Ω m) includes both a transition layer composed of a mixture of sand and clay (with some organics) and a clayey mineral layer.

7.1.3. Electromagnetic induction

Electromagnetic induction (EMI) instruments are one of the most popular proximal soil sensors as they do not require physical contact with the soil (Saey et al., 2012; Huang et al., 2016). Commercially available instruments (e.g., Geonics EM38 and DUALEM-1) which allow sensing on-the-go are widely used in precision agriculture.

The EMI sensor transmits a primary electromagnetic field which induces electrical currents in the soil. These currents generate a secondary electromagnetic field which is detected by the sensor's receiver. The secondary field is proportional to the ground current and is used to calculate the "apparent" or "bulk" electrical conductivity (ECa) for the volume of soil. A multi-coil offset electromagnetic induction instrument, capable of simultaneously recording several integral depths, could be used to map peat depth as the apparent electrical conductivity (ECa) of peat materials (and its large water content) have distinct values from mineral materials.

Linear regression relating peat thickness and ECa has been developed. Theimer et al. (1994) related EM31 measurements with peat thickness, with an average value of 10 mS/m for a 50 cm peat and 25 mS/m for a 2 m thick peat thick. They attributed the increase of ECa to the increase in pore water electrical conductivity. Altdorff et al. (2016) used measurements of different ECa depth ranges to predict peat thickness and C stock for a field in Germany. Theoretically, the ECa data can be inverted to represent EC values with depth. However, the authors did not provide meaningful estimates of peat layer depth, possibly because of the small depth range of the peat layer. Koszinski et al. (2015) used the EM38DD device in several peatlands in Germany and a two-layer model (Saey et al., 2012) to relate ECa measurement with peat thickness or the depth to mineral soil. Probing data using a linear regression model as the two-layer model proved to be inaccurate. Efficient ECa inversion algorithms for EMI instruments (Huang et al., 2016) could offer more accurate mapping of peat thickness.

Airborne multi-frequency EMI surveys, mostly used for near-surface geology and mining studies, can penetrate 70–100 m. In a 124 ha area of Soidinsuo in Central Finland, airborne electromagnetic data was inverted using a 1-D electromagnetic induction model calibrated using field data. The resulting peat thickness map is agreeable with GPR data (Fig. 19).

The results from these studies suggest that to predict peat thickness or depth to mineral layer, EMI instruments need to be calibrated to local conditions.

7.1.4. Seismic reflection, gravity, and magnetic methods

Various geophysical methods have been used to survey and locate coal deposits. These include broad scale airborne geophysical surveys (gravity, magnetic, or electromagnetic induction) to delineate

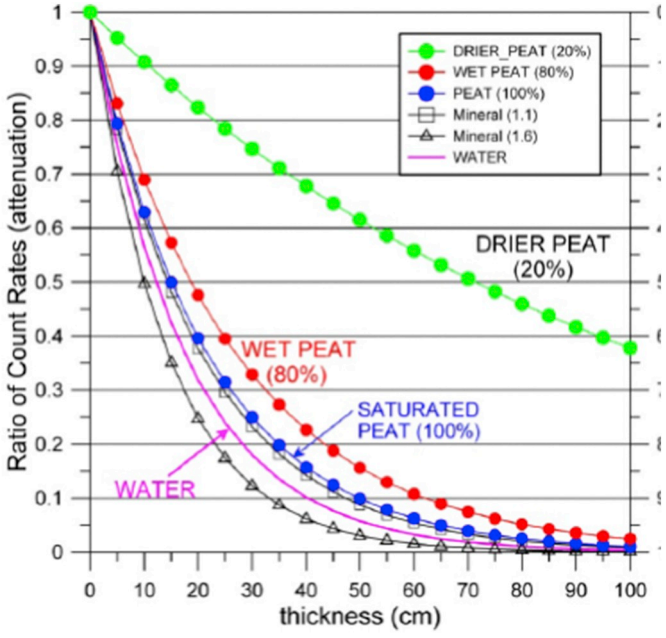

Fig. 20. Theoretical attenuation behaviour of gamma radiometric signal for peats at different moisture content and variation with thickness assuming a uniform half-space. A 90% attenuation level provides a reference level. (From Beamish, 2013, Creative Common License.)

sedimentary areas, followed by detailed ground surveys (Kang, 2009). Seismic refraction tomography was used to interpret shallow subsurface geology and Avalos et al. (2016) demonstrated that low seismic velocity can be used to infer peat deposits. Gravity and magnetic survey are well-developed for coal exploration but they have not been widely used for peat mapping. Their depth of penetration is much deeper than peat deposits and most of these instruments do not directly measure peat.

7.2. Remote sensing of peats

For large scale peat mapping, proximal sensors have little value. Remote sensors operate at a horizontal resolution of around 1 m–1 km, which can cover areas from a field (0.1 ha) to the globe. According to Lawson et al. (2015), tropical (and other) peatland has unique characteristics that make it mappable via remote sensing. Characteristics include distinctive vegetation types and structures, unique topography, and a high water table.

Geophysical airborne surveys, usually used to survey high economic value minerals and hydrocarbons, have also proved to be useful for mapping soils and peatlands. Examples in Finland and Sweden (section 5) show these surveys can identify parent materials as well as mapping peat thickness. Fine to medium resolution spatial and temporal data are now freely available from the Landsat, Sentinel and MODIS satellite platforms. Satellites that measure earth's surface moisture may be useful to generate rough peat maps. Gravity Recovery and Climate Experiment (GRACE) is available at 0.5 degree resolution (about 50 km), and Soil Moisture Active Passive (SMAP) available at 3 km resolution. These images provide a very coarse resolution which may only be useful for continental or global coarse mapping.

This section discusses some common remote sensing instruments, satellites, and airborne sensors that could map peatlands.

7.2.1. Gamma radiometrics

A gamma radiometer records the amount of radioactive isotopes in the soil. It is based on the principle that each gamma ray photon relates to a discrete energy window which is characteristic of the source isotope. Radiometric mapping predominantly reflects the variation in the amount of naturally occurring radioisotopes of potassium (^{40}K), uranium (^{238}U-series) and thorium (^{232}Th-series) as they produce high-energy gamma-rays with sufficient intensities to be picked up by a detector.

Radionuclides in the soil are adsorbed by clay minerals, iron oxides, and organic matter. Due to weathering processes, radionuclides are lost from the soil, which results in a characteristic gamma-ray spectrum. The soil's gamma intensity is directly related to the mineralogy and geochemistry of the parent material and its degree of weathering. Radiometric surveys, mainly aerial-based, have therefore been used for uranium exploration and geological mapping on a large scale (Wilford and Minty, 2006). Gamma radiometrics have also been widely used as covariates to map soils and regolith distribution in Australia (Wilford, 2012). A proximal gamma radiometer survey also allows fine-scale characterisation of soils (Stockmann et al., 2015).

Gamma-ray attenuation theory predicts that the behaviour of wet peat is distinct from most other soil types. The peat gamma signal is distinct mainly due to its high water content and low density (Fig. 20) (Beamish, 2013).

Based on the attenuation theory, Beamish (2013) speculated that the attenuation levels observed across wet peatlands could not, in general, be used to map variations in peat thickness. Beamish (2013) noted that the low gamma values form spatially-coherent zones (natural clusters) and can be interpreted as areas of increased water content for each soil type. Peat, in particular, is remarkably skewed to low count behaviour in its radiometric response. The higher amplitude intra-peat zones may be due to areas with thin peat cover while the areas with the lowest amplitudes coincide with the highest water content. Nevertheless, Keaney et al. (2013) and others found that the airborne gamma radiometrics data are highly correlated to peat thickness.

National gamma radiometric surveys have been undertaken in Australia (Wilford, 2012), Finland (Airo et al., 2014), Sweden (Lunden et al., 2001), Northern Ireland (Beamish, 2014) and other countries. These products have proved to be an invaluable data source for mapping peat extent. Berglund and Berglund (2010) calibrated ^{40}K concentrations in a peatland area in Sweden. The ^{40}K content of peatland was on average 1% compared to a non-peat area which has a concentration of 2%. They used a threshold value of 1.4% for classifying peat areas. The Finland survey (Airo et al., 2014) also found that ^{40}K was an invaluable measure of peat occurrence. The ^{40}K concentration was used to distinguish shallow (< 0.6 m) and deep peat (> 0.6 m).

Rawlins et al. (2009) encountered a problem when mapping soil carbon distribution in Northern Ireland—carbon has a bimodal distribution due to the presence of peat and mineral soils. They developed a linear mixed model into 3 regions based on peat, organo-mineral, and mineral soil. Gamma ^{40}K proved to be an important covariate for mapping C concentrations in all 3 soil classes.

In another detailed study, Keaney et al. (2013) mapped peat thickness for an area in the Republic of Ireland using field data cokriged with a total count of airborne gamma radiometrics data (Fig. 21). They further demonstrated that the gamma count coincides with peat thickness as measured by GPR.

Radiometric data components, potassium (K), thorium (Th) and uranium (U) and their ratios have proved to be useful to assist mapping peat deposits (Hyvönen et al., 2003; Hyvönen et al., 2002). Nevertheless, as gamma radiometric surveys mainly capture surface information (top 30–50 cm), they cannot infer peat of greater thickness. Additionally, airborne radiometric data are strongly dependent on variations of gamma radiation or conductivity in bedrock, which can obscure the signal on peats.

7.2.2. Visible and infrared sensors

Satellite images that provide earth's surface reflectance from the visible, to near- and mid-infrared spectrum (400–13,000 nm) are now widely available as low resolution (e.g. MODIS at 250 m), medium resolution (Landsat at 30 m, Sentinel 2 at 20 m), and high resolution

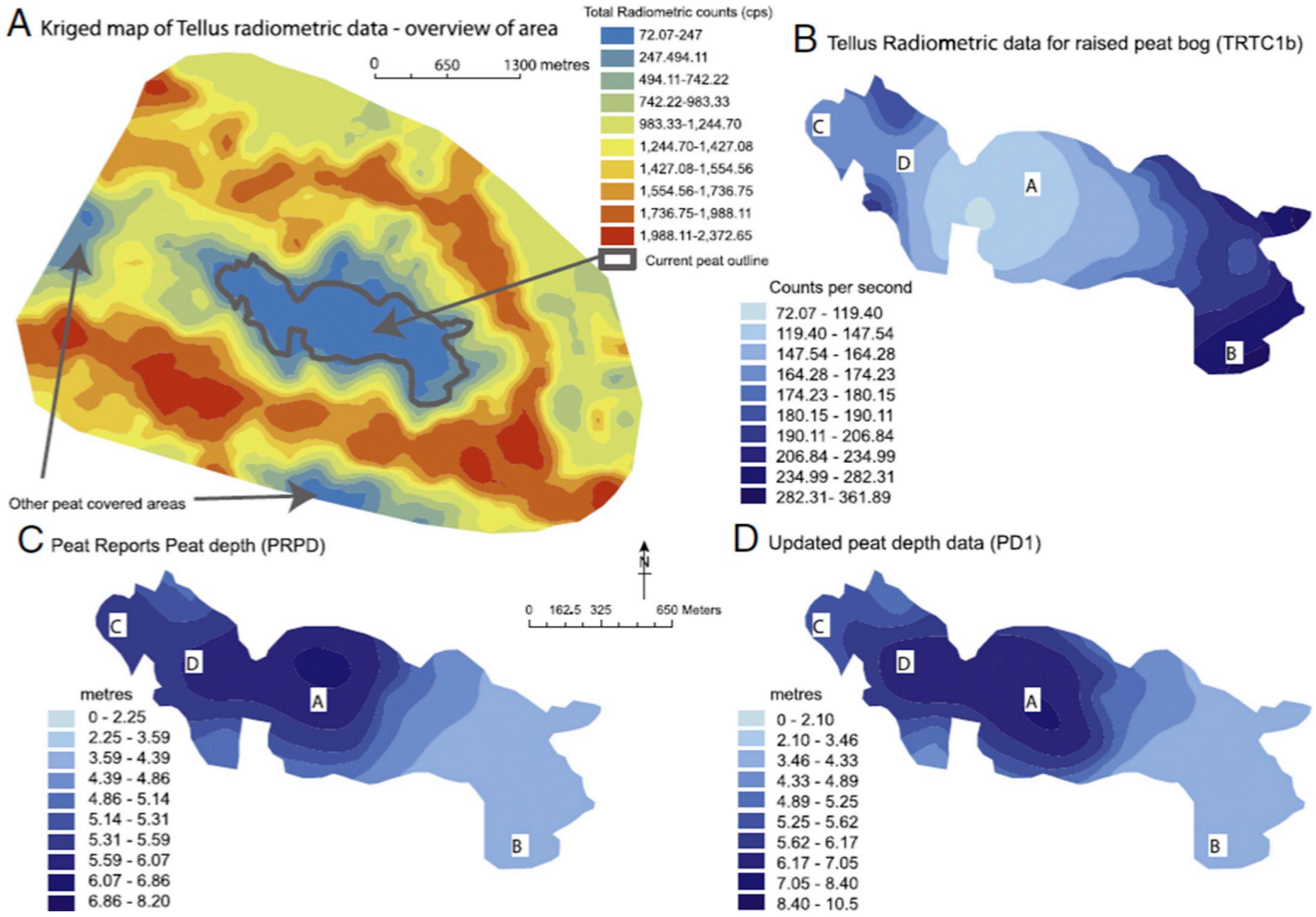

Fig. 21. (A) Radiometric data for an area in Ireland; (B) radiometric data for peat bog; (C) 1996 Peat thickness data from legacy data; and (D) updated peat thickness map cokriged from legacy data and gamma radiometrics. (from Keaney et al., 2013).

(SPOT, QuickBird at ~2.5 m) (Dissanska et al., 2009). These images can be trained to distinguish land cover or vegetation type, which may be related to peat type. Temporal spectral indices have been investigated to distinguish peat types (Fig. 22), while fine-resolution object-based classification may be able to map features such as drains. The resolution of the images can affect the accuracy of the prediction. High-spatial resolution imagery could improve peatland classification by reducing the uncertainty of mixed pixels (Rampi et al., 2014).

As an organic matter, peat has a unique spectral signature, with lower reflectance in the near- and shortwave-infrared part of the electromagnetic spectrum (Krankina et al., 2008). However, as most peatland is covered with vegetation we cannot directly identify peat in the visible and infrared regions. Many studies since the 1980s have delineated peat based on Landsat multispectral satellite data (from 500 to 1100 nm), which reflects land cover or vegetation type (Stove, 1983a; Stove and Hulme, 1980).

Harris and Bryant (2009) used spectra from Sphagnum mosses as proxy indicators of near-surface hydrology in peatlands. Spectral indices calculated from the near infra-red (NIR) and shortwave infrared (SWIR) liquid water absorption bands were used to indicate peat moisture status. Airborne hyperspectral imaging (in the visible and NIR range) has been trialled for small areas for mapping peatland vegetation types (Harris et al., 2015).

Shimada et al. (2016) postulated that peat thickness in a swamp forest in Indonesia could be estimated from forest phenology via multitemporal satellite images (Shimada et al., 2016). They used monthly NDVI values from a time series of MODIS satellite data. As vegetation can be affected by season (especially dry seasons) and groundwater level, seasonal NDVI fluctuation within a year may be indicative of peat thickness. Such a model may be applicable in natural forest areas.

7.2.3. Radar

Radio detection and ranging (Radar) is one remote sensing technology that operates in the microwave portion (1 cm to 1 m) of the electromagnetic spectrum. Radar imagery represents the amount of energy backscattered from a surface which varies with the degree of roughness of the surface (geometry), and with the type of object and its received site environment. Radar has been prominent in wetland mapping (Li and Chen, 2005) because:

- Unlike visible and infrared images, it is not susceptible to atmospheric scattering and the environment (e.g., night or day, rain or snow, fog or clear sky).
- It is relatively low cost.
- It offers real-time image processing.

In areas such as the tropics, Brazil, and Scotland, where cloud cover is persistent throughout the year, radar data proves to be invaluable for mapping peatlands (Poggio and Gimona, 2014). Microwave sensor systems are commonly divided into two categories according to their modes of operation—active and passive. Radar is categorized as an active microwave sensor which provides the source of microwave radiation to illuminate the target. Its basic principles are the transmission and reception of pulses where high energy pulses are emitted, and the returning echoes are recorded in the same antenna. The sensor can receive information such as magnitude, phase, time interval between

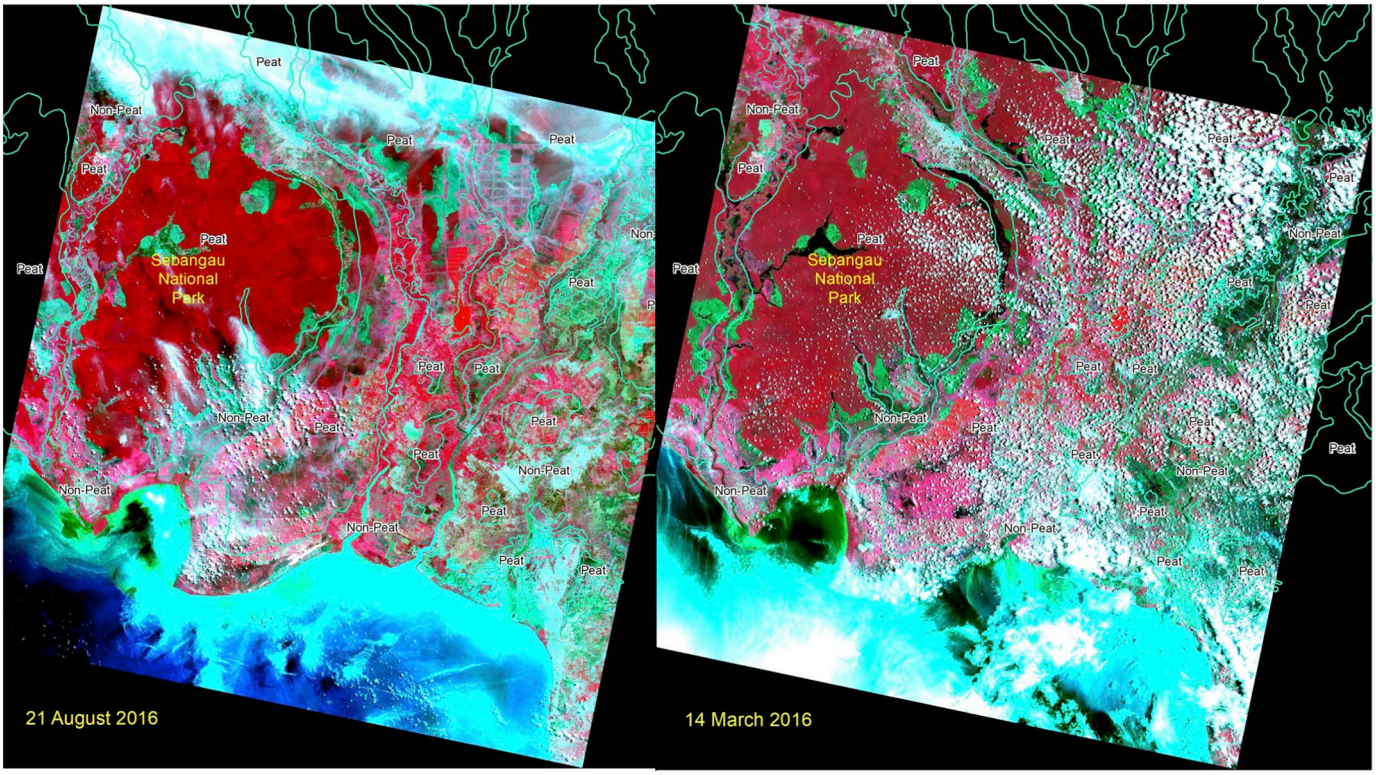

Fig. 22. A composite of Landsat 8 Band 543 in Central Kalimantan, Indonesia, showing peatland polygon at 2 periods: dry season (21/8/2016) and the end of the rainy season (14/03/2016). These two images show that peatland can be identified from the higher red tones during the dry season (compared to the rainy which looks similar between peat and non-peatland), as long as the peatlands are still intact (with forest cover). For the deforested area, the red tone difference cannot be observed. Note that one of the challenges in the tropics is the high cloud cover. (For interpretation of the references to colour in this figure legend, the reader is referred to the web version of this article.)

pulse emission and return from the object, polarization, and Doppler frequency.

There are two basic elements in an imaging radar system; Real Aperture Radar or Side Looking Airborne Radar (RAR or SLAR) and Synthetic Aperture Radar (SAR). Recent radar applications use SAR to generate high-resolution images of the earth's surface, including properties such as slope, roughness, humidity, textural in-homogeneities, and dielectric constant. Radar interferometry combines two or more radar images over the same area to detect change. Radar interferometry provides 3-D terrain and topographic features through an elevation model. As radar can penetrate the vegetation canopy, it has been used to retrieve soil surface moisture contents.

Some common spaceborne radar satellite platform and sensors include: ALOS-PALSAR (Advanced Land Observing Satellite); ENVISAT (ESA); ERS1/2 (European Remote Sensing Satellite 1 and 2); JERS-1 (Japanese Earth Resources Satellite-1); LightSAR (a low cost, lightweight L-band system); RADARSAT-2 (Canadian Space Program); Sentinel-1 (European Space Agency); SEISM (Solid Earth Interferometric Space Borne Mission); SIR-C/X-SAR (Shuttleborne Imaging Radar); and TerraSAR-X (German Aerospace Centre). Some products such as ERS-1/2, JERS-1, ENVISAT ASAR, and RADARSAT-1/2 are available at a spatial resolution of 10 m or finer. Compared to optical satellite data, radar imagery is available at a higher temporal frequency.

The standard radar image processing procedures consist of digital signal processing and image processing to extract information from objects of interest. In soil mapping, identifying the polarization type and data combination is an important part of radar image process. As radar image is based on detecting the dielectric constant, not all types of polarization are effective in mapping soil properties. Polarization refers to the orientation and shape of the pattern traced by the tip of the radar vector. The measurement of the energy at emission and at the reception after backscattering by the observed target are identified by the combination of the horizontal (H) and vertical (V) linearly polarized radar waves (Henderson and Lewis, 2008).

A radar system covers several levels of polarization complexity, i.e., single polarized (HH or VV of HV or VH), dual polarized (HH and HV, VV and VH, or HH and VV; and four polarizations (HH, VV, HV and VH). This polarimetric scattering mechanism represents the characteristics of soil status, especially those related to roughness, wetness, tillage, bare soils, etc. In tropical regions, vegetation cover becomes the main problem in predicting soil properties. A combination of different image polarization indices (such as HH/VV) provide complementary information on peat properties.

Lower frequency systems (P-band, L-band, and C-band) could retrieve soil characteristics over vegetation because they can penetrate deeper compared to the higher frequency systems (Zribi et al., 2014). C– Band in the HH polarization mode was recognised to be most sensitive to soil moisture and least sensitive to the surface roughness in the presence of low biomass.

Recent advances use temporal (two or more dates) of L-band (such as ALOS PALSAR) and/or C-band (e.g., ERS or Sentinel-1) SAR imagery to distinguish different peatland types based on moisture or flooding conditions. L- and/or C-band SAR have also been combined with optical (vis-IR) data (such as Landsat) to further enhance discrimination of peatland vegetation types (Bourgeau-Chavez et al., 2017; Hribljan et al., 2017). Hoekman (2007) used JERS-1 time series to map out flooding characteristics in the Mawas area in Central Kalimantan. He further postulated that the flooding intensity of the peat swamp forest is related to peat thickness, and thus peat thickness can be estimated (Fig. 23).

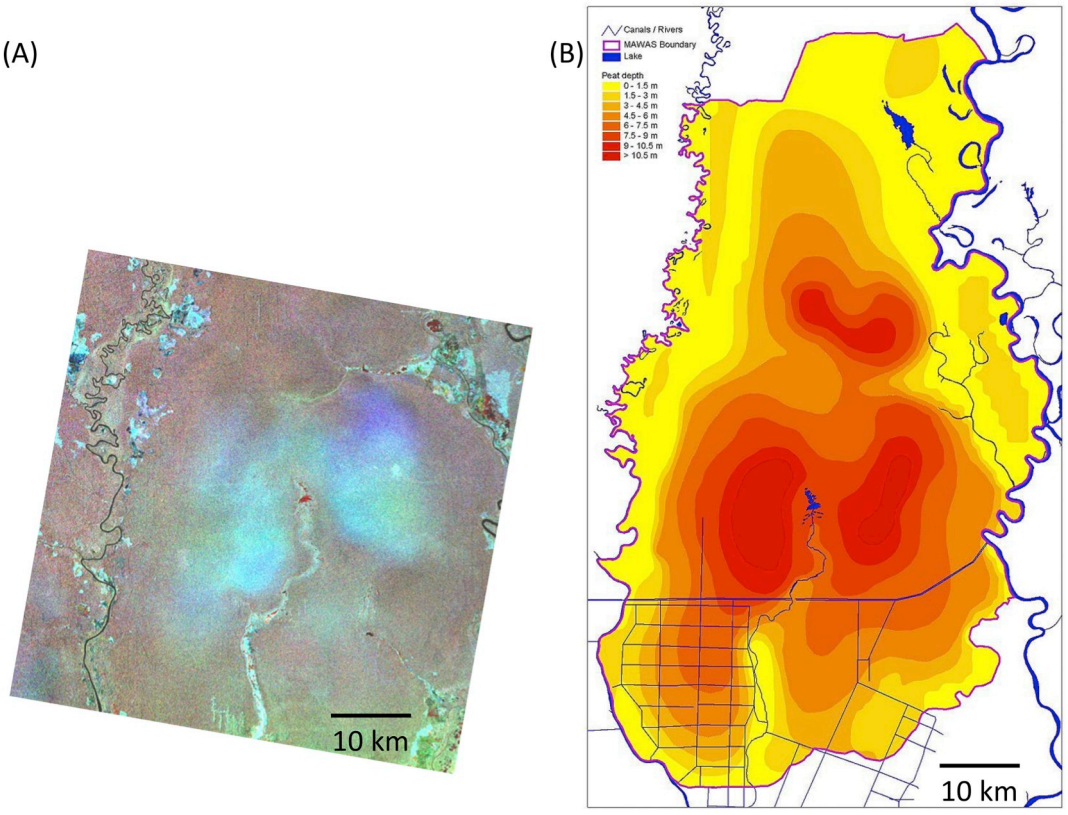

Fig. 23. A. JERS-1 multi-temporal composite image of a peat dome in Mawas, Central Kalimantan, (B) Peat thickness map on a 300,000 ha section of Mawas area derived from flood dynamics as detected from the JERS-1 time series. Figure courtesy of Dirk Hoekman used with permission.

7.2.3.1. Digital elevation model. Elevation and its derivatives from a DEM are important predictors of peatlands. Although peatlands in tropical regions such as Indonesia are in a relatively flat area, elevation appears to be an important predictor in peat thickness modelling because peat accumulates in dome-shaped structures (Figs. 2 and 24) (Anderson, 1964, 1961; Jaenicke et al., 2008).

There are several sources of data that can be used to derive a DEM.

SRTM DEM: the SRTM (Shuttle Radar Topography Mission) was flown on board the Space Shuttle Endeavor and mapped 80% of the Earth's land mass from 11 to 22 February of 2000. The sensor was a C-band Interferometric Synthetic Aperture Radar (InSAR) instrument. Due to the relatively short wavelength (5.6 cm), the majority of the return electromagnetic energy was affected by vegetation canopy (Hensley et al., 2000). The freely-available 1 arc-second (around 30 m resolution) DEM from the Shuttle Radar Topography Mission (SRTM) proves to be an important covariate for mapping peats (Table 4).

ASTER Global DEM: Advanced Spaceborne Thermal Emission and Reflection Radiometer (ASTER) provides a global DEM at a resolution

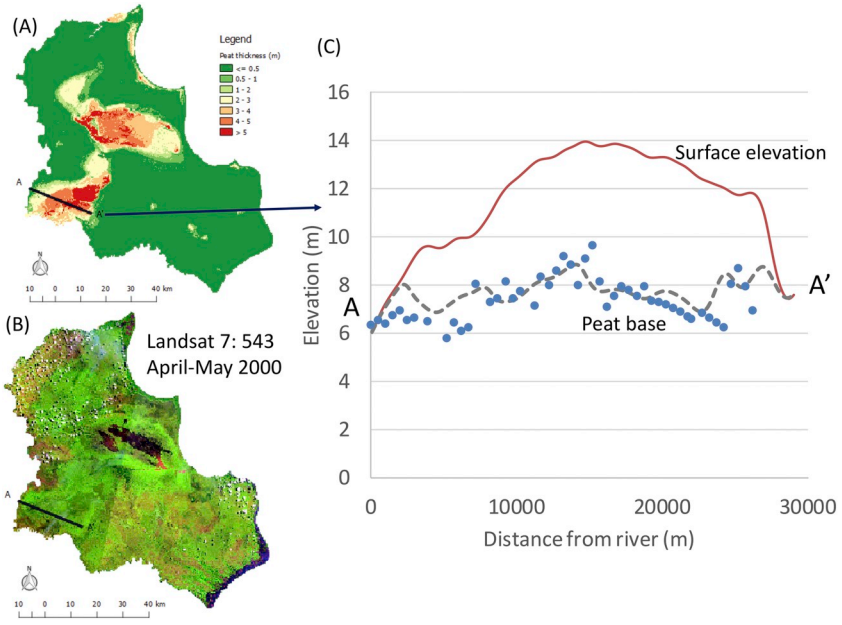

Fig. 24. (A) A map of peat thickness in Ogan Komerang Ilir, South Sumatra, Indonesia. (B) Landsat image. (C) The relationship between peat thickness and elevation along a transect across the peat dome. The dots refer to field observations of peat depth, and the dashed line is modelled peat depth based on a digital mapping model. (Based on Rudiyanto et al. (2016b)).

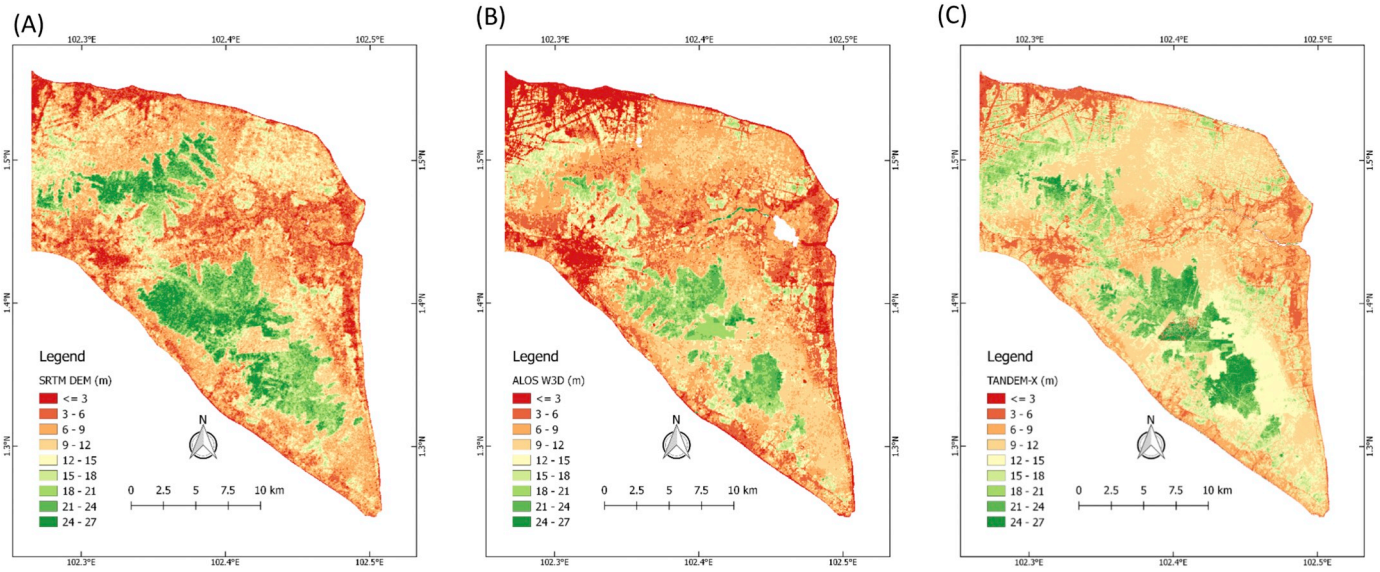

Fig. 25. Three sources of DEM of the eastern part of Bengkalis Island, Indonesia: (A) SRTM, (B) ALOS W3D, and (C) TanDEM-X.

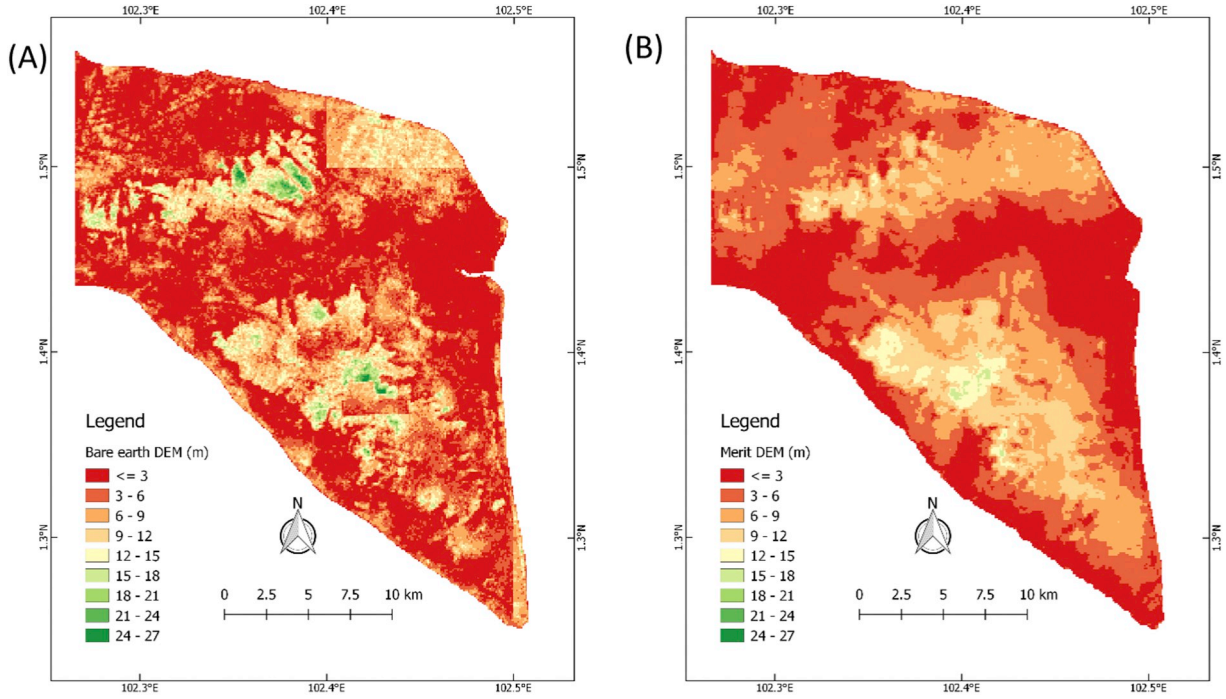

Fig. 26. Corrected DEM (or DTM) based on bare-earth SRTM and Merit DEM of Bengkalis island (Fig. 24).

of 90 m based on stereoscopic pairs and digital image correlation methods (Hirano et al., 2003). This DEM has artefacts due to poor stereo coverage at high latitudes, cloud interference, and water masking issues (Reuter et al., 2009).

ALOS World 3D (AW3D): a global DEM, digital surface model, and ortho-rectified image (ORI) was derived from the archived data of the Panchromatic Remote-sensing Instrument for Stereo Mapping (PRISM) onboard the Advanced Land Observing Satellite (ALOS), which operated from 2006 to 2011 (Tadono et al., 2014). It is freely available at a resolution of 30 m DEM. The 5 m digital surface model product is commercial.

TanDEM-X and WorldDEM: TanDEM-X (TerraSAR-X add-on for Digital Elevation Measurement) was launched in June 2010 by the German Aerospace Center (DLR). It is a synthetic aperture radar (SAR) which generated a global DEM based on two satellites flying in close formation (TanDEM-X and TerraSAR-X). It provides a 12 m resolution DEM. The DLR, in conjunction with Airbus DS, commercially produced and distributed the data (DEM and digital surface model) under the brand name WorldDEM (Collins et al., 2015).

DEM products vary in resolution and quality. In lowland areas with rapid land use changes, it is challenging to use the raw DEM as covariates for mapping. Fig. 25 shows three DEM products for the eastern part of Bengkalis Island in Indonesia. The two main elevated areas are peat domes. The difference in elevation is due to tree height differences from deforestation and afforestation. Various algorithms were developed to retrieve a digital surface model out of a DEM.

Various terrain attributes can be derived from a DEM. Local attributes such as slope and curvatures commonly describe local processes (Holden and Connolly, 2011), while regional attributes such as topographic wetness index combined with upslope contributing flow area

and slope describe hydrological processes. MrVBF multiresolution index of valley bottom flatness (Gallant and Dowling, 2003), a topographic index to identify areas of deposition at a range of scales, was shown to be a good predictor of peat thickness in lowland area in Indonesia (Rudiyanto et al., 2018). Margono et al. (2014a) calculated relative changes in height with respect to hydrological stream flow which proved to be a good predictor for wetland classification. Distances to a river or other landscape features are also important covariates as found by Mirmanto et al. (2003) and Rudiyanto et al. (2018). Depending on the topography and formation of peats, different terrain attributes may have different prediction capacities.

DEM resolution may also affect the predictability of peat areas. Fine resolution LiDAR DEM characterises local topography, while a coarser resolution DEM characterises local relief. A common unsupported belief is that the use of a finer resolution DEM will improve the accuracy and precision of the prediction over a coarser DEM. Knight et al. (2013) compared DEMs derived from LiDAR at a 3 m resolution with a national DEM at a 10 m resolution for mapping a palustrine wetland in Minnesota, USA. They also used a variety of datasets including high resolution optical imagery, and radar. The study found that the choice of topographic attributes and resolution did not have statistically significant influences on accuracy. The site was a relatively low wetland and topographic diversities captured by the coarser DEM were sufficient. In a more general DSM study, Samuel-Rosa et al. (2015) demonstrated that using more detailed or fine scale covariates only slightly improved the spatial prediction of soil properties. They further concluded that the modest increase in accuracy might not outweigh the extra costs of using more detailed covariates. Cavazzi et al. (2013) found that in flat homogeneous areas, coarser resolution DEMs perform best in terms of accuracy in prediction. Areas which are morphologically varied, such as abrupt changes in topography reflected in steep slopes, are better mapped with fine resolution DEM.

7.2.4. DEM correction

As shown in Fig. 25, the DEM is affected by vegetation height (O'Loughlin et al., 2016), especially in lowlands, which may affect prediction accuracy if used in modelling. O'Loughlin et al. (2016) produced a 'Bare-Earth' DEM based on the SRTM. Tree cover per cent was estimated from the MODIS satellite, and a global vegetation height map (Simard et al., 2011) was used to remove the vegetation height. Subsequently, Yamazaki et al. (2017) produced a global Multi-Error-Removed Improved-Terrain DEM (MERIT DEM) at 3 arc sec resolution (~90 m resolution) by removing bias, stripe noise, speckle noise, and tree height using multiple satellite data sets and filtering techniques. They used SRTM DEM (below N60°) and the AW3D DEM (above N60°) as the baseline DEMs. The Geoscience Laser Altimeter System (GLAS) aboard ICESat (Ice, Cloud, and land Elevation Satellite) that provided global LiDAR data were used as the reference ground elevation for correcting bias. A global tree density map and tree height map was used to correct for vegetation. Further noise was removed by applying an adaptive smoothing filter.

Fig. 26 shows the vegetation corrected DEM based on the bare-earth (O'Loughlin et al., 2016) and the Merit DEM (Yamazaki et al., 2017) products. Artefacts can be seen on the bare-earth model which suggest that local correction for vegetation is essential. Meanwhile, the Merit DEM seems to be over-smoothed.

Different DEM products captured in different years in areas with dynamic land use allows us to estimate tree heights in the deforested area (Avtar and Sawada, 2013). The tree height for the whole area can be estimated using Landsat images, providing an accurate way to correct the DEM for trees. Fig. 14 shows the difference between SRTM and AW3D DEM which has a time lag of 8 years, representing trees that were lost due to deforestation. The tree height data were intersected with a cloud-free Landsat 5 Thematic Mapper (TM) image that was acquired close to the SRTM period. A neural network model was generated to predict vegetation height throughout the area based on Landsat bands allowing the creation of a fine-scale tree height corrected DEM (Fig. 27).

7.2.5. LiDAR

LiDAR (Light Detection and Ranging), often used in airborne mapping, can create a 3-D model of the earth's surface (Hopkinson et al., 2005). Laser pulses reflect objects both on and above the ground surface, enabling estimation of both ground surfaces and aboveground objects such as trees. LiDAR is mostly useful for estimating tree biomass and above ground C stock, but it can also be used to generate Digital Terrain Models (DTM). To do this, ground points (points from LiDAR pulses reflected from the ground surface) are first separated from vegetation points, then interpolated for the whole area based on morphology and terrain (Maguya et al., 2014).

As the acquisition of LiDAR is expensive, it is commonly used in areas < 400 km^2 (Table 4) for mapping peat burn depth, gully

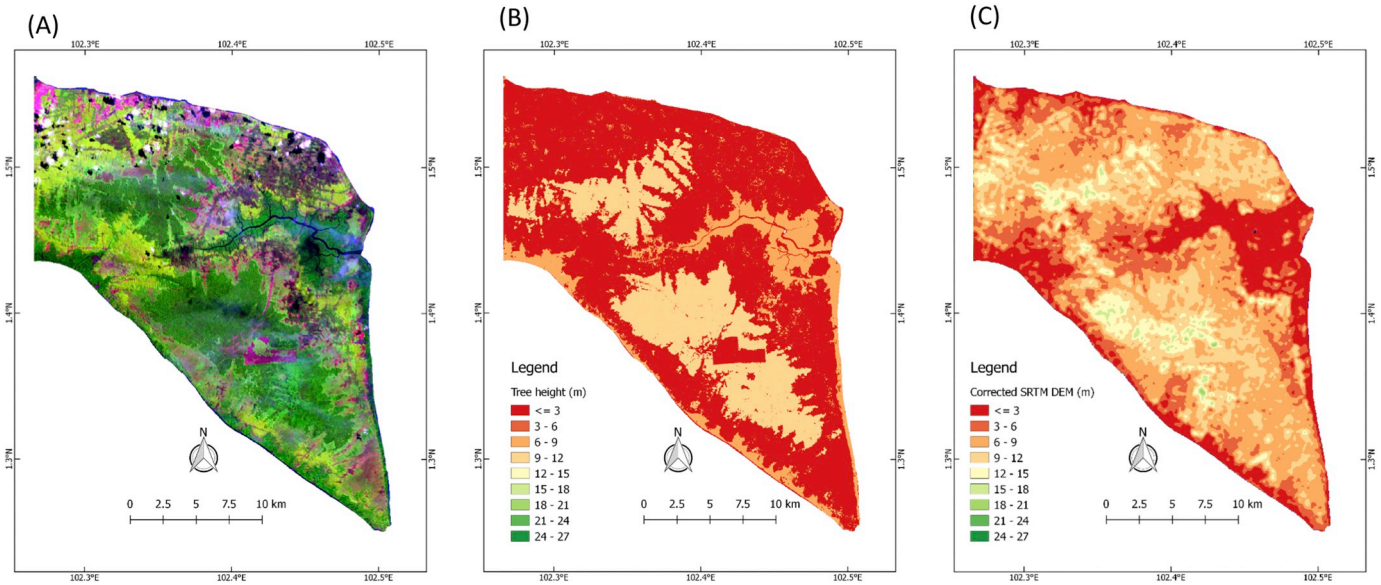

Fig. 27. (A) Landsat image is used to generate a land cover map, (B) modelled tree height estimated from the difference between AW3D DEM and SRTM, and (C) tree corrected SRTM.

networks, or as a covariate for mapping peat thickness (Gatis et al., 2019). While LiDAR can provide high resolution DEM and DTM, it can have errors in areas with dense, short-sward vegetation which disrupt the return of the laser pulse from the ground surface. This underestimates the vegetation canopy height and surface-drainage network depth (Luscombe et al., 2015).

7.2.6. Structure from Motion DEM

Digital elevation models can be created by overlapping aerial photographs taken from different viewing angles collected from a low-altitude unmanned aerial vehicle (UAV) system (Simpson et al., 2016). The Structure from Motion technique (Fonstad et al., 2013) can be used to reconstruct point clouds to produce DTMs (or vegetation corrected DEMs). Fonstad et al. (2013) demonstrated this over a 5.2 ha peatland in Jambi, Indonesia, by estimating burn depth based on pre-and post-fire DTMs. The Fonstad et al. (2013) paper shows that it is possible to use UAV to provide detailed optical and elevation data for areas that required detailed study.

8. Conclusions and further research

Peatlands hold about 5–20% of global carbon stocks and provide a variety of ecosystem services. Climate change and rapid land use change are degrading peatlands, liberating their stored C into the atmosphere.

Various countries have regulations on the protection of peatlands (Law et al., 2015), and some restoration efforts are underway. In 2016, the Indonesian government established the peatland restoration agency (Badan Restorasi Gambut, BRG) to coordinate and facilitate peat restoration. In Ireland, protected peatlands are linked to Natura 2000, an EU network of nature protection sites. Restoration works following peat extraction are underway and specific emission factors for rewetted peatlands (Wilson et al., 2016a, 2016b) are being explored. In some countries, however, peat has limited protection. In Chile, for example, peatlands are currently recognised as a non-metallic resource in the Mining Code, giving priorities to extraction over conservation.

Peatlands have been discussed at the global level by various UN agencies (Crump, 2017). From 2021, the EU requires that member states report on the emission and removals of greenhouse gases from wetlands (European-Parliament, 2018). Such reporting requires understanding and quantifying current peatland extent, condition, C stocks, and land use (Connolly, 2018). Bord na Mona (1984) argued “peat for fuel” as a motivation for mapping and inventory. Now we must map peatlands to mitigate climate change.

Current global peatland knowledge and mapping are poor. Peatlands are fragmented, cover a relatively small land area (around 3% globally), and are often overlooked in large-scale soil surveys. There is considerable uncertainty on the spatial extent of peatlands and their C stock, both nationally and globally, with global estimates of C stored in peatland ranging from 113 to 612 Pg.

Accurate peatland mapping is essential to secure and restore degraded peatlands, to better estimate soil C stocks, and to achieve the Paris Agreement. Digital soil mapping is an avenue to map and quantify global peatlands. Despite varying peat types across the globe (i.e., Northern, tropical vs Southern latitude), the framework using DSM methods is universal. Local calibration of field observations and covariates is essential for more accurate peat maps and estimates of carbon stocks. Models calibrated in Scotland, for example, cannot be applied in Indonesia.

Based on this review and experiences from different countries, some emerging research questions that can be addressed using DSM:

- What is the global extent of current peatland and its C stock?
- How do current global peatlands respond to climate change?
- Can we map areas with the most rapid peat changes stemming from land use change?
- How can DSM further understanding of how peatlands are distributed across the globe and hydrological units?

Immediate technical challenges and opportunities for mapping peatlands include:

1. **Methodological challenges**

- Open digital mapping

The proliferation of satellite data available in an open-access format, availability of machine learning algorithms in open source computing environment and (not so free) high-performance computing facility such as Google Earth Engine (Hird et al., 2017; Padarian et al., 2015) have enhanced the way soil can be mapped. There are advantages to using this information to generate efficient and accountable digital soil maps. Rudiyanto et al. (2018) proposed an open digital mapping methodology which used open-access data in an open source computing environment for mapping peatlands. This approach is transparent, and therefore repeatable and accountable. A similar procedure has been demonstrated in Scotland and mapping wetlands in Canada (Hird et al., 2017). Open-access methods can be scaled to a national extent for countries such as Brazil and Indonesia by performing fieldwork and computer modelling in parallel.

- Covariates

Gamma radiometrics appear to be the most efficient covariate for delineating peat extent. However, not all countries have such data. In the absence of gamma radiometrics, there are other, powerful covariates for peatland mapping. Rather than relying on a single covariate such as LiDAR data, multi-source remotely-sensed data derived from geographical information, optical, and radar images produce better predictions. Adding multi-temporal dimensions to optical and radar information has been shown to be effective in mapping peat and possibly providing information on peat thickness.

- A better sampling methodology

Many ecological studies sample based on transects and use this data to calibrate spatial models. While transect sampling is efficient for field observation, it usually gives a biased prediction when the data is used for model calibration (Hengl et al., 2003). Sampling based on the covariates or sampling the feature space is more effective for model calibration in DSM (Brungard and Boettinger, 2010). For example, a conditioned Latin hypercube sampling (cLHS) approach that samples along the distribution of the covariates has been found to be effective for developing DSM models. Sampling should also consider limited access, as natural peat is commonly not easily accessible (Dargie et al., 2017). The cLHS approach incorporating operational constraints such as access (Roudier et al., 2012) has been developed, and it would be an advantage to apply it to mapping peat areas.

- Mapping the thickness of the organic horizon

Mapping peat thickness and C stock in an area usually involves a two-step approach because peat occurs together with mineral soils. Peat thickness data is called ‘zero-inflated’. The first step models peat extent, the second step maps peat thickness. Mapping peat thickness is more accurate than assuming a constant peat thickness throughout a peat type.

The mixture model, which models peat thickness or C content distributions as a mixture of mineral and organic soils could be a useful technique. The model defines peat and mineral components where each could have a different distributional type, can potentially be used to describe these types of data. The Bayesian method can be used to

estimate the parameters of the distribution directly from the data (Leisch, 2004). This mixture model is promising and yet to be explored for peat mapping.

- Uncertainty of peat extent, thickness, and C stock.

All mapping procedures and products need to be accompanied by the uncertainty of estimates. As there are many definitions and quantification methods, the uncertainty also needs to be clearly defined (Heuvelink, 2014). One statistical approach is to represent the uncertainty of the map as probability distributions. The uncertainty used in the GlobalSoilMap specification is defined as the 90% Prediction Interval (PI) which reports the range of values within which the true value is expected to occur 9 times out of 10 (Arrouays et al., 2014). The lower (5 percentile), median, and upper (95 percentile) estimate can be presented for maps of peat C stock (e.g., Rudiyanto et al., 2018).

2. **Global Challenge—to come up with a consistent peat map and C stock estimates with uncertainty.**

There is currently no high resolution and reliable peatland map of the world. Maps of wetlands and vegetation are frequently used as a proxy for peatlands, however coarse-scale peatland maps such as Xu et al. (2018) cannot capture local peatlands. Combining peat maps from various countries as a bottom-up approach following the GlobalSoilMap (Arrouays et al., 2014) approach would be ideal. Key challenges include defining a consistent set of peat classes and definitions across all countries and recognising legacy maps from different countries. The GlobalSoilMap needs to differentiate the properties of peat from mineral soils. Adding the thickness of organic horizon to the GlobalSoilMap data is one option. Technical challenges remain in distinguishing peatlands from wetlands and peat-containing permafrost soils.

While mapping peat on a global and national scale is important, DSM is also useful for detailed soil surveys in priority areas. This requires fine resolution images or remote sensing covariates.

3. Can digital mapping be used to monitor peat degradation or changes?

Earth observation satellites are now able to provide coverage of earth's condition, detecting changes in vegetation (Hansen et al., 2013). Satellite data such as from Sentinel 1 and 2 can provide temporal information (e.g. monthly), and using DSM modelling there is a possibility to map changes in peatland coverage over time. We still do not have a good estimate of contemporary potential C sequestration of peatlands in various ecosystems. Current global studies on peatland degradation are based on rough inventory estimates and a broad LULCF emission factor which is full of uncertainty (Leifeld and Menichetti, 2018).

4. **Knowledge discovery from peatland mapping**

Machine learning models provide non-linear relationships between covariates and peat occurrence and can reveal spatial correlations of the covariates. While correlation does not mean causation, DSM can provide new insights and formulate further questions regarding peat distribution, formation and management in different parts of the world.

Acknowledgements

Budiman Minasny received funding from the Australis-Indonesia Institute to conduct a part of the review. Zamir Libohova from the USDA NRCS helped in calculating and providing maps of organosols in the USA. Linda Gregory from CSIRO provided the calculation of the organic soil area in Australia. Alisa Bryce helped in reading and editing the manuscript.

References

Adams, W., 1973. The effect of organic matter on the bulk and true densities of some uncultivated podzolic soils. Eur. J. Soil Sci. 24, 10–17.
Airo, M.-L., Hyvönen, E., Lerssi, J., Leväniemi, H., Ruotsalainen, A., 2014. Tips and tools for the application of GTK's airborne geophysical data. In: Gelogical Survey of Finland, Report of Investigation. vol. 215. pp. 33.
Aitkenhead, M., 2017. Mapping peat in Scotland with remote sensing and site characteristics. Eur. J. Soil Sci. 68, 28–38.
Akumu, C.E., McLaughlin, J.W., 2014. Modeling peatland carbon stock in a delineated portion of the Nayshkootayaow river watershed in Far North, Ontario using an integrated GIS and remote sensing approach. CATENA 121, 297–306.
Altdorff, D., Bechtold, M., van der Kruk, J., Vereecken, H., Huisman, J.A., 2016. Mapping peat layer properties with multi-coil offset electromagnetic induction and laser scanning elevation data. Geoderma 261, 178–189.
Anderson, K., Bennie, J., Milton, E., Hughes, P., Lindsay, R., Meade, R., 2010. Combining LiDAR and IKONOS data for eco-hydrological classification of an ombrotrophic peatland. J. Environ. Qual. 39, 260–273.
Andriesse, J., 1988. Nature and management of tropical peat soils. In: Food & Agriculture Organisation, Rome.
Antropov, O., Rauste, Y., Astola, H., Praks, J., Hame, T., Hallikainen, M.T., 2014. Land cover and soil type mapping from spaceborne PolSAR data at L-band with probabilistic neural network. IEEE Trans. Geosci. Remote Sens. 52, 5256–5270.
Arrouays, D., Grundy, M.G., Hartemink, A.E., Hempel, J.W., Heuvelink, G.B., Hong, S.Y., Lagacherie, P., Lelyk, G., McBratney, A.B., McKenzie, N.J., 2014. GlobalSoilMap: Toward a Fine-Resolution Global Grid of Soil Properties, Advances in Agronomy. Elsevier, pp. 93–134.
Ausseil, A.-G., Jamali, H., Clarkson, B., Golubiewski, N., 2015. Soil carbon stocks in wetlands of New Zealand and impact of land conversion since European settlement. Wetl. Ecol. Manag. 23, 947–961.
Avalos, E.B., Malone, D.H., Peterson, E.W., Anderson, W.P., Gehrels, R.W., 2016. Two-dimensional seismic refraction tomography of a buried bedrock valley at Hallsands beach, Devon, United Kingdom. Environ. Geosci. 23, 179–193.
Avtar, R., Sawada, H., 2013. Use of DEM data to monitor height changes due to deforestation. Arab. J. Geosci. 6, 4859–4871.
Ballhorn, U., Siegert, F., Mason, M., Limin, S., 2009. Derivation of burn scar depths and estimation of carbon emissions with LIDAR in Indonesian peatlands. Proc. Natl. Acad. Sci. 106, 21213–21218.
Bartsch, A., Kidd, R.A., Pathe, C., Scipal, K., Wagner, W., 2007. Satellite radar imagery for monitoring inland wetlands in boreal and sub-arctic environments. Aquat. Conserv. Mar. Freshwat. Ecosyst. 17, 305–317.
Batjes, N.H., 1996. Total carbon and nitrogen in the soils of the world. Eur. J. Soil Sci. 47, 151–163.
Bauer, I.E., Bhatti, J.S., Cash, K.J., Tarnocai, C., Robinson, S.D., 2006. Developing statistical models to estimate the carbon density of organic soils. Can. J. Soil Sci. 86, 295–304.
Bazanov, V., Berezin, A., Savichev, O.G., Skugarev, A., 2009. The phytoindication method for mapping peatlands in the taiga zone of the West-Siberian Plain. Int. J. Environ. Stud. 66, 473–484.
BBSDLP, 2011. Peta Lahan Gambut Indonesia Skala 1: 250.000 (Indonesian Peatland Map at the Scale 1: 250,000). Indonesian Center for Agricultural Land Resources Research and Development, Bogor, Indonesia.
Beamish, D., 2013. Gamma ray attenuation in the soils of Northern Ireland, with special reference to peat. J. Environ. Radioact. 115, 13–27.
Beamish, D., 2014. Peat mapping associations of airborne radiometric survey data. Remote Sens. 6, 521–539.
Beilman, D.W., Vitt, D.H., Bhatti, J.S., Forest, S., 2008. Peat carbon stocks in the southern Mackenzie River Basin: Uncertainties revealed in a high-resolution case study. Glob. Chang. Biol. 14, 1221–1232.
Berglund, Ö., Berglund, K., 2008. Odlad organogen jord i Sverige 2003 - Areal och grödfördelning uppskattad med hjälp av digitaliserade databaser. In: 1653–6797, SLU, Inst. för Markvetenskap, avd. för hydroteknik, Uppsala.
Berglund, Ö., Berglund, K., 2010. Distribution and cultivation intensity of agricultural peat and gyttja soils in Sweden and estimation of greenhouse gas emissions from cultivated peat soils. Geoderma 154, 173–180.
Beutler, S.J., Pereira, M.G., Tassinari, W.d.S., Menezes, M.D.d., Valladares, G.S., Anjos, L.H.C.d., 2017. Bulk density prediction for Histosols and soil horizons with high organic matter content. Revista Brasileira de Ciência do Solo 41.
Bjelm, L., 1980. Geological interpretation with subsurface interface radar in peat lands. In: Proceedings of the 6th International Peat Congress, Duluth, USA.
Bord na Mona, 1984. Fuel Peat in Developing Countries. Washinton D.C., USA.
Bourgeau-Chavez, L.L., Endres, S., Powell, R., Battaglia, M.J., Benscoter, B., Turetsky, M., Kasischke, E.S., Banda, E., 2017. Mapping boreal peatland ecosystem types from multitemporal radar and optical satellite imagery. Can. J. For. Res. 47, 545–559.
Bronge, L.B., Näslund-Landenmark, B., 2002. Wetland classification for Swedish CORINE Land Cover adopting a semi-automatic interactive approach. Can. J. Remote. Sens. 28, 139–155.
Brown, E., Aitkenhead, M., Wright, R., Aalders, I., 2007. Mapping and classification of peatland on the Isle of Lewis using Landsat ETM+. Scott. Geogr. J. 123, 173–192.
Bruneau, P.M.C., Johnson, S.M., 2014. Scotland's peatland-definitions & information resources (No. 701). Scottish Natural Heritage, Scotland, UK.
Brungard, C., Boettinger, J., 2010. Conditioned Latin Hypercube Sampling: Optimal Sample Size for Digital Soil Mapping of Arid Rangelands in Utah, USA, Digital Soil Mapping. Springer, pp. 67–75.
Buffam, I., Carpenter, S.R., Yeck, W., Hanson, P.C., Turner, M.G., 2010. Filling holes in

regional carbon budgets: predicting peat depth in a north temperate lake district. Journal of Geophysical Research: Biogeosciences (G1), 115.
Camporese, M., Ferraris, S., Putti, M., Salandin, P., Teatini, P., 2006. Hydrological modeling in swelling/shrinking peat soils. Water Resour. Res. 42.
Campos, J.R.D.R., Christófaro Silva, A., Nanni, M.R., dos Santos, M., Vidal-Torrado, P., 2017. Influence of the structural framework on peat bog distribution in the tropical highlands of Minas Gerais, Brazil. Catena 156, 228–236.
Cavazzi, S., Corstanje, R., Mayr, T., Hannam, J., Fealy, R., 2013. Are fine resolution digital elevation models always the best choice in digital soil mapping? Geoderma 195, 111–121.
Charman, D.J., Amesbury, M.J., Hinchliffe, W., Hughes, P.D.M., Mallon, G., Blake, W.H., Daley, T.J., Gallego-Sala, A.V., Mauquoy, D., 2015. Drivers of Holocene peatland carbon accumulation across a climate gradient in northeastern North America. Quat. Sci. Rev. 121, 110–119.
Chasmer, L., Hopkinson, C., Montgomery, J., Petrone, R., 2016. A physically based terrain morphology and vegetation structural classification for wetlands of the Boreal Plains, Alberta, Canada. Can. J. Remote. Sens. 42, 521–540.
Chasmer, L., Hopkinson, C., Petrone, R., Sitar, M., 2017. Using multitemporal and multispectral airborne lidar to assess depth of peat loss and correspondence with a new active normalized burn ratio for wildfires. Geophys. Res. Lett. 44, 11851–11859.
Clarke, D., 2010. Brown Gold: A History of Bord Na Móna and the Peat Industry in Ireland. Gill & Macmillan.
Cobb, A.R., Hoyt, A.M., Gandois, L., Eri, J., Dommain, R., Salim, K.A., Kai, F.M., Su'ut, N.S.H., Harvey, C.F., 2017. How temporal patterns in rainfall determine the geomorphology and carbon fluxes of tropical peatlands. Proc. Natl. Acad. Sci. 114 (26), E5187–E5196.
Collins, J., Riegler, G., Schrader, H., Tinz, M., 2015. Applying terrain and hydrological editing to TanDEM-X data to create a consumer-ready WorldDEM product. In: The International Archives of Photogrammetry, Remote Sensing and Spatial Information Sciences. vol. 40. pp. 1149.
Comas, X., Slater, L., 2004. Low-frequency electrical properties of peat. Water Resour. Res. 40 (12).
Comas, X., Terry, N., Slater, L., Warren, M., Kolka, R., Kristijono, A., Sudiana, N., Nurjaman, D., Darusman, T., 2015. Imaging tropical peatlands in Indonesia using ground penetrating radar (GPR) and electrical resistivity imaging (ERI): implications for carbon stock estimates and peat soil characterization. Biogeosciences 12.
Connolly, J., 2018. Baseline mapping of land use on Irish peatlands using medium resolution satellite imagery. Ir. Geogr. 51 (2), 187–204.
Connolly, J., Holden, N.M., 2009. Mapping peat soils in Ireland: updating the derived Irish peat map. Ir. Geogr. 42, 343–352.
Connolly, J., Holden, N., 2017. Detecting peatland drains with Object based image Analysis and Geoeye-1 imagery. Carbon balance and management 12, 7.
Connolly, J., Holden, N.M., Ward, S.M., 2007. Mapping peatlands in Ireland using a rule-based methodology and digital data. Soil Sci. Soc. Am. J. 71, 492–499.
Coombs, D.B., Thie, J., 1979. The Canadian Land Inventory System. In: Beatty, M., Petersen, G., LD, S. (Eds.), Planning the Uses and Management of Land. American Society of Agronomy, Madison, Wisconsin, pp. 909–933.
Cotching, W.E., Lynch, S., Kidd, D.B., 2009. Dominant soil orders in Tasmania: distribution and selected properties. Soil Research 47, 537–548.
Creamer, R., Simo, I., Reidy, B., Fealy, R., Mayr, T., Hallett, S., Holden, N., Schulte, R., 2014. Irish Soil Information System. TResearch, Soils Special Autumn. pp. 16–17.
Crichton, K., Anderson, K., Bennie, J., Milton, E., 2015. Characterizing peatland carbon balance estimates using freely available Landsat ETM+ data. Ecohydrology 8, 493–503.
Crooks, S., Herr, D., Tamelander, J., Laffoley, D., Vandever, J., 2011. Mitigating climate change through restoration and management of coastal wetlands and near-shore marine ecosystems: Challenges and opportunities. In: Environment Department Paper 121. World Bank, Washington, DC.
Cruickshank, M., Tomlinson, R., 1990. Peatland in Northern Ireland: inventory and prospect. Ir. Geogr. 23, 17–30.
Crump, J., 2017. Smoke on Water–Countering Global Threats from Peatland Loss and Degradation. A UNEP Rapid Response Assessment. United Nations Environment Programme and GRID-Arendal, Nairobi and Arendal.
Daily, W., Ramirez, A., LaBrecque, D., Nitao, J., 1992. Electrical resistivity tomography of vadose water movement. Water Resour. Res. 28 (5), 1429–1442.
Dargie, G.C., Lewis, S.L., Lawson, I.T., Mitchard, E.T., Page, S.E., Bocko, Y.E., Ifo, S.A., 2017. Age, extent and carbon storage of the Central Congo Basin peatland complex. Nature 542, 86–90.
De Bakker, H., Schelling, J., 1989. System of Soil Classification for the Netherlands: The Higher Levels, 2nd edition. Winand Staring Centre, Wageningen.
De Vries, F., Lesschen, J., van den Akker, J., Petrescu, A., van Huissteden, J., van den Wyngaert, I., 2009. Bodemgerelateerde emissie van broeikasgassen in Drenthe: de huidige situatie. 1566–7197, Alterra.
De Vries, F., Brus, D.J., Kempen, B., Brouwer, F., Heidema, A., 2014. Actualisatie bodemkaart veengebieden: deelgebied en 2 in Noord Nederland. 1566–7197, Alterra Wageningen UR.
Dissanska, M., Bernier, M., Payette, S., 2009. Object-based classification of very high resolution panchromatic images for evaluating recent change in the structure of patterned peatlands. Can. J. Remote. Sens. 35, 189–215.
Dos Santos, H., Carvalho Junior, W., Dart, R., Áglio, M., de Sousa, J., Pares, J., Fontana, A., Martins, A.D.S., de oliveira, A., 2011. O novo mapa de solos do Brasil: legenda atualizada. In: Embrapa Solos-Documentos (INFOTECA-E).
Draper, F.C., Roucoux, K.H., Lawson, I.T., Mitchard, E.T., Coronado, E.N.H., Lähteenoja, O., Montenegro, L.T., Sandoval, E.V., Zaráte, R., Baker, T.R., 2014. The distribution and amount of carbon in the largest peatland complex in Amazonia. Environ. Res. Lett. 9, 124017.
Ek, B., Aaro, S., Näslund-Landenmark, B., 1992. Utnyttjande av flygradiometriska data och IR-bilder vid inventering av sumpskogar och andra våtmarker. SGU och Lantmäteriverket, Uppsala.
Embrapa Solos, 2013. Sistema brasileiro de classificação de solos. Centro Nacional de Pesquisa de Solos, Rio de Janeiro, Brazil.
European Parliament, 2018. Inclusion of greenhouse gas emissions and removals from land use, land use change and forestry into the 2030 climate and energy framework. In: Parliament, E. (Ed.), P8_TA-PROV(2018)0096, Strasbourg.
Evans, M., Lindsay, J., 2010. High resolution quantification of gully erosion in upland peatlands at the landscape scale. Earth Surf. Process. Landf. 35, 876–886.
Fan, S., 1988. Applications of Remote-Sensing Techniques in Peat Resource Investigations in Zoigê. Acta Geologica Sinica (English Edition) 1, 101–112.
Farmer, J., Matthews, R., Smith, P., Langan, C., Hergoualc'h, K., Verchot, L., Smith, J.U., 2014. Comparison of methods for quantifying soil carbon in tropical peats. Geoderma 214-215, 177–183.
Fonstad, M.A., Dietrich, J.T., Courville, B.C., Jensen, J.L., Carbonneau, P.E., 2013. Topographic structure from motion: a new development in photogrammetric measurement. Earth Surf. Process. Landf. 38, 421–430.
Fournier, R.A., Grenier, M., Lavoie, A., Hélie, R., 2007. Towards a strategy to implement the Canadian Wetland Inventory using satellite remote sensing. Can. J. Remote. Sens. 33, S1–S16.
Gallant, J.C., Dowling, T.I., 2003. A multiresolution index of valley bottom flatness for mapping depositional areas. Water Resour. Res. 39.
Gardiner, M., Radford, T., 1980. Ireland: General Soil Map, 2nd edition. Teagasc, Dublin, Ireland.
Gatis, N., Luscombe, D.J., Carless, D., Parry, L.E., Fyfe, R.M., Harrod, T.R., Brazier, R.E., Anderson, K., 2019. Mapping upland peat depth using airborne radiometric and lidar survey data. Geoderma 335, 78–87.
Geboy, N.J., Olea, R.A., Engle, M.A., Martín-Fernández, J.A., 2013. Using simulated maps to interpret the geochemistry, formation and quality of the Blue Gem coal bed, Kentucky, USA. Int. J. Coal Geol. 112, 26–35.
Grenier, M., Labrecque, S., Garneau, M., Tremblay, A., 2008. Object-based classification of a SPOT-4 image for mapping wetlands in the context of greenhouse gases emissions: the case of the Eastmain region, Québec, Canada. Can. J. Remote. Sens. 34, S398–S413.
Greve, M.H., Christensen, O.F., Greve, M.B., Kheir, R.B., 2014. Change in peat coverage in Danish cultivated soils during the past 35 years. Soil Sci. 179, 250–257.
Grover, S., 2006. Carbon and Water Dynamics of Peat Soils in the Australian Alps (PhD Thesis). La Trobe University, Bundoora, Victoria, pp. 205.
Grundy, M., Viscarra Rossel, R.A., Searle, R., Wilson, P., Chen, C., Gregory, L., 2015. The Soil and Landscape Grid of Australia. Soil Research 53, 835–844.
Gumbricht, T., Roman-Cuesta, R.M., Verchot, L., Herold, M., Wittmann, F., Householder, E., Herold, N., Murdiyarso, D., 2017. An expert system model for mapping tropical wetlands and peatlands reveals South America as the largest contributor. Glob. Chang. Biol. 23, 3581–3599.
Haapanen, R., Tokola, T., 2007. Creating a digital treeless peatland map using satellite image interpretation. Scand. J. For. Res. 22, 48–59.
Hallgren, G., Berglund, G., 1962. De odlade myrjordarnas omfattning och användning. Skrivelse till styrelsen för lantbrukshögskolan och statens lantbruksförsök. Swedish University of Agricultural Sciences, Uppsala.
Hammond, R.F., 1979. The Peatlands of Ireland, to Accompany New Peatland Map of Ireland and Ireland Peatland Map. Foras Talúntais.
Hansen, M.C., Potapov, P.V., Moore, R., Hancher, M., Turubanova, S., Tyukavina, A., Thau, D., Stehman, S., Goetz, S., Loveland, T., 2013. High-resolution global maps of 21st-century forest cover change. Science 342, 850–853.
Harris, A., Bryant, R.G., 2009. A multi-scale remote sensing approach for monitoring northern peatland hydrology: present possibilities and future challenges. J. Environ. Manag. 90, 2178–2188.
Harris, A., Charnock, R., Lucas, R., 2015. Hyperspectral remote sensing of peatland floristic gradients. Remote Sens. Environ. 162, 99–111.
Heagy, L.J., Cockett, R., Kang, S., Rosenkjaer, G.K., Oldenburg, D.W., 2017. A framework for simulation and inversion in electromagnetics. Comput. Geosci. 107, 1–19.
Henderson, F.M., Lewis, A.J., 2008. Radar detection of wetland ecosystems: a review. Int. J. Remote Sens. 29, 5809–5835.
Hengl, T., Rossiter, D.G., Stein, A., 2003. Soil sampling strategies for spatial prediction by correlation with auxiliary maps. Soil Research 41, 1403–1422.
Hengl, T., de Jesus, J.M., Heuvelink, G.B., Gonzalez, M.R., Kilibarda, M., Blagotić, A., Shangguan, W., Wright, M.N., Geng, X., Bauer-Marschallinger, B., 2017. SoilGrids250m: Global gridded soil information based on machine learning. PLoS One 12, e0169748.
Hensley, S., Rosen, P., Gurrola, E., 2000. Topographic Map Generation from the Shuttle Radar Topography Mission C-Band SCANSAR Interferometry.
Hergoualc'h, K., Gutiérrez-Vélez, V.H., Menton, M., Verchot, L.V., 2017. Characterizing degradation of palm swamp peatlands from space and on the ground: an exploratory study in the Peruvian Amazon. For. Ecol. Manag. 393, 63–73.
Heuvelink, G.B., 2014. Uncertainty quantification of GlobalSoilMap products. In: GlobalSoilMap: Basis of the Global Spatial Soil Information System. Proceedings of 1st GlobalSoilMap Conference, pp. 335–340.
Hewitt, A.E., 2010. New Zealand Soil Classification. Landcare Research Science Series, New Zealand.
Hirano, A., Welch, R., Lang, H., 2003. Mapping from ASTER stereo image data: DEM validation and accuracy assessment. ISPRS J. Photogramm. Remote Sens. 57, 356–370.
Hird, J.N., DeLancey, E.R., McDermid, G.J., Kariyeva, J., 2017. Google Earth Engine, Open-Access Satellite Data, and Machine Learning in support of Large-Area Probabilistic Wetland Mapping. Remote Sens. 9, 1315.

Hoekman, D.H., 2007. Satellite radar observation of tropical peat swamp forest as a tool for hydrological modelling and environmental protection. Aquat. Conserv. Mar. Freshwat. Ecosyst. 17, 265–275.
Hoekman, D.H., Vissers, M.A., Wielaard, N., 2010. PALSAR wide-area mapping of Borneo: methodology and map validation. IEEE Journal of Selected Topics in Applied Earth Observations and Remote Sensing 3, 605–617.
Holden, N.M., Connolly, J., 2011. Estimating the carbon stock of a blanket peat region using a peat depth inference model. CATENA 86, 75–85.
Holden, J., Burt, T., Vilas, M., 2002. Application of ground-penetrating radar to the identification of subsurface piping in blanket peat. Earth Surf. Process. Landf. 27, 235–249.
Hoogland, T., van den Akker, J.J.H., Brus, D.J., 2012. Modeling the subsidence of peat soils in the Dutch coastal area. Geoderma 171-172, 92–97.
Hooijer, A., Vernimmen, R., 2013. Peatland maps for Indonesia. Including accuracy assessment and recommendations for improvement, elevation mapping and evaluation of future flood risk. Quick Assessment and Nationwide Screening (QANS) of Peat and Lowland Resources and Action Planning for the Implementation of a National Lowland Strategy-PVW3A10002.
Hopkinson, C., Chasmer, L.E., Sass, G., Creed, I.F., Sitar, M., Kalbfleisch, W., Treitz, P., 2005. Vegetation class dependent errors in lidar ground elevation and canopy height estimates in a boreal wetland environment. Can. J. Remote. Sens. 31, 191–206.
Householder, J.E., Janovec, J.P., Tobler, M.W., Page, S., Lähteenoja, O., 2012. Peatlands of the Madre de Dios River of Peru: distribution, geomorphology, and habitat diversity. Wetlands 32, 359–368.
Hribljan, J.A., Suarez, E., Bourgeau-Chavez, L., Endres, S., Lilleskov, E.A., Chimbolema, S., Wayson, C., Serocki, E., Chimner, R.A., 2017. Multidate, multisensor remote sensing reveals high density of carbon-rich mountain peatlands in the páramo of Ecuador. Glob. Chang. Biol. 23, 5412–5425.
Huang, J., Monteiro Santos, F., Triantafilis, J., 2016. Mapping soil water dynamics and a moving wetting front by spatiotemporal inversion of electromagnetic induction data. Water Resour. Res. 52, 9131–9145.
Hugelius, G., Virtanen, T., Kaverin, D., Pastukhov, A., Rivkin, F., Marchenko, S., Romanovsky, V., Kuhry, P., 2011. High-resolution mapping of ecosystem carbon storage and potential effects of permafrost thaw in periglacial terrain, European Russian Arctic. Journal of Geophysical Research: Biogeosciences 116.
Hugelius, G., Routh, J., Kuhry, P., Crill, P., 2012. Mapping the degree of decomposition and thaw remobilization potential of soil organic matter in discontinuous permafrost terrain. Journal of Geophysical Research: Biogeosciences 117.
Hyvönen, E., Turunen, P., Vanhanen, E., Arkimaa, H., Sutinen, R., 2002. Airborne Gamma-Ray Surveys in Finland.
Hyvönen, E., Lerssi, J., Väänänen, T., 2003. Airborne Geophysical Surveys Assessing the General Scale Quaternary Mapping Project in Finland, 9th EAGE/EEGS Meeting.
Illés, G., Sutikno, S., Szatmári, G., Sandhyavitri, A., Pásztor, L., Kristijono, A., Molnár, G., Yusa, M., Székely, B., 2019. Facing the peat CO_2 threat: digital mapping of Indonesian peatlands—a proposed methodology and its application. J. Soils Sediments 1–16. https://doi.org/10.1007/s11368-019-02328-0.
Ingram, H., 1982. Size and shape in raised mire ecosystems: a geophysical model. Nature 297, 300–303.
Isbell, R., 2002. The Australian Soil Classification - Revised Edition, Australian Soil and Land Survey Handbooks Series 4. CSIRO PUBLISHING, Australia.
Itoh, M., Okimoto, Y., Hirano, T., Kusin, K., 2017. Factors affecting oxidative peat decomposition due to land use in tropical peat swamp forests in Indonesia. Sci. Total Environ. 609, 906–915.
Izquierdo, A.E., Foguet, J., Grau, H.R., 2015. Mapping and spatial characterization of argentine High Andean peatbogs. Wetl. Ecol. Manag. 23, 963–976.
Jackson, R.B., Lajtha, K., Crow, S.E., Hugelius, G., Kramer, M.G., Piñeiro, G., 2017. The ecology of soil carbon: pools, vulnerabilities, and biotic and abiotic controls. Annu. Rev. Ecol. Evol. Syst. 48, 419–445.
Jaenicke, J., Rieley, J.O., Mott, C., Kimman, P., Siegert, F., 2008. Determination of the amount of carbon stored in Indonesian peatlands. Geoderma 147, 151–158.
Joosten, H., 2009. The Global Peatland CO2 Picture: Peatland Status and Drainage Related Emissions in all Countries of the World.
Joosten, H., Clarke, D., 2002. Wise Use of Mires and Peatlands. vol. 304 International Mire Conservation Group and International Peat Society.
Joosten, H., Tapio-Biström, M.-L., Tol, S., 2012. Peatlands: Guidance for Climate Change Mitigation through Conservation, Rehabilitation and Sustainable Use. Food and Agriculture Organization of the United Nations.
Jowsey, P., 1966. An improved peat sampler. New Phytol. 65, 245–248.
Kang, L., 2009. Coal exploration and mining. In: Gao, J. (Ed.), Coal, Oil Shale, Natural Bitumen, Heavy Oil and Peat-Volume I. Eolss Publishers, Oxford, UK, pp. 92–112.
Keaney, A., McKinley, J., Graham, C., Robinson, M., Ruffell, A., 2013. Spatial statistics to estimate peat thickness using airborne radiometric data. Spatial Statistics 5, 3–24.
Kempen, B., Brus, D.J., Heuvelink, G.B., Stoorvogel, J.J., 2009. Updating the 1: 50,000 Dutch soil map using legacy soil data: a multinomial logistic regression approach. Geoderma 151, 311–326.
Kempen, B., Brus, D.J., Heuvelink, G.B., 2012a. Soil type mapping using the generalised linear geostatistical model: a case study in a Dutch cultivated peatland. Geoderma 189, 540–553.
Kempen, B., Brus, D.J., Stoorvogel, J.J., Heuvelink, G., de Vries, F., 2012b. Efficiency comparison of conventional and digital soil mapping for updating soil maps. Soil Sci. Soc. Am. J. 76, 2097–2115.
Kempen, B., Brus, D.J., de Vries, F., 2015. Operationalizing digital soil mapping for nationwide updating of the 1: 50,000 soil map of the Netherlands. Geoderma 241, 313–329.
Kennedy, C.D., Wilderotter, S., Payne, M., Buda, A.R., Kleinman, P.J.A., Bryant, R.B., 2018. A geospatial model to quantify mean thickness of peat in cranberry bogs. Geoderma 319, 122–131.
Kidd, D., Webb, M., Malone, B., Minasny, B., McBratney, A., 2015. Eighty-metre resolution 3D soil-attribute maps for Tasmania, Australia. Soil Research 53, 932–955.
Kimmel, K., Mander, U., 2010. Ecosystem services of peatlands: Implications for restoration. Prog. Phys. Geogr. 34, 491–514.
Klingenfuß, C., Roßkopf, N., Walter, J., Heller, C., Zeitz, J., 2014. Soil organic matter to soil organic carbon ratios of peatland soil substrates. Geoderma 235-236, 410–417.
Knight, J.F., Tolcser, B.P., Corcoran, J.M., Rampi, L.P., 2013. The effects of data selection and thematic detail on the accuracy of high spatial resolution wetland classifications. Photogramm. Eng. Remote Sens. 79, 613–623.
Köchy, M., Hiederer, R., Freibauer, A., 2015. Global distribution of soil organic carbon–part 1: Masses and frequency distributions of SOC stocks for the tropics, permafrost regions, wetlands, and the world. Soil 1, 351–365.
Kolka, R., Bridgham, S.D., Ping, C.-L., 2016. Soils of peatlands: Histosols and Gelisols. In: Vepraskas, M.J., Craft, C.L. (Eds.), Wetland Soils: Genesis, Hydrology, Landscapes, and Classification. CRC Press, Boca Raton, pp. 277–309.
Kool, D.M., Buurman, P., Hoekman, D.H., 2006. Oxidation and compaction of a collapsed peat dome in Central Kalimantan. Geoderma 137, 217–225.
Korpela, I., Koskinen, M., Vasander, H., Holopainen, M., Minkkinen, K., 2009. Airborne small-footprint discrete-return LiDAR data in the assessment of boreal mire surface patterns, vegetation, and habitats. For. Ecol. Manag. 258, 1549–1566.
Koszinski, S., Miller, B.A., Hierold, W., Haelbich, H., Sommer, M., 2015. Spatial Modeling of organic carbon in degraded Peatland soils of Northeast Germany. Soil Sci. Soc. Am. J. 79, 1496–1508.
Krankina, O., Pflugmacher, D., Friedl, M., Cohen, W., Nelson, P., Baccini, A., 2008. Meeting the challenge of mapping peatlands with remotely sensed data. Biogeosciences 5, 1809–1820.
Kumpula, T., Colpaert, A., Qian, W., Manderscheid, A., 2004. Remote sensing in inventory of high altitude pastures of the eastern Tibetan Plateau. Rangifer 24, 53–63.
Lähteenoja, O., Ruokolainen, K., Schulman, L., Oinonen, M., 2009. Amazonian peatlands: an ignored C sink and potential source. Glob. Chang. Biol. 15, 2311–2320.
Lähteenoja, O., Reátegui, Y.R., Räsänen, M., Torres, D.D.C., Oinonen, M., Page, S., 2012. The large Amazonian peatland carbon sink in the subsiding Pastaza-Marañón foreland basin, Peru. Glob. Chang. Biol. 18, 164–178.
Landcare-Research, 2000. Fundamental Soil Layer - New Zealand Soil Classification. https://lris.scinfo.org.nz/layer/48079-fsl-new-zealand-soil-classification/.
Latifovic, R., Pouliot, D., Olthof, I., 2017. Circa 2010 Land Cover of Canada: Local Optimization Methodology and Product Development. Remote Sens. 9, 1098.
Law, E.A., Bryan, B.A., Torabi, N., Bekessy, S.A., McAlpine, C.A., Wilson, K.A., 2015. Measurement matters in managing landscape carbon. Ecosystem Services 13, 6–15.
Lawson, I.T., Kelly, T., Aplin, P., Boom, A., Dargie, G., Draper, F., Hassan, P., Hoyos-Santillan, J., Kaduk, J., Large, D., 2015. Improving estimates of tropical peatland area, carbon storage, and greenhouse gas fluxes. Wetl. Ecol. Manag. 23, 327–346.
Leifeld, J., Menichetti, L., 2018. The underappreciated potential of peatlands in global climate change mitigation strategies. Nat. Commun. 9, 1071.
Leisch, F., 2004. Flexmix: a general framework for finite mixture models and latent class regression in R. J. Stat. Softw. 11, 1–18.
Li, J., Chen, W., 2005. A rule-based method for mapping Canada's wetlands using optical, radar and DEM data. Int. J. Remote Sens. 26, 5051–5069.
Lilburne, L., Hewitt, A., Webb, T., 2012. Soil and informatics science combine to develop S-map: a new generation soil information system for New Zealand. Geoderma 170, 232–238.
Lilja, H., Nevalainen, R., 2006. Chapter 5 developing a Digital Soil Map for Finland. In: Lagacherie, P., McBratney, A.B., Voltz, M. (Eds.), Developments in Soil Science. Elsevier, pp. 67–603.
Limpens, J., Berendse, F., Blodau, C., Canadell, J., Freeman, C., Holden, J., Roulet, N., Rydin, H., Schaepman-Strub, G., 2008. Peatlands and the carbon cycle: from local processes to global implications–a synthesis. Biogeosciences 5, 1475–1491.
Llanos, R., Moreira-Turcq, P., Huaman, Y., Espinoza, R., Apaestegui, J., Turcq, B., Willems, B., 2017. Carbon accumulation in high-altitude peatlands of the Central Andes of Peru. EGU General Assembly Conference Abstracts 10157.
Loftin, C.S., Rasberry, W., Kitchens, W.M., 2000. Development of a grid-cell topographic surface for Okefenokee Swamp, Georgia. Wetlands 20, 487–499.
Lottes, A.L., Ziegler, A.M., 1994. World peat occurrence and the seasonality of climate and vegetation. Palaeogeogr. Palaeoclimatol. Palaeoecol. 106, 23–37.
Lunden, B., Wang, G., Wester, K., 2001. A GIS based analysis of data from Landsat TM, airborne geophysical measurements, and digital maps for geological remote sensing in the Stockholm region, Sweden. Int. J. Remote Sens. 22, 517–532.
Luscombe, D.J., Anderson, K., Gatis, N., Wetherelt, A., Grand-Clement, E., Brazier, R.E., 2015. What does airborne LiDAR really measure in upland ecosystems? Ecohydrology 8, 584–594.
Lynn, I.H., Manderson, A.K., Page, M.J., Harmsworth, G.R., Eyles, G.O., Douglas, G.B., Mackay, A.D., Newsome, P.J.F., 2009. Land Use Capability survey handbook – a New Zealand handbook for the classification of land. AgResearch Hamilton; Manaaki Whenua Lincoln; GNS Science Lower Hutt, New Zealand.
Maguya, A.S., Junttila, V., Kauranne, T., 2014. Algorithm for extracting digital terrain models under forest canopy from airborne LiDAR data. Remote Sens. 6, 6524–6548.
Maltby, E., Immirzi, P., 1993. Carbon dynamics in peatlands and other wetland soils regional and global perspectives. Chemosphere 27, 999–1023.
Margono, B.A., Bwangoy, J.-R.B., Potapov, P.V., Hansen, M.C., 2014a. Mapping wetlands in Indonesia using Landsat and PALSAR data-sets and derived topographical indices. Geo-spatial Information Science 17, 60–71.
Margono, B.A., Potapov, P.V., Turubanova, S., Stolle, F., Hansen, M.C., 2014b. Primary forest cover loss in Indonesia over 2000–2012. Nat. Clim. Chang. 4, 730.
McBratney, A.B., Mendonça Santos, M.L., Minasny, B., 2003. On digital soil mapping. Geoderma 117, 3–52.

McCulloch, R.D., Davies, S.J., 2001. Late-glacial and Holocene palaeoenvironmental change in the Central Strait of Magellan, southern Patagonia. Palaeogeogr. Palaeoclimatol. Palaeoecol. 173, 143–173.
McKenzie, N., Jacquier, D., Isbell, R., Brown, K., 2004. Australian Soils and Landscapes: An illustrated compendium. CSIRO publishing, Melbourne, Australia.
Mercer, J.J., Westbrook, C.J., 2016. Ultrahigh-resolution mapping of peatland microform using ground-based structure from motion with multiview stereo. Journal of Geophysical Research: Biogeosciences 121, 2901–2916.
Merchant, M.A., Adams, J.R., Berg, A.A., Baltzer, J.L., Quinton, W.L., Chasmer, L.E., 2017. Contributions of C-Band SAR Data and Polarimetric Decompositions to Subarctic Boreal Peatland Mapping. IEEE Journal of Selected Topics in Applied Earth Observations and Remote Sensing 10, 1467–1482.
Middleton, M., Närhi, P., Arkimaa, H., Hyvönen, E., Kuosmanen, V., Treitz, P., Sutinen, R., 2012. Ordination and hyperspectral remote sensing approach to classify peatland biotopes along soil moisture and fertility gradients. Remote Sens. Environ. 124, 596–609.
Millard, K., Richardson, M., 2013. Wetland mapping with LiDAR derivatives, SAR polarimetric decompositions, and LiDAR–SAR fusion using a random forest classifier. Can. J. Remote. Sens. 39, 290–307.
Millard, K., Richardson, M., 2015. On the importance of training data sample selection in random forest image classification: a case study in peatland ecosystem mapping. Remote Sens. 7, 8489–8515.
Minasny, B., McBratney, A.B., 2016. Digital soil mapping: a brief history and some lessons. Geoderma 264, 301–311.
Minasny, B., McBratney, A.B., Malone, B.P., Wheeler, I., 2013. Digital mapping of soil carbon. Adv. Agron. 118, 1–47.
Mirmanto, E., Tsuyuzaki, S., Kohyama, T., 2003. Investigation of the effects of distance from river and peat depth on tropical wetland forest communities. Tropics 12, 287–294.
Mitra, S., Wassmann, R., Vlek, P.L., 2005. An appraisal of global wetland area and its organic carbon stock. Curr. Sci. 88 (1), 25–35.
MLURI, 1984. Organisation and Methods of the 1:250 000 Soil Survey of Scotland. Macaulay Institute for Soil Research, Aberdeen.
Moore, P.D., Bellamy, D.J., 1974. Peatlands. Elek Science, London, UK.
Morton Rowland, C., Wood, C., Meek, L., Marston, C., Smith, G., Wadsworth, R., Simpson, I.C., 2011. Final Report for LCM2007 - the new UK land cover map. (No. Countryside Survey Technical Report No 11/07 112pp. (CEH Project Number: C03259).). NERC/Centre for Ecol. Hydrol.
Nachtergaele, F., van Velthuizen, H., Verelst, L., Batjes, N., Dijkshoorn, K., van Engelen, V., Fischer, G., Jones, A., Montanarella, L., Petri, M., Prieler, S., 2009. Harmonized World Soil Database. FAO, Rome.
National Wetlands Working Group, 1997. The Canadian wetland classification system. In: Warner, B.G., Rubec, C.D.A. (Eds.), Wetlands, 2nd Ed. Research Centre, University of Waterloo, Waterloo, ON, Canada.
Novresiandi, D.A., Nagasawa, R., 2017. Polarimetric synthetic aperture radar application for tropical peatlands classification: a case study in Siak River Transect, Riau Province, Indonesia. J. Appl. Remote. Sens. 11 (1), 016040.
O'Sullivan, G., 1992. CORINE land cover project (Ireland). Surv. Ireland 24, 32–35.
O'Loughlin, F.E., Paiva, R.C.D., Durand, M., Alsdorf, D.E., Bates, P.D., 2016. A multi-sensor approach towards a global vegetation corrected SRTM DEM product. Remote Sens. Environ. 182, 49–59.
Padarian, J., Minasny, B., McBratney, A.B., 2015. Using Google's cloud-based platform for digital soil mapping. Comput. Geosci. 83, 80–88.
Page, S.E., Siegert, F., Rieley, J.O., Boehm, H.-D.V., Jaya, A., Limin, S., 2002. The amount of carbon released from peat and forest fires in Indonesia during 1997. Nature 420, 61.
Page, S., Wűst, R., Weiss, D., Rieley, J., Shotyk, W., Limin, S.H., 2004. A record of late Pleistocene and Holocene carbon accumulation and climate change from an equatorial peat bog (Kalimantan, Indonesia): implications for past, present and future carbon dynamics. J. Quat. Sci. 19, 625–635.
Pahkakangas, S., Berglund, Ö., Lundblad, M., Karltun, E., 2016. Markanvändning på organogena jordar i Sverige.
Päivänen, J., 1969. The bulk density of peat and its determination. Silva Fennica 3, 1–19.
Pala, S., 1982. A method for peat inventory based on Landsat data and computerized mapping. In: Proc. National Conference on Energy Resource Management, Baltimore, 1982. vol. 2. pp. 518–534.
Parry, L.E., Charman, D.J., 2013. Modelling soil organic carbon distribution in blanket peatlands at a landscape scale. Geoderma 211, 75–84.
Parry, L.E., Charman, D.J., Noades, J.P.W., 2012. A method for modelling peat depth in blanket peatlands. Soil Use Manag. 28, 614–624.
Parry, L., West, L., Holden, J., Chapman, P., 2014. Evaluating approaches for estimating peat depth. Journal of Geophysical Research: Biogeosciences 119, 567–576.
Pemberton, M., 1989. Land Systems of Tasmania. Region 7, South West. Department of Agriculture.
Pemberton, M., 2005. Australian peatlands: a brief consideration of their origin, distribution, natural values and threats. J. R. Soc. West. Aust. 88, 81–89.
Pereira, M.G., Anjos, L.H.C., Valladares, G.S., 2005. Organossolos: Ocorrência, gênese, classificação, alterações pelo uso agrícola e manejo. In: Torrado, P.V., Alleoni, L.R.F., Cooper, M., Silva, A.P., Cardoso, E.J. (Eds.), Tópicos em ciência do solo. 4. Sociedade Brasileira de Ciência do Solo, Viçosa, MG, pp. 233–276.
Pflugmacher, D., Krankina, O.N., Cohen, W.B., 2007. Satellite-based peatland mapping: potential of the MODIS sensor. Glob. Planet. Chang. 56, 248–257.
Plado, J., Sibul, I., Mustasaar, M., Joeleht, A., 2011. Ground-penetrating radar study of the Rahivere peat bog, eastern Estonia. Estonian journal of earth sciences 60, 31.
Poggio, L., Gimona, A., 2014. National scale 3D modelling of soil organic carbon stocks with uncertainty propagation—an example from Scotland. Geoderma 232, 284–299.
Poggio, L., Lassauce, A., Gimona, A., 2019. Modelling the extent of northern peat soil and its uncertainty with Sentinel: Scotland as example of highly cloudy region. Geoderma 346, 63–74.
Racine, M.-J., Bernier, M., Ouarda, T., 2005. Evaluation of RADARSAT-1 images acquired in fine mode for the study of boreal peatlands: a case study in James Bay, Canada. Can. J. Remote. Sens. 31, 450–467.
Rampi, L.P., Knight, J.F., Pelletier, K.C., 2014. Wetland mapping in the upper Midwest United States. Photogramm. Eng. Remote Sens. 80, 439–448.
Rawlins, B., Marchant, B., Smyth, D., Scheib, C., Lark, R., Jordan, C., 2009. Airborne radiometric survey data and a DTM as covariates for regional scale mapping of soil organic carbon across Northern Ireland. Eur. J. Soil Sci. 60, 44–54.
Reddy, A.D., Hawbaker, T.J., Wurster, F., Zhu, Z., Ward, S., Newcomb, D., Murray, R., 2015. Quantifying soil carbon loss and uncertainty from a peatland wildfire using multi-temporal LiDAR. Remote Sens. Environ. 170, 306–316.
Renou-Wilson, F., Bolger, T., Bullock, C., Convery, F., Curry, J., Ward, S., Wilson, D., Müller, C., 2011. BOGLAND: Sustainable Management of Peatlands in Ireland. STRIVE Report Series 181.
Reuter, H.I., Neison, A., Strobl, P., Mehl, W., Jarvis, A., 2009. A first assessment of Aster GDEM tiles for absolute accuracy, relative accuracy and terrain parameters. In: Geoscience and Remote Sensing Symposium, 2009 IEEE International, IGARSS 2009. IEEE, pp. V–240-V-243.
Rodrigo, P., Orrego, J.P., 2007. In: Libros, Ocho (Ed.), Patagonia chilena¡ Sin represas. Santiago de Chile.
Rosa, E., Larocque, M., Pellerin, S., Gagné, S., Fournier, B., 2009. Determining the number of manual measurements required to improve peat thickness estimations by ground penetrating radar. Earth Surf. Process. Landf. 34, 377–383.
Rothwell, J.J., Lindsay, J.B., 2007. Mapping contemporary magnetic mineral concentrations in peat soils using fine-resolution digital terrain data. CATENA 70, 465–474.
Rothwell, J.J., Lindsay, J.B., Evans, M.G., Allott, T.E., 2010. Modelling suspended sediment lead concentrations in contaminated peatland catchments using digital terrain analysis. Ecol. Eng. 36, 623–630.
Roudier, P., Beaudette, D., Hewitt, A., 2012. A conditioned Latin hypercube sampling algorithm incorporating operational constraints. In: Digital Soil Assessments and beyond. CRC Press, Sydney, NSW, Australia, pp. 227–231.
Rudiyanto, R., Setiawan, B.I., Arief, C., Saptomo, S.K., Gunawan, A., Kuswarman, Sungkono, Indriyanto, H., 2015. Estimating distribution of Carbon Stock in Tropical Peatland using a Combination of an Empirical Peat Depth Model and GIS. Procedia Environ. Sci. 24, 152–157.
Rudiyanto, R., Minasny, B., Setiawan, B.I., 2016a. Further results on comparison of methods for quantifying soil carbon in tropical peats. Geoderma 269, 108–111.
Rudiyanto, R., Minasny, B., Setiawan, B.I., Arif, C., Saptomo, S.K., Chadirin, Y., 2016b. Digital mapping for cost-effective and accurate prediction of the depth and carbon stocks in Indonesian peatlands. Geoderma 272, 20–31.
Rudiyanto, R., Minasny, B., Setiawan, B.I., Saptomo, S.K., McBratney, A.B., 2018. Open digital mapping as a cost-effective method for mapping peat thickness and assessing the carbon stock of tropical peatlands. Geoderma 313, 25–40.
Saey, T., Islam, M.M., De Smedt, P., Meerschman, E., Van De Vijver, E., Lehouck, A., Van Meirvenne, M., 2012. Using a multi-receiver survey of apparent electrical conductivity to reconstruct a Holocene tidal channel in a polder area. CATENA 95, 104–111.
Saito, H., Yoshino, K., Ishida, T., Nagano, T., Sirichuaychoo, W., Jongskul, A., Haraguchi, N., 2005. Geostatistical estimation of tropical peat-soil volume at Bacho, Thailand: impact of spatial support size and censored information. Geoderma 125, 235–247.
Samuel-Rosa, A., Heuvelink, G., Vasques, G., Anjos, L., 2015. Do more detailed environmental covariates deliver more accurate soil maps? Geoderma 243, 214–227.
Sheng, Y., Smith, L.C., MacDonald, G.M., Kremenetski, K.V., Frey, K.E., Velichko, A.A., Lee, M., Beilman, D.W., Dubinin, P., 2004. A high-resolution GIS-based inventory of the west Siberian peat carbon pool. Glob. Biogeochem. Cycles 18.
Shimada, S., Takada, M., Takahashi, H., 2016. Peat Mapping, Tropical Peatland Ecosystems. Springer, pp. 455–467.
Silc, T., Stanek, W., 1977. Bulk density estimation of several peats in northern Ontario using the von Post humification scale. Can. J. Soil Sci. 57, 75.
Silva, M.L.d., Silva, A.C., Silva, B.P.C., Barral, U.M., Soares, P.G., Vidal-Torrado, P., 2013. Surface mapping, organic matter and water stocks in peatlands of the Serra do Espinhaço Meridional-Brazil. Revista Brasileira de Ciência do Solo 37, 1149–1157.
Simard, M., Pinto, N., Fisher, J.B., Baccini, A., 2011. Mapping forest canopy height globally with spaceborne lidar. Journal of Geophysical Research: Biogeosciences 116.
Simpson, J.E., Wooster, M.J., Smith, T.E., Trivedi, M., Vernimmen, R.R., Dedi, R., Shakti, M., Dinata, Y., 2016. Tropical peatland burn depth and combustion heterogeneity assessed using UAV photogrammetry and airborne LiDAR. Remote Sens. 8, 1000.
Sirin, A., Maslov, A., Valyaeva, N., Tsyganova, O., Glukhova, T., 2014. Mapping of peatlands in the Moscow oblast based on high-resolution remote sensing data. Contemp. Probl. Ecol. 7, 808–814.
Slater, L.D., Reeve, A., 2002. Investigating peatland stratigraphy and hydrogeology using integrated electrical geophysics. Geophysics 67, 365–378.
Soil Classification Working Group, 1998. The Canadian System of Soil Classification. NRC Research press, Ottawa, Canada.
Soil Survey of Scotland, 1984. Organization and Methods of the 1:250 000 Soil Survey of Scotland. The Macaulay Institute for Soil Research, Aberdeen, UK.
Squeo, F.A., Warner, B.G., Aravena, R., Espinoza, D., 2006. Bofedales: high altitude peatlands of the Central Andes. Rev. Chil. Hist. Nat. 79, 245–255.
Stockmann, U., Malone, B., McBratney, A.B., Minasny, B., 2015. Landscape-scale exploratory radiometric mapping using proximal soil sensing. Geoderma 239, 115–129.
Stove, G., 1983a. The current use of remote-sensing data in peat, soil, land-cover and crop inventories in Scotland. Phil. Trans. R. Soc. Lond. A 309, 271–281.

Stove, G., 1983b. Improved peatland classification using principal components analysis based on synthetic variables: A remote sensing methodology for peat resource surveys in Scotland. In: Remote Sensing in Peat and Terrain Resource Surveys, Proceedings of Symposium of IPS Commission I, pp. 75–86.
Stove, G., Hulme, P., 1980. Peat resource mapping in Lewis using remote sensing techniques and automated cartography. Int. J. Remote Sens. 1, 319–344.
Subardja, D., Ritung, S., Anda, M., Sukarman, S.E., Subandiono, R.E., 2016. Petunjuk Teknis Klasifikasi Tanah Nasional. Edisi Ke-2. Balai Besar Penelitian dan Pengembangan Sumberdaya Lahan Pertanian, Badan Penelitian dan Pengembangan Pertanian, Bogor, Indonesia.
Tadono, T., Ishida, H., Oda, F., Naito, S., Minakawa, K., Iwamoto, H., 2014. Precise global DEM generation by ALOS PRISM. In: ISPRS Annals of the Photogrammetry, Remote Sensing and Spatial Information Sciences. vol. 2. pp. 71.
Takada, M., Mishima, Y., Natsume, S., 2009. Estimation of surface soil properties in peatland using ALOS/PALSAR. Landsc. Ecol. Eng. 5, 45–58.
Tanneberger, F., Tegetmeyer, C., Busse, S., Barthelmes, A., Shumka, S., Moles Mariné, A., Jenderedjian, K., Steiner, G.M., Essl, F., Etzold, J., Mendes, C., Kozulin, A., Frankard, P., Milanović, D., Ganeva, A., Apostolova, I., Alegro, A., Delipetrou, P., Navrátilová, J., Risager, M., Leivits, A., Fosaa, A.M., Tuominen, S., Muller, F., Bakuradze, T., Sommer, M., Christanis, K., Szurdoki, E., Oskarsson, H., Brink, S.H., Connolly, J., Bragazza, L., Martinelli, G., Aleksāns, O., Priede, A., Sungaila, D., Melovski, L., Belous, T., Saveljić, D., de Vries, F., Moen, A., Dembek, W., Mateus, J., Hanganu, J., Sirin, A., Markina, A., Napreenko, M., Lazarević, P., Šefferová Stanová, V., Skoberne, P., Heras Pérez, P., Pontevedra-Pombal, X., Lonnstad, J., Küchler, M., Wüst-Galley, C., Kirca, S., Mykytiuk, O., Lindsay, R., Joosten, H., 2017. The peatland map of Europe. Mires and Peat 19, 1–17.
Tarnocai, C., 1984. Peat Resources of Canada. Land Resources Research Institute, Research Branch, Agriculture, Canada.
Tarnocai, C., Kettles, I., Lacelle, B., 2011. Peatlands of Canada. In: Geological Survey of Canada, Open File 6551. vol. 10 Natural Resources Canada, Ottawa, ON.
Tharp, W.E., 1924. Mapping peat soils. American Soil Survey Association Bulletin 5, 51–52.
Theimer, B.D., Nobes, D.C., Warner, B.G., 1994. A study of the geoelectrical properties of peatlands and their influence on ground-penetrating radar surveying. Geophys. Prospect. 42, 179–209.
Thomas, V., Treitz, P., Jelinski, D., Miller, J., Lafleur, P., McCaughey, J.H., 2003. Image classification of a northern peatland complex using spectral and plant community data. Remote Sens. Environ. 84, 83–99.
Thompson, D.K., Waddington, J.M., 2014. A Markov chain method for simulating bulk density profiles in boreal peatlands. Geoderma 232-234, 123–129.
Thompson, D.K., Simpson, B.N., Beaudoin, A., 2016. Using forest structure to predict the distribution of treed boreal peatlands in Canada. For. Ecol. Manag. 372, 19–27.
Tonks, A.J., Aplin, P., Beriro, D.J., Cooper, H., Evers, S., Vane, C.H., Sjögersten, S., 2017. Impacts of conversion of tropical peat swamp forest to oil palm plantation on peat organic chemistry, physical properties and carbon stocks. Geoderma 289, 36–45.
Torbick, N., Persson, A., Olefeldt, D., Frolking, S., Salas, W., Hagen, S., Crill, P., Li, C., 2012. High resolution mapping of peatland hydroperiod at a high-latitude Swedish mire. Remote Sens. 4, 1974–1994.
Upton, A., Vane, C.H., Girkin, N., Turner, B.L., Sjögersten, S., 2018. Does litter input determine carbon storage and peat organic chemistry in tropical peatlands? Geoderma 326, 76–87.
Väänänen, T., Hyvönen, E., Jakonen, M., Kupila, J., Lerrsi, J., Leskinen, J., Liwata, P., Nevalainen, R., Putkinen, S., Virkki, H., 2007. Maaperän yleiskartan tulkinta- ja kartoitusprosessi.
Valladares, G., 2003. Caracterização de Organossolos, auxílio à sua classificação. Universidade Federal Rural do Rio de Janeiro, Rio de Janeiro (142 pp).
Van Breemen, N., 1995. How Sphagnum bogs down other plants. Trends Ecol. Evol. 10, 270–275.
Villagrán, M.C., Castro, R.V., 1997. Etnobotánica y manejo ganadero de las vegas, bofedales y quebradas en el Loa superior, Andes de Antofagasta, Segunda Región, Chile. Chungara. pp. 275–304.
Vitt, D.H., Halsey, L.A., Bauer, I.E., Campbell, C., 2000. Spatial and temporal trends in carbon storage of peatlands of continental western Canada through the Holocene. Can. J. Earth Sci. 37, 683–693.
Wahyunto, R.S., Subagjo, H., 2003. Maps of Area of Peatland Distribution and Carbon Content in Sumatera, 1990–2002. Wetlands Int-Indonesia Programm and Wildl Habitat Canada, Bogor, Indonesia.
Wahyunto, R.S., Subagjo, H., 2004. Map of Peatland Distribution Area and Carbon Content in Kalimantan, 2000–2002. Wetlands International—Indonesia Programme & Wildlife Habitat Canada (WHC), Bogor, Indonesia.
Wahyunto, H.B., Bekti, H., Widiastuti, F., 2006. Maps of Peatland Distribution, Area and Carbon Content in Papua, 2000–2001. Wetlands International-Indonesia Programme & Wildlife Habitat Canada (WHC), Bogor.
Walter, J., Lueck, E., Bauriegel, A., Richter, C., Zeitz, J., 2015. Multi-scale analysis of electrical conductivity of peatlands for the assessment of peat properties. Eur. J. Soil Sci. 66, 639–650.
Warner, B.G., Nobes, D.C., Theimer, B.D., 1990. An application of ground penetrating radar to peat stratigraphy of Ellice Swamp, southwestern Ontario. Can. J. Earth Sci. 27, 932–938.
Warren, M.W., Kauffman, J.B., Murdiyarso, D., Anshari, G., Hergoualc'h, K., Kurnianto, S., Purbopuspito, J., Gusmayanti, E., Afifudin, M., Rahajoe, J., Alhamd, L., 2012. A cost-efficient method to assess carbon stocks in tropical peat soil. Biogeosciences 9 (11), 4477–4485.
Warren, M., Hergoualc'h, K., Kauffman, J.B., Murdiyarso, D., Kolka, R., 2017. An appraisal of Indonesia's immense peat carbon stock using national peatland maps: uncertainties and potential losses from conversion. Carbon balance and management 12, 12.
Weissert, L.F., Disney, M., 2013. Carbon storage in peatlands: a case study on the Isle of Man. Geoderma 204-205, 111–119.
Whinam, J., Hope, G., 2005. The Peatlands of the Australasian Region. In: Steiner, G.M. (Ed.), Moore - von Sibirien bis Feuerland Mires - from Siberia to Tierra del Fuego. Biologiezentrum der Oberoesterreichischen, Linz, pp. 397–434.
White, L., Millard, K., Banks, S., Richardson, M., Pasher, J., Duffe, J., 2017. Moving to the RADARSAT constellation mission: comparing synthesized compact polarimetry and dual polarimetry data with fully polarimetric RADARSAT-2 data for image classification of peatlands. Remote Sens. 9.
Wieder, R.K., Vitt, D.H., Benscoter, B.W., 2006. Peatlands and the Boreal Forest, Boreal Peatland Ecosystems. Springer, pp. 1–8.
Wiesmeier, M., Urbanski, L., Hobley, E., Lang, B., von Lützow, M., Marin-Spiotta, E., van Wesemael, B., Rabot, E., Ließ, M., Garcia-Franco, N., Wollschläger, U., 2019. Soil organic carbon storage as a key function of soils-a review of drivers and indicators at various scales. Geoderma 333, 149–162.
Wijaya, A., Reddy Marpu, P., Gloaguen, R., 2010. Discrimination of peatlands in tropical swamp forests using dual-polarimetric SAR and Landsat ETM data. International Journal of Image and Data Fusion 1, 257–270.
Wijedasa, L.S., Sloan, S., Michelakis, D.G., Clements, G.R., 2012. Overcoming limitations with Landsat imagery for mapping of peat swamp forests in Sundaland. Remote Sens. 4, 2595–2618.
Wilford, J., 2012. A weathering intensity index for the Australian continent using airborne gamma-ray spectrometry and digital terrain analysis. Geoderma 183, 124–142.
Wilson, D., Blain, D., Couwenberg, J., Evans, C., Murdiyarso, D., Page, S., Renou-Wilson, F., Rieley, J., Sirin, A., Strack, M., 2016a. Greenhouse gas emission factors associated with rewetting of organic soils. Mires and Peat 17.
Wilson, D., Farrell, C.A., Fallon, D., Moser, G., Müller, C., Renou-Wilson, F., 2016b. Multiyear greenhouse gas balances at a rewetted temperate peatland. Glob. Chang. Biol. 22, 4080–4095.
World-Energy-Council, 2013. World Energy Resources: Peat, London, UK.
Wu, Y., Chan, J.R., Verseghy, D.L., 2017. A Map of Global Peatland Distribution Created Using Machine Learning for Use in Terrestrial Ecosystem and Earth System Models.
Wulder, M.A., White, J.C., Cranny, M., Hall, R.J., Luther, J.E., Beaudoin, A., Goodenough, D.G., Dechka, J.A., 2008. Monitoring Canada's forests. Part 1: completion of the EOSD land cover project. Can. J. Remote. Sens. 34, 549–562.
Xing, W., Bao, K., Gallego-Sala, A.V., Charman, D.J., Zhang, Z., Gao, C., Lu, X., Wang, G., 2015. Climate controls on carbon accumulation in peatlands of Northeast China. Quat. Sci. Rev. 115, 78–88.
Xu, J., Morris, P.J., Liu, J., Holden, J., 2018. PEATMAP: refining estimates of global peatland distribution based on a meta-analysis. CATENA 160, 134–140.
Yamazaki, D., Ikeshima, D., Tawatari, R., Yamaguchi, T., O'Loughlin, F., Neal, J.C., Sampson, C.C., Kanae, S., Bates, P.D., 2017. A high accuracy map of global terrain elevations. Geophys. Res. Lett. 44 (11), 5844–5853.
Yoshino, K., Ishida, T., Nagano, T., Setiawan, Y., 2010. Land cover pattern analysis of tropical peat swamp lands in Southeast Asia. In: Kajiwara, K. (Ed.), International Archives of the Photogrammetry Remote Sensing and Spatial Information Sciences. ISPRS, Kyoto, pp. 941–946.
Young, D.M., Parry, L.E., Lee, D., Ray, S., 2018. Spatial models with covariates improve estimates of peat depth in blanket peatlands. PLoS One 13 (9), e0202691.
Yu, Z., Loisel, J., Brosseau, D.P., Beilman, D.W., Hunt, S.J., 2010. Global peatland dynamics since the last Glacial Maximum. Geophys. Res. Lett. 37.